Control of Systems with Limited Capacity

Solyom, Stefan

2004

Document Version:
Publisher's PDF, also known as Version of record

Control of Systems with Limited Capacity

Control of Systems with Limited Capacity

Stefan Solyom

Department of Automatic Control
Lund Institute of Technology
Lund, August 2004

Department of Automatic Control
Lund Institute of Technology
Box 118
SE-221 00 LUND
Sweden

ISSN 0280–5316
ISRN LUTFD2/TFRT--1069--SE

Printed in Sweden by Media-Tryck.
Lund 2004

Contents

Preface

Virtually all real life systems are such that they present some kind of limitation on one or many of its variables, physical quantities. In some cases this is a direct consequence of the laws of physics. In others it is an engineering constraint. Usually, the operating points of the system are such that these limitations are of little or no concern. However, there exist several systems where these limitations are critical and can lead to undesirable behaviors.

Nevertheless, all of these systems can be classified as systems with limited capacity. This thesis is treating control related problems of a subclass of such systems, where the limitation is a critical factor.

The thesis is composed of four parts. The first and the fourth part is treating two industrial applications, the control of tire slip in a braking car and, the voltage stability control in power systems. The capacity limited factor in theses cases are the friction coefficient between the tire and the road and the maximum transferable power through a power network. The second and third part treats two nonlinear control related problems, of a more theoretical nature. The second part introduces a tuning method for PI(D) controllers that can be used for a class of systems with limited capacity. The third part is treating the trajectory following problem in piecewise linear systems with focus on anti-windup compensation of saturated systems. These latter processes fall naturally in the class of systems with limited capacity.

The Anti-lock Braking System (ABS) is an important component of a complex steering system for the modern car. In the latest generation of brake-by-wire systems, the performance requirements on the ABS have changed. The controllers have to maintain a specified tire slip for each wheel during braking. This thesis proposes a design model and based on that a hybrid controller that regulates the tire-slip. Simulation and results from drive tests are presented.

In the second part, a design method for robust PID controllers is pre-

sented. Robustness is ensured with respect to a cone bounded static nonlinearity acting on the plant. Additional constraints on maximum sensitivity are also considered. The design procedure has been successfully applied in the synthesis of the proposed ABS controller.

The third part studies the trajectory convergence for a general class of nonlinear systems. The servo problem for piecewise linear systems is presented. Convex optimization is used to describe the behavior of system trajectories of a piecewise linear system with respect to some input signals. The obtained results are then applied for the study of anti-windup compensators.

The last part of this thesis is treating the problem of voltage stability in power systems. Voltage at the load end of a power system has to be controlled within prescribed tolerances, in order to guarantee a satisfactory voltage for the consumers. Even in case of normal operation, this task is non-trivial due to the ever-changing load conditions. Moreover, in case of emergencies such as sudden line failures, this task can be very difficult and sometimes impossible. The main contribution of this chapter is a method for improving the stability properties of the grid by dynamic compensation of the reference load voltage. Moreover, a complete compensation scheme is proposed that has load shedding as secondary control variable. This control scheme is shown to stabilize different power system models, meanwhile attempts to minimize the amount of disconnected load.

Acknowledgments

First of all I would like to thank my supervisor Professor Anders Rantzer for his guidance and support. He was a great source of inspiration from the moment I met him. His influence during these years has profoundly contributed to the value of this thesis.

Many thanks to Andrey Ghulchak for his excellent courses and inspiring discussions, as well as his patience in answering so many questions of mathematical nature.

I am grateful to Professor Björn Wittenmark and Professor Tore Hägglund for their valuable comments and suggestions regarding the manuscript. Special thanks to Karl Johan Åström for his help with formulating the introductory chapter.

I would like to express my appreciation to the team at DaimlerChrysler that made possible the real-life testing of this work. In particular, to Dr. Jens Kalkkuhl at DaimlerChrysler for inspiring discussions and insightful suggestions regarding the work in the second chapter of this thesis.

During the work on power systems I had the opportunity of working together with Professor Sture Lindahl and Dr. Mats Larsson. Their constant encouragement and support contributed significantly to this thesis. Also here would like to thank Inés Romero Navarro, who answered so many power systems related questions.

Sincere gratitude to Professor Stefan Preitl and Professor Paul M. Frank who made possible my first more profound contact with the field of control during my master thesis.

It has been grate fun to work together with Ari Ingimundarson on the problems presented in Chapter 3 of this thesis as well as with Bo Lincoln on our short, but rewarding endeavor in the realm of power systems.

I would like to thank all my colleagues at the department for their support. It is elevating to be part of such a great collective. Special thanks to Leif Andersson for his help in (m)any computer related questions that

appeared over these years. Here is to mention you guys, who helped with the proofreading of the thesis Henrik, Jacob, Staffan, Stéphane. I am obliged!

Financial support from the EU projects Heterogeneous Hybrid Control ($\mathcal{H}^2\mathcal{C}$), and Computation and Control ($\mathcal{CC}$) is gratefully acknowledged.

I would like to thank my parents for their understanding and support during these years. Thanks goes also to my friends here in Lund, who made the rainy days and nights more fun.

Many, many thanks to Diana for her patience, encouragement and her courage to give up a life and career in Romania and move here to Sweden and start allover. Your love and support in the last couple of years were invaluable.

Stefan

1

Introduction

This thesis has four parts that are addressing four different nonlinear control problems in the framework of systems with limited capacity. The work presented here is based on a total of six papers.

The first and fourth part handles industrial applications, the control of tire slip during braking of a vehicle and voltage stability problem in power networks respectively.

In the second part, a method for tuning PI(D) controllers is presented that can be used for a class of systems with limited capacity. The theory developed here has been applied in the tire slip control problem.

The third part is concentrating on a more theoretical issue, the trajectory following in piecewise linear systems. Also a practical application of the theory is presented by in the context of anti-windup compensators.

1.1 Contributions of the Thesis

Chapter 2 of this thesis is concerned with an industrial application, an Anti-lock Braking System for a passenger vehicle. It introduces an effective design model that is shown to capture the main control difficulties of the problem. A novel control system is proposed. The resulting controller is a gain scheduled nonlinear PI(D). Simulation and test results show the efficiency of the controller. An extended introduction of this work is presented in Section 1.4. This chapter is is an extended version of:

Solyom, S., A. Rantzer, and J. Lüdemann (2003): "Synthesis of a model-based tire slip controller." *Vehicle System Dynamics*, **41:6**, pp. 477–511.

Furthermore, the Appendix B of Chapter 2 contains a benchmark for Anti-lock Braking Systems that is based on:

Solyom, S., J. Kalkkuhl, and Rantzer (2002): "A benchmark for control of anti-lock braking systems." In *http://www.control.lth.se/H2C*.

Chapter 3 is treating a synthesis method for robust PI(D) controllers for a class of systems with limited capacity. Due to the involved nonlinearity, no classical PID tuning methods can be used to guarantee stability of the system.This work proposes a novel design method based on the Circle Criterion that guarantees stability of the closed loop nonlinear system. The method is used in the tuning of the PI(D) controllers used in the tire slip controller. An extended introduction of this work is presented in Section 1.5. This chapter is based on the results in:

Solyom, S. and A. Ingimundarson (2002): "A synthesis method for robust PID controllers for a class of uncertain systems." *Asian Journal of Control*, **4:4**, pp. 381–387.

Chapter 4 is treating the servo problem for piecewise linear systems, that is, the trajectory convergence of piecewise linear systems in presence of exogenous output signals. This problem is shown to be solvable in terms of LMI-based convex optimization. As a case study, the class of saturated systems with anti-windup compensation is explored. An extended introduction of this work is presented in Section 1.6. This chapter is based on the results in:

Solyom, S. and A. Rantzer (2002): "The servo problem for piecewise linear systems." In *Proceedings of the Fifteenth International Symposium on Mathematical Theory of Networks and Systems*. Notre Dame, IN.

Solyom, S. (2003): "A synthesis method for static anti-windup compensators." In *Proceedings of the European Control Conference, ECC03*. Cambridge, UK.

Chapter 5 is concerned with voltage stability of power systems. This work analyses a simple model that is shown to capture the control difficulties of this problem. A new stabilization method is introduced and a controller is proposed that improves the stability properties of a power network. An extended introduction of this work is presented in Section 1.7. This chapter is based on the results in:

Solyom, S., B. Lincoln, and A. Rantzer (2004a): "A novel method for voltage stability control in power systems." In *Proceedings of the World Automation Congress*.

Solyom, S., B. Lincoln, and A. Rantzer (2004b): "Power systems." In *Patent application nr. 040031-8, Svenska Patentverket*.

Other related publications:

Solyom, S. and A. Rantzer (2003): "ABS control - a design model and control structure." In *Nonlinear and Hybrid Systems in Automotive Control*, pp. 85–96. Springer Verlag.

Ingimundarson, A. and S. Solyom (2003): "On a synthesis method for robust PID controllers for a class of uncertainties." In *Proceedings of the European Control Conference, ECC03*. Cambridge, UK.

1.2 Background and Motivation

I started my research activities at the department within the frame of the European project on Heterogeneous and Hybrid Control, $\mathcal{H}^2\mathcal{C}$. Its objective was to develop innovative theory for heterogeneous and hybrid control while proving the industrial relevance of this technology. The analyzed benchmark was the tire slip control problem for a braking vehicle. This work led to the results in the Chapters 2 and 3. It also inspired us to formulate the servo problem in Chapter 4. After the project finished, I got involved in another European project, named Computation and Control, $\mathcal{CC}$. This project involved a benchmark devoted to the voltage stability of power systems. To our surprise, we realized that the two systems present in essence the same type of limitations.

1.3 Systems with Limited Capacity

The term *capacity* has several meanings, the one used in this thesis can be described by the following definition, according to Webster Dictionary: *"the facility or power to produce, perform, or deploy"*.

The majority of real life systems are such that they present some kind of limitation on one or many of its variables, physical quantities. In some cases this is a direct consequence of the laws of physics. In others it is an engineering constraint. Usually, the operating points of the system are such that these limitations are of little or no concern. However, there exist several systems where these limitations are critical and can lead to undesirable behaviors. Nevertheless, all of these systems can be classified as systems with limited capacity. Some typical example are:

- the amount of water contained in a water tank is limited by the size of the tank,
- information transmission rate is limited by the capacity of the used network,

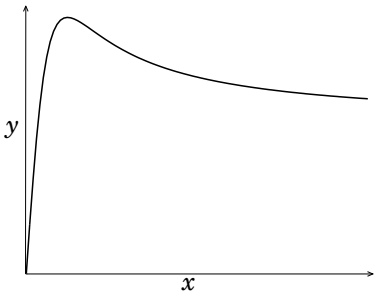

Figure 1.1 Nonlinearity that can give rise to system with limited capacity. The value of y can not increase above a maximum value.

- the maximum attainable friction force between two surfaces is limited by the maximum friction coefficient between the two surfaces,
- the maximum electrical power transmitted through a network with limited power source is limited by the impedances in the network,
- actuators in a sontrol system have limited range and velocity.

This work addresses a special class of systems, where the capacity limitation is given by a nonlinearity of the type shown in Figure 1.1. Moreover, in the studied processes the nonlinearity has a critical influence on the behavior of the system. As seen in the figure, the variable y can not increase above a given maximum value. A dynamical system with such limitation on one of its variables is said to have *limited capacity of delivering the quantity* y.

This thesis studies three different class of systems with limited capacity:

- an Anti-lock Braking System, where the capacity limited factor is the deliverable friction force between the tires and the surface,
- a power system, where the capacity limited factor is the deliverable power through the network. This reaches its maximum when the impedance of the network and the load are matched.
- saturated control systems, where the limited variable is the control authority of the actuators.

It is shown that these apparently very different systems are technically, quite similar from the control point of view.

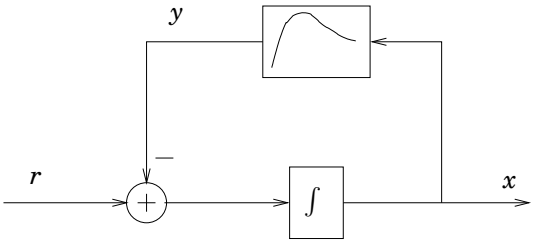

Figure 1.2 Dynamical system with limited capacity. This system describes the control difficulties of both an anti-lock braking system (ABS) of a car and voltage stability control in power systems.

The dynamical system, in Figure 1.2 is investigated. It is shown that this system describes the control difficulties of both an Anti-lock Braking System (ABS) for a car and voltage stability control in power systems. In case of *ABS control* the quantities in the figure have the following physical interpretation:

- x - tire slip,
- y - torque caused by the friction between the tire and the road,
- r - braking torque.

The tire-road friction coefficient is the capacity limited factor. In case of *voltage stability control in power systems* the quantities in the figure have the following physical interpretation:

- x - load admittance,
- y - the power transfered through the network,
- r - the power requested by the load.

Here, the power transfered through the network is the capacity limited factor. It is well known that the transmitted power is maximized when the impedances of the load and network are matched.

Even in the simplest case, when a linear system is combined with such a nonlinearity (Figure 1.1), there are several *control difficulties* arising:

- Depending on the interconnection, the resulting system can have one, two, or no equilibrium points. This can give rise to interesting behaviors of the nonlinear system.
- When the system has two equilibrium points, it can exhibit qualitatively different behaviors depending on the equilibrium. One equilibrium point is typically stable while the other is unstable.

- Limitation of one or more quantities in the system can have serious repercussions on the global behavior of the nonlinear system.

These problems can not be solved by classical linear system theory. This work uses Lyapunov theory to formulate some approaches and solutions.

1.4 Anti-Lock Braking Systems and Tire Slip Control

"While the development of braking systems has come a long way, the progress is just beginning." [Buckman, 1998]

Introduction

In the 1970's government mandated standards started to emerge that regulated the exhaust emissions and fuel economy of the vehicles. Car manufacturers realized that automatic control systems are a viable solution for this problem. Since then automatic control systems have been used to improve almost every function of a vehicle. Major fields of applications are improvement of passenger safety. Arguably the most important contribution has been in the area of braking, traction and stability control. In these application the control system aids the driver and corrects its mistakes [Jurgen, 1999].

One of the most important subsystems in any vehicle is its braking system. In the last century, braking systems have evolved considerably. It started with primitive systems, consisting of a block rubbing against the wheel rim. Today, the braking is electronically controlled by Anti-lock Braking Systems (ABS).

The first ABS systems were implemented in the late 1970's, the main objective of the control system being prevention of wheel-lock and they typically made use of hydraulic actuators.

In the latest generation of brake-by-wire systems, electro-mechanical actuators are capable of delivering continuously varying and different brake forces independently to the four wheels. Such actuators are capable of superior performance, needing novel slip controllers that can fully exploit these capabilities. The control objective of these systems shifts to maintain a specified tire slip rather then just preventing wheel-lock. The set-point slip is supposed to be provided by a higher level in the hierarchy (e.g. an Electronic Stability Program), and can be used for stabilizing the steering dynamics of the car while braking.

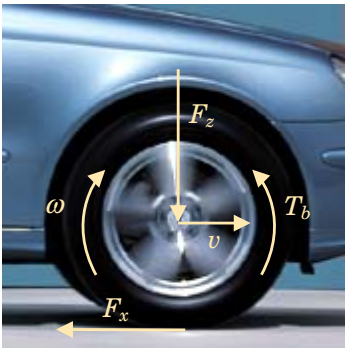

Figure 1.3 The tire slip is the normalized difference between the linear velocity of the wheel ωr and the velocity of the vehicle v.

Tire Slip Control

Consider the wheel of a vehicle (see Figure 1.3), then the tire slip λ is defined as the normalized difference between the linear velocity of the wheel ωr and the velocity of the vehicle v:

$$\lambda = \frac{v - \omega r}{v}$$

Tire slip control aims at the control of the tire slip λ. This is a nonlinear control problem. Additionally, the friction characteristics between the tire and the surface introduces significant uncertainty into the problem.

Chapter 2 is based on the results in [Solyom and Rantzer, 2003; Solyom *et al.*, 2004]. It introduces a simple design model (see Figure 1.4) that is shown to capture the main control difficulties of the problem. Due to the nonlinearity introduced by the friction curve, this problem clearly belongs

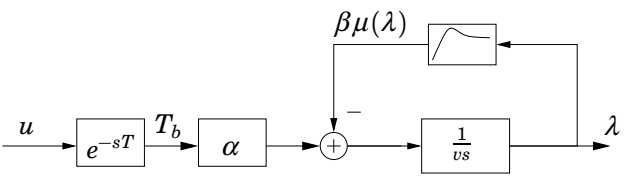

Figure 1.4 Proposed design model for an ABS. The nonlinearity is in feed-back with an integrator scaled by the linear velocity. Note that the system can have two equilibrium points. The one to the left of the peak of the friction curve is stable while the one to the right is unstable.

to the class of systems with limited capacity. The limited variable in this case is the friction coefficient between the road and the tire.

Based on this model, a systematic design procedure is proposed. The resulting controller is a gain-scheduled nonlinear PI(D) controller. The controller is using information about the vehicle velocity, the angular velocity of the wheel and an estimate of the maximum friction between the road and the tire.

Both simulation and experimental results show the viability of the proposed method. The experimental testing was carried out in a modified Mercedes E220 passenger vehicle that has been provided by DaimlerChrysler. The vehicle was fitted with brake-by-wire system and state of the art electromechanical brake actuators. The tests consisted in controlled emergency-braking on dry surface. The braking distance for the proposed controller, from an initial velocity of 30 m/s, was between 36−41 meters. The proposed controller outperformed the production ABS and some other controllers that have been tested.

1.5 PI(D) Control of a System with Limited Capacity

"The PID controller can be said to be the 'bread and butter' of control engineering." [Åström, 1995]

PID Control

One of the most commonly used controllers is the PID controller. In process control, more than 95% of the control loops are of PID type. The popularity of this type of controllers is mainly due to fact that inspite of its simple structure, it provides some important functions such as: feedback, ability to eliminate steady state offsets through integral action and it can anticipate the future through derivative action [Åström and Hägglund, 1995].

Over the past 50 years several design methods for PID controllers have been presented. Some of the methods need only superficial information about the process, in form of simple parameter models (e.g. Ziegler-Nichols, λ tuning method). These parameters can be easily identified by simple experiments (e.g. by measurement of the natural frequency of the plant, or by examining the step response of the plant). Other design methods need a more in-depth knowledge of the process (H_∞ synthesis).

Optimal control synthesis is a widely studied problem in the control engineering community. These methods are usually computationally involved and almost exclusively need a good process knowledge. In case of output feedback controllers, the resulting controllers have typically com-

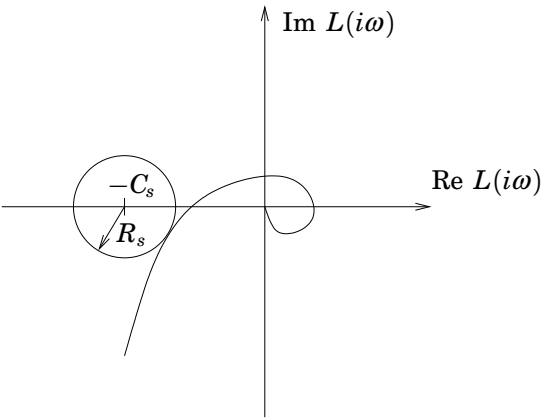

Figure 1.5 The radius R_s of the circle centered in $-C_s$ is a robustness measure of the closed loop system. When the robustness is measured by the maximum sensitivity function, the center $-C_s$ becomes -1 and $R_s = 1/\|(1+L)^{-1}\|_\infty$.

parable number of states as the plant. It has been shown in several occasions that the synthesis of optimal controllers with fixed number of states is a difficult problem. Nevertheless, in the case of PID controllers there have been several successful attempts to solve this problem [Ho, 2001; Panagopoulos, 2000].

In the latter mentioned work a design procedure for PI(D) controllers was presented which minimizes the effect of load disturbances. This is achieved by maximizing the integral gain while making sure that the closed loop system is stable. Furthermore, robustness is conferred by guaranteeing that the Nyquist curve of the loop transfer function is outside a circle with center $-C_s$ and radius R_s (see Figure 1.5). When the robustness is measured by the maximum sensitivity function, the center of the circle becomes -1 and

$$R_s = \frac{1}{\|(1+L(s))^{-1}\|_\infty}$$

where $L(s)$ is the loop transfer function. This way $M_s = 1/R_s$ can be used as a design parameter. The value of this parameter will influence the damping of the closed loop system.

These type of constraints will give rise to regions in the parameter space of the controller that are delimited by ellipsoids. Although a nonlinear optimization problem, it has been shown to be solvable for a class of systems.

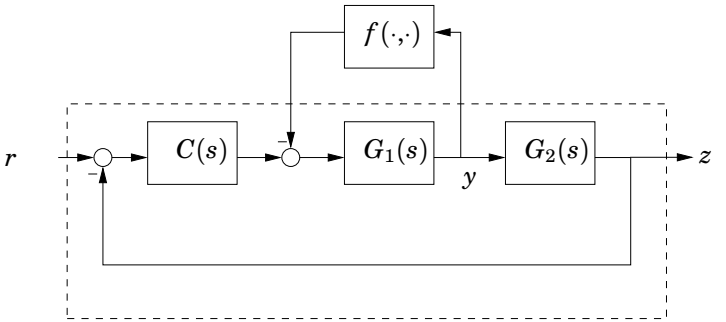

Figure 1.6 Block diagram showing nonlinearity, plant, and controller.

PI(D) Control of Systems with Limited Capacity

Chapter 3 is based on the results in [Solyom and Ingimundarson, 2002; Ingimundarson and Solyom, 2003]. The extension presented in this chapter guarantees, in addition, asymptotic stability of the system when a cone bounded nonlinearity is present in feedback with part of the plant, as shown in Figure 1.6. In particular this procedure can be used for systems with limited capacity that have a cone bounded nonlinearity in feedback with a linear plant.

The method is based on the Circle Criterion [Khalil, 1992]. In Chapter 3 it is shown that similarly to the M_s constraints, the Circle Criterion will induce regions in the controller parameter space bounded by ellipsoids. In case of PI control the optimal solution can easily be picked through visual inspection. However, for PID controllers optimization routines are desirable.

As a case study, the ABS control problem is revisited and a local design procedure is outlined which in combination with gain-scheduling gives the controller in Chapter 2.

1.6 Piecewise Linear Systems and Trajectory Following

Introduction

One type of nonlinear systems are the so called piecewise linear systems. These are dynamical systems of the form:

$$\begin{aligned} \dot{x} &= A_i x + a_i + B_i u \\ y &= C_i x + c_i + D_i u \end{aligned} \quad \text{for } x \in X_i \tag{1.1}$$

The state space of such systems is partitioned in a finite number of regions X_i, so that the system dynamics undergoes switching when passing from one operating regime to the other.

Many engineering applications can be modeled by piecewise linear systems. This specific structure can appear either inherently, as in the case of actuator saturations, or by piecewise linear approximation of nonlinearities. Either way, such system have an essential nonlinear character, exhibiting behaviors that can not be predicted by classical linear system theory.

One appealing property of such systems is that in many situations they can be analyzed by various computationally tractable methods. Stability of such systems can be investigated using Lyapunov theory. It has been shown by several authors that quadratic and piecewise quadratic Lyapunov functions for piecewise linear systems can be computed using convex optimization. The analysis problem usually results in a set of Linear Matrix Inequalities (LMIs), which can be solved by efficient convex optimization algorithms.

Stability of Piecewise Linear Systems

All the results related to piecewise linear systems that are presented in this work assume stability in the sense of the next theorems [Boyd and Yang, 1989; Hassibi and Boyd, 1998]:

THEOREM 1.1
Consider the system in (1.1). If there exist $P > 0$ such that

$$\begin{bmatrix} x \\ 1 \end{bmatrix}^T \begin{bmatrix} A_i^T P + P A_i & P a_i \\ a_i^T P & 0 \end{bmatrix} \begin{bmatrix} x \\ 1 \end{bmatrix} < 0 \quad \text{for } x \in X_i \setminus \{0\} \tag{1.2}$$

then the system is said to be quadratically stable. □

Condition (1.2) can be transformed to an LMI with the help of the S-procedure [Boyd *et al.*, 1994].

A less conservative result than quadratic stability was introduced in [Johansson, 1999], where piecewise quadratic Lyapunov functions are used instead of a quadratic one.

THEOREM 1.2
Consider the system in (1.1). If there exist a continuous function $V(x)$ such that

$$V(x) = \begin{bmatrix} x \\ 1 \end{bmatrix}^T \bar{P}_i \begin{bmatrix} x \\ 1 \end{bmatrix} > 0 \quad \text{for } x \in X_i \setminus \{0\}$$

and

$$\begin{bmatrix} x \\ 1 \end{bmatrix}^T \left(\begin{bmatrix} A_i^T & a_i \\ 0 & 0 \end{bmatrix}^T \bar{P}_i + \bar{P}_i \begin{bmatrix} A_i^T & a_i \\ 0 & 0 \end{bmatrix} \right) \begin{bmatrix} x \\ 1 \end{bmatrix} < 0 \quad \text{for } x \in X_i \setminus \{0\}$$

Then every trajectory $x(t) \in \bigcup X_i$ satisfying (1.1) with $u = 0$ for all $t > 0$ tends to zero exponentially. □

Also these inequality conditions can be converted to LMIs, using the S-procedure. By parameterizing the Lyapunov functions with respect to the cell boundaries, continuity at the switching hyperplanes can be imposed.

If the input signal of the system is different from 0, the equilibrium will be moved from the origin. To determine the stability properties of this equilibrium point, a new analysis is needed. That is, the analysis of the system for one input signal will, in general, not give enough information about the system behavior if the input signal is changed. Moreover, it is also interesting to characterize the system behavior when the input signal is time varying.

Trajectory Following

Behavior of trajectories for piecewise linear systems in presence of an input signal, is an important issue from a control theoretic point of view. Most analysis results on piecewise linear systems are oriented towards stability of the origin for the unforced system [DeCarlo *et al.*, 2000; Hassibi and Boyd, 1998; Johansson and Rantzer, 1998]. The convergence of trajectories of the *unforced piecewise linear system* as defined in [Johansson and Rantzer, 1998] is not sufficient in general, to guarantee good behavior when input signals are applied to the system. Even if the unforced system is proved to be *stable*, applying an input might change the equilibrium point in such a way that the system behavior becomes unsatisfactory. Moreover, the time varying nature of the input signal can easily lead to an unacceptable behavior of the system.

The so called servo problem studies the behavior of the system trajectory with respect to time varying reference signal. It gives information about the convergence of the system trajectory when disturbed by a time varying input signal (see Figure 1.7).

One way to approach this problem is by looking at the input-output stability of the system. In case of $\mathcal{L}_2$ analysis, one is interested in a finite γ such that

$$\int_0^T |x|^2 \mathrm{dt} \leq \gamma^2 \int_0^T |r|^2 \mathrm{dt}$$

This relation gives a good idea about the behavior of the system trajectory for some time varying input signal. Nevertheless, it does not give

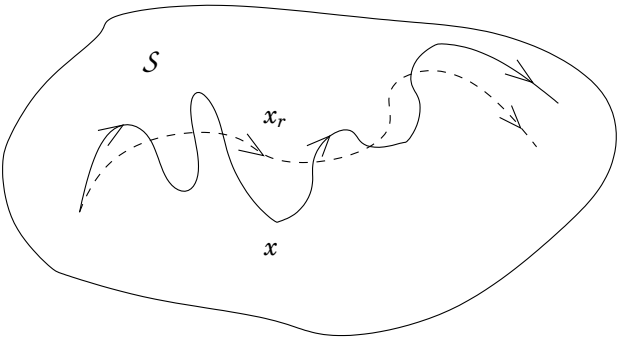

Figure 1.7 The servo problem studies the system trajectory x with respect to some time varying reference signal r. In this work, a particular reference trajectory is used to describe the system behavior. The reference trajectory is defined such that each constant reference value r corresponds to an equilibrium point x_r. Thus, for a slowly varying r the distance between x and x_r should be small. This way, the system behavior for time varying reference signals can be analyzed by characterizing the distance between x and x_r. Moreover it is desirable to distinguish the influence of the variations in the reference signal r.

direct information about the behavior of the system trajectory with respect to the variations of the reference signal.

Consider now a trajectory x_r that is defined such that each x_r is the value at rest of the system trajectory x corresponding to a constant reference signal r. Then an inequality of the form:

$$\int_0^T |x - x_r|^2 \mathrm{dt} \leq \gamma^2 \int_0^T |\dot{r}|^2 \mathrm{dt}\,.$$

describes how a disturbance in form of variations in r, will affect the system trajectory in comparison to its value at rest. Note that this relation gives information also about the input-output stability of the system.

Chapter 4 presents a method to solve the problem above. Computing the $\mathcal{L}_2$ gain from the derivative of the input signal $(\dot{r})$ to the "distance" between system trajectory (x) and reference trajectory (x_r), one obtains information relating the convergence of the system trajectories.

Chapter 4 is based on the results in [Solyom and Rantzer, 2002; Solyom, 2003]. The contribution of this work is to give a quantitative bound on the neighborhood of the equilibria when the variation of the parameter is a continuous function. For piecewise linear systems, a computational method using Linear Matrix Inequalities is proposed.

One possible application of this theory is in the field of anti-windup compensation. This will be addressed in the following.

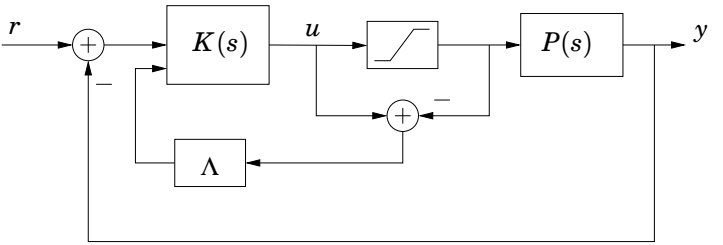

Figure 1.8 The considered anti-windup scheme. Λ represents a block of static compensators.

Anti-Windup Compensation

All real world control systems must deal with actuator saturation. This give rise to interesting control challenges. As a result of actuator saturation the plant input will be different from the controller output. When this happens the control loop is broken and the controller output does not drive the plant. Thus the states of the controller are updated incorrectly, resulting in serious performance deterioration [Kothare *et al.*, 1994].

Figure 1.8 shows the typical system setup. A linear plant with saturation-type limitations on the input, is controlled by a linear controller. When the actuator saturates, that is the system enters the affine region of operation, the control loop is broken. The regulator has no more control authority and the controller states will exhibit undesirable behavior.

A well-known and successful methodology to cope with this problem is anti-windup compensation or conditioning. This methodology gives rise to a compensator that during saturation improves the performance of the closed loop system. In Figure 1.8, the anti-windup compensator block is denoted by Λ. The input signal for this compensator block is zero as long as the system does not saturate. In case of saturation, its input signal becomes the difference between the desired and saturated control signal. It is customary to use linear filters as anti-windup compensators. Both static and dynamic compensators are reported in the literature.

In [Fertik and Ross, 1967; Teel and Kapoor, 1997] the problem of anti-windup compensation has been recognized as being that of returning the system to linear behavior. That is, return of the system output to the one that would have been without saturation. Thus it is clear that the anti-windup problem can naturally be posed as a servo problem for a nonlinear system. The goal is to return to the behavior of the linear system as well as possible. In this context, x_r can be viewed as a trajectory that describes the linear behavior of the system. Computing the $\mathcal{L}_2$ gain from the derivative of the input signal to $x - x_r$, gives a measure on the behavior of the

system trajectories with respect to x_r. Notice that the reference signal is smoothly time varying. Chapter 4 presents a method for designing static anti-windup compensators that fulfill the above mentioned criterion.

1.7 Voltage Collapse in Power Systems

Introduction

A power system consists of several electrical components (e.g. generators, transmission lines, loads) connected together, its purpose being transfer and usage of electrical power. Power systems are referred to as the largest machines built by man. Geographically they stretch over entire continents including hundreds of generators and millions of costumers.

An important feature of electrical energy is that it cannot be easily stored in large quantities. This basically means that at any instant in time the energy demand has to be met by corresponding generation. This suggests that keeping the balance between consumption and generation is a difficult problem.

In case of special events in the network, such as faults or unexpected increase of power demand, the balance between the generation and consumption can be disturbed. Such disturbances can have catastrophic consequences, such that major parts of the grid can be disabled. In the year 2003, several power blackouts occurred throughout the globe. A major blackout stroke on August 14 in the US. Over 60 MW of load and over 50 million people were affected. Geographically, it spread over eight states of the US and part of Ontario. The estimated costs of this power outage are between 4.5 – 8.2 billion dollars [Jones, 2004]. Such events are studied in the frame of power system stability and are of major concern in the power system community.

Voltage Stability in Power Systems

Due to the complexity of a power system, instabilities can be manifested in different ways. In general, *power system stability* can be defined as the property of the power system that enables it to remain in a state of equilibrium under normal operating conditions and to regain an acceptable state of equilibrium after being subject to a disturbance [Kundur, 1993].

The type of power system stability studied in this work is *voltage stability*. Voltage at the load end of a power system has to be controlled within prescribed tolerances to guarantee a satisfactory voltage for the consumers. Even in the case of normal operation, this task is not trivial due to the ever-changing load conditions. Moreover, in case of emergencies

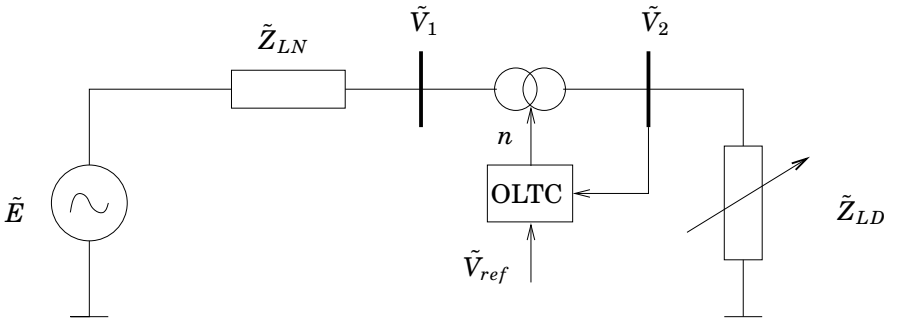

Figure 1.9 The considered two-node system with generator, transmission line, transformer and load.

this task can be very difficult and sometimes impossible.

Chapter 5 is based on the results in [Solyom *et al.*, 2004a; Solyom *et al.*, 2004b]. The power system considered in this work is shown in Figure 1.9. It is a radial system containing a generator E, a transmission line with impedance $\tilde{Z}_{LN}$, a transformer with an on-load tap changer (OLTC) and a load with impedance $\tilde{Z}_{LD}$. The system can be thought of as having two nodes, generation (i.e. the generator source) and consumption (i.e. the load). The on-load tap changer regulates the voltage on the load side at a desired value V_{ref}. In a power system, the loads have a built-in control system that tries to achieve some control objective. Usually this control objective is to keep the absorbed power at a given value. In turns this means that the load will dynamically change its impedance.

It is shown that this simple system exhibits the typical nonlinear behaviors that appear in a voltage collapse scenario. Furthermore, it is shown that also this system fits the framework of systems with limited capacity. The limited variable, in this case being the transferred power.

In Section 5.4 it is shown that in some scenarios, the stability of the power system can be maintained by dynamic compensation of the reference signal V_{ref}.

Furthermore, a complete compensation scheme is proposed that has load shedding as secondary control variable. This control scheme is shown to stabilize different power system models, at the same time it attempts to minimize the amount of disconnected load. The structure can be easily expanded, integrating additional control variables (e.g. capacitor banks).

1.8 Future Work

In the first part of this thesis a model based Anti-lock Braking System is presented. Simulation and test results are presented. In order to fully validate the proposed controller, more tests are needed, especially for low friction surfaces. Furthermore, in the control design only longitudinal slip has been considered. It is the belief of the author that the controller can be easily adapted for the cases when side-slip is present. Using the multi-model observer, the estimate of the maximum friction coefficient is obtained rather fast, although it is usually not precise. This information could be used also in a feedforward fashion to improve the transient response of the controller in case of changing road surfaces.

Chapter 3 of the thesis treats a synthesis procedure for PID controllers for a class of uncertain systems. It solves the problem for a cone bounded nonlinearity in feedback with a part of the plant. It is of interest to investigate the case when multiple cone bounded nonlinearities are present in the system.

Chapter 4 presents a result for analysis of piecewise linear systems. Behavior of system trajectory is analyzed with respect to some input signal. The theory has been used in the study of static anti-windup compensator. It would be of interest to explore the case when the anti-windup compensators are dynamic (having same order as the plant or with reduced order). In presented results, LMIs are used as computational tools. It would be of interest to study the results with a more flexible computational tool, such as the recently, increasingly popular sum of squares approach.

In Chapter 5 the voltage stability of power systems is analyzed. A simple model is used that describes a radial system. It is of significant importance how such system would interact if interconnected, moreover how the proposed solution will influence neighboring systems.

References

Åström, K. J. and T. Hägglund (1995): *PID Controllers: Theory, Design, and Tuning*. Instrument Society of America, Research Triangle Park, North Carolina.

Boyd, S., L. El Ghaoui, E. Feron, and V. Balakrishnan (1994): *Linear Matrix Inequalities in System and Control Theory*. SIAM.

Boyd, S. and Y. Q. (1989): "Structured and simultaneous Lyapunov functions for system stability problems." *International Journal of Control*, pp. 2215 – 2240.

DeCarlo, R. A., M. S. Branicky, S. Pettersson, and B. Lennartson (2000): "Perspectives and results on the stability and stabilizability of hybrid systems." In *Proceedings of IEEE*, pp. 1069 – 1082.

Fertik, H. A. and C. Ross (1967): "Direct digital control algorithm with anti-windup feature." *Instrument Society of America*, **10:1**.

Hassibi, A. and S. Boyd (1998): "Quadratic Stabilization and Control of Piecewise-Linear Systems." In *Proceedings of the American Control Conference*, pp. 3659 – 3664.

Ho, M.-T. (2001): "Synthesis of H_∞ PID controllers." In *Proceedins of the 40th Conference on Decision and Control*, pp. 255–260.

Ingimundarson, A. and S. Solyom (2003): "On a synthesis method for robust PID controllers for a class of uncertainties." In *Proceedings of the European Control Conference, ECC03*. Cambridge, UK.

Johansson, M. (1999): *Piecewise Linear Control Systems*. PhD thesis ISRN LUTFD2/TFRT--1052--SE, Department of Automatic Control, Lund Institute of Technology, Sweden.

Johansson, M. and A. Rantzer (1998): "Computation of piecewise quadratic Lyapunov functions for hybrid systems." *IEEE Transactions on Automatic Control*, **43:4**, pp. 555 –559.

Jones, L. (2004): "Tvärteknik 2004, Solvina - Göteborg." – Conference preprints.

Jurgen, R. K. (1999): *Electronic Braking, Traction and Stability Controls – Safer stopping and going via electronics*. Society of Autmotive Engineers, Inc.

Khalil, H. K. (1992): *Nonlinear Systems*. MacMillan, New York.

Kothare, M. V., P. J. Campo, M. Morari, and C. N. Nett (1994): "A unified framework for the study of anti-windup designs." *Automatica*, **30:12**, pp. 1869–1883.

Kundur, P. (1993): *Power System Stability and Control*. McGraw-Hill, Inc.

Panagopoulos, H. (2000): *PID Control, Design, Extension, Application*. PhD thesis, Lund Institute of Technology, Department of Automatic Control.

Solyom, S. (2003): "A synthesis method for static anti-windup compensators." In *Proceedings of the European Control Conference, ECC03*. Cambridge, UK.

Solyom, S. and A. Ingimundarson (2002): "A synthesis method for robust PID controllers for a class of uncertain systems." *Asian Journal of Control*, **4:4**, pp. 381–387.

Solyom, S., J. Kalkkuhl, and Rantzer (2002): "A benchmark for control of Anti-lock Braking Systems." http://www.control.lth.se/H2C.

Solyom, S., B. Lincoln, and A. Rantzer (2004a): "A novel method for voltage stability control in power systems." In *Proceedings of the World Automation Congress*.

Solyom, S., B. Lincoln, and A. Rantzer (2004b): "Power systems." In *Patent application nr. 040031-8, Svenska Patentverket*.

Solyom, S. and A. Rantzer (2002): "The servo problem for piecewise linear systems." In *Proceedings of the Fifteenth International Symposium on Mathematical Theory of Networks and Systems*. Notre Dame, IN.

Solyom, S. and A. Rantzer (2003): "ABS control - a design model and control structure." In *Nonlinear and Hybrid Systems in Automotive Control*, pp. 85–96. Springer Verlag.

Solyom, S., A. Rantzer, and J. Lüdemann (2004): "Synthesis of a model-based tire slip controller." *Vehicle System Dynamics*, **41:6**, pp. 477–511.

Teel, A. R. and N. Kapoor (1997): "The $\mathcal{L}_2$ anti-windup problem: Its definition and solution." In *Proceedings of the European Control Conference*.

2

Synthesis of a Model-Based Tire Slip Controller

2.1 Introduction

The Anti-lock Braking System (ABS) is an important component of a complex steering system for the modern car. It is now available on most of the vehicles, enhancing their braking capabilities.

The early development of anti-lock system for vehicle brakes began in Europe in the mid 1920's [Buckman, 1998]. One of the first patents in Europe was issued in 1932 entitled "An Improved Safety Device for Preventing the Jamming of the Running Wheels of Automobiles when Braking". In the US the first patent was issued in 1936, named "Apparatus for Preventing Wheel Sliding". Contrary to the common belief, the first practical application of an anti-lock system to a vehicle was done to railroad trains and not to aircrafts. The first occurred around 1943, while the latter appeared in the late 1940's and early 1950's. In 1951 an anti-lock braking system for highway vehicles was presented. These early systems were mechanical systems and performed with varying degrees of efficiency, but they significantly improved vehicle steerability during braking. This ability of the early systems encouraged further development. In 1968 an optional equipment for Thunderbirds was a rear axle hydraulic ABS. The control algorithm of this system was implemented on analog computers with primarily discrete components, resulting in low reliability. In 1978, Mercedes-Benz offered anti-lock braking system as an optional equipment for its S-class vehicles. In the beginning of the 1980's the algorithms were migrated to micro-computers and ABS development started to progress strongly. By 1985, Mercedes, BMW and Audi introduced Bosch ABS systems. Meanwhile Ford introduced its first Teves systems. In the

late 1980's ABS systems were offered on many luxury and sports cars. Today, ABS systems can be found on most of the vehicles, tending to be a standard equipment.

The main objective of most of these control system is prevention of wheel-lock while braking. This is important for two main reasons. First, to maintain steering ability of the car while hard and emergency braking, enabling obstacle avoidance in such situations. Second, to decrease the braking distance in case of an emergency braking. The later is due to the fact that the maximum friction between the road and the tires is, in most of the cases, achieved when the wheel is still rotating and not when it is locked.

It turns out that this task is not trivial, one of the main reasons being the high amount of uncertainty involved. Most uncertainty arises from the friction between the tires and the road surface. In addition, the tire-road characteristics is highly nonlinear, which burdens even further the control task.

The brake actuators play an important role in slip control, influencing the performance of the control system. Most of the ABS available on the market are making use of hydraulic actuators. These are simple hydraulic valves, usually with three-point-characteristics. In the new generation of ABS, electro-hydraulic actuators are used and in the next generation of brake-by-wire systems electro-mechanic actuators will be used. In a brake-by-wire system the drivers action on the brake pedal is converted into electrical signals that are transmitted via microcontrollers to the brake actuators. This way there is no hydraulic connection between the pedal and the actuators. The brake actuators used in these systems have the advantage of allowing continuous and more accurate adjustment of the brake force. These braking systems enable control of tire slip at arbitrary set-points which can be used to improve the driving characteristics of the vehicle. This means that to fully exploit the capabilities of such braking systems, there is a need for new high performance control systems. In particular, these controllers should be able to regulate the slip at different set-points. These reference values are to be specified by other systems, such as an Electronic Stabilization Program (ESP).

The key word for novel vehicle dynamics control systems is integration. Different levels, in a hierarchical structure of controllers with different functionalities are interacting in order to improve the driving characteristics of the vehicle. Such a high level integration and interaction is not possible without brake-by-wire technology. To fully use the capabilities offered by this technology, new analysis and synthesis approaches are to be developed.

This chapter is addressing the ABS system for a vehicle equipped with brake-by-wire technology. A novel model based control approach for slip

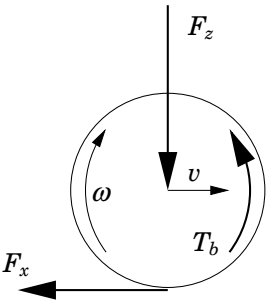

Figure 2.1 The quarter car consists of a single wheel attached to a mass.

control is proposed. A systematic synthesis method is proposed. The resulting controller is a hybrid nonlinear PI(D) controller. Tests have been carried out in a Mercedes E220 vehicle, provided by DaimlerChrysler, equipped with electro-mechanical brakes and brake-by-wire system.

2.2 Process Description

The easiest way to understand the underlying control problem is by looking at the so called quarter car model. This model consists of a single wheel attached to a mass, as shown in Figure 2.1.

The equations of motion of the quarter car during braking are:

$$\begin{aligned} J\dot{\omega} &= rF_x - T_b \\ m\dot{v} &= -F_x \end{aligned} \tag{2.1}$$

where:

m - mass of the quarter car

v - velocity over ground of the car

ω - angular velocity of the wheel

F_z - vertical force

F_x - tire friction force

T_b - brake torque

r - wheel radius

J - wheel inertia

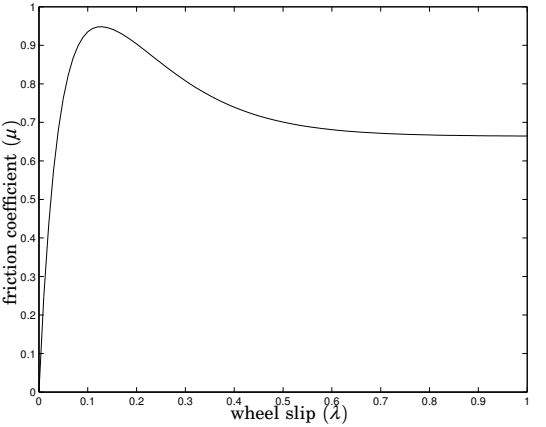

Figure 2.2 Typical tire friction curve. It describes the nonlinear dependence between the friction and the wheel slip.

The longitudinal tire slip is defined as:

$$\lambda = \frac{v - \omega r}{v} \tag{2.2}$$

hence, a locked wheel ($\omega = 0$) is described by $\lambda = 1$, while the free motion of the wheel ($\omega r = v$) is described by $\lambda = 0$.
The tire friction force, F_x, is determined by:

$$F_x = F_z \mu(\lambda, \mu_H, \alpha, F_z, v)$$

where $\mu(\lambda, \mu_H, \alpha, F_z)$ is the road-tire friction coefficient, a nonlinear function with a typical dependence on the slip shown in Figure 2.2 (μ_H denotes the maximum friction coefficient). The most common tire friction model used in the literature is the "Magic Formula" [Bakker *et al.*, 1989], or the Pacejka model. This model uses static maps to describe the dependence between slip and friction. In the literature, there are several dynamical friction models reported [Bliman *et al.*, 1995; Canudas de Wit and Tsiotras, 1999; Svendenius, 2003], that attempt to capture more accurately the transient behavior of the tire-road contact forces. However, in this work a Pacejka model will be used for simulations as well as design. This function depends also on the normal force (F_z), steering angle (α), road surface, tire characteristics and velocity of the car. For ease of writing in the following the arguments of μ will be dropped. Substituting (2.2) into

(2.1), the system becomes:

$$\begin{aligned} \dot{\lambda} v &= -\frac{F_z \mu}{J} r^2 - \frac{F_z \mu}{m}(1-\lambda) + \frac{r}{J} T_b \\ \dot{v} &= -\frac{F_z \mu}{m} \end{aligned} \tag{2.3}$$

This is a nonlinear differential equation where the parameters v, μ are time varying. Notice that the slip dynamics is scaled by the inverse of the velocity over ground of the vehicle. This will have an important effect on the control performance.

As mentioned before, the tire-road friction coefficient is itself a nonlinear function. Depending on the road condition and the tire characteristics, the peek of the friction curve will be more or less pronounced and the value of the maximum friction coefficient (μ_H) will be different. To the left of the peak the tire slip dynamics is stable. While on the right of the peak, where the slope of the curve is negative, the slip dynamics becomes unstable. The easiest way to see this is by linearizing in operating points that are in the positive respectively negative slope regions of the curve. Another factor that is influencing the tire-road friction curve is the side-slip angle. In case of steering while free rolling, side slip together with a side force occur. This phenomenon is more pronounced in case of simultaneous braking and steering. In general, the larger the tire slip angle is the smaller the longitudinal friction will be. Naturally, this will lead to reduction of the braking force when braking in a curve and consequently will increase the braking distance.

Consider the tire friction curve shown in Figure 2.2 (this curve corresponds to a high friction surface, e.g. dry asphalt). Then by fixing the braking torque T_b, one can draw the phase plane of (2.3). Figure 2.3 shows the normalized vector field of (2.3) together with some simulated solutions. The thick dashed lines represent the slip coordinate of the two equilibrium points close to the peak of the tire friction curve. These equilibrium points are on different sides of the peak (see Figure 2.2)). One of them is a stable equilibrium point $(0.079, 0)$ while the other is unstable $(0.205, 0)$. The position of these points (for a fixed curve) depends on the braking torque (T_b). It can be seen from the phase-plot that the velocity over ground dynamics is much slower than the slip dynamics. Furthermore, the slip dynamics is somewhat faster for low velocities than for high velocities. Figure 2.3 is drawn for fixed $T_b = 1300$ Nm, one can see the specific behavior of the slip dynamics, namely that for an initial slip higher than a given value (in this case 0.205), the slip dynamics becomes unstable. This would basically mean, that for a given constant braking torque $T_b = 1300$ Nm, if the point $\lambda = 0.205$ is passed, the wheel will lock.

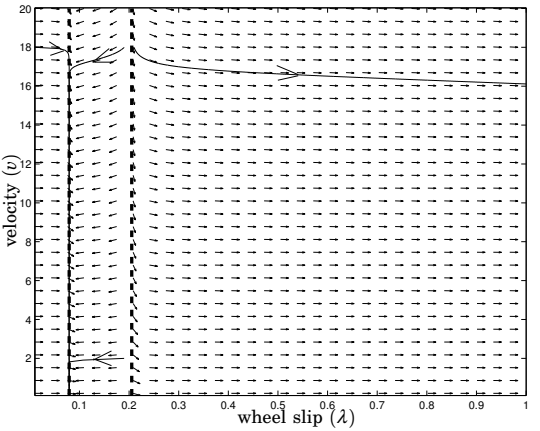

Figure 2.3 Phase plane for the quarter-car model with a fixed braking torque. There is one stable and one unstable equilibrium point indicated by the thick dashed lines.

Notice that this model is a quite simple description of the slip dynamics for a wheel. It does not capture pitching motion of the car body while braking, suspension dynamics, actuator dynamics, tire dynamics nor camber angle (in the above given model, the tire is consider perpendicular on the road surface).

2.3 Existing ABS Solutions

Most ABS controllers available on the market are table and relay-feedback based, making use of hydraulic actuators to deliver the braking force [Hattwig, 1993; Maier and Müller, 1995; Maisch *et al.*, 1993; Wellstead and Pettit, 1997].

The existing ABS control strategies can be divided, conceptually in two groups: wheel acceleration control and slip control. The first group of ABS uses the measured angular velocity of the wheels. This control strategy is regulating the slip indirectly by controlling the wheel deceleration/acceleration. It is used mainly for hydraulic brakes with three-point-characteristics. The idea is to measure the wheel rotational velocity and compute the wheel deceleration. Then, given some thresholds for the wheel deceleration and acceleration, the pressure is increased, held, or decreased preventing wheel lock during braking [Kiencke and Nielsen, 2000]. By appropriately selecting these thresholds, the slip will oscillate

around the "critical slip". This way, the friction force between the tires and the surface is close to its maximum value and the braking distance is minimized. This kind of algorithm will have as side-effect vibrations which are noticeable while braking. Todays production ABS are rule based control system, having exhaustive tables for different braking scenarios. These controllers are tuned in trial and error manner, using simulations and exhaustive field testing. The level of complexity they reach is a serious limitation for the analysis and further development of this kind of ABS.

These difficulties naturally lead to model based approaches where the parameters have physical meaning. An immediate advantage for the model based controllers is that they are easier to migrate to different vehicles. In the literature several such approaches are reported. In the following some of these results are presented.

In [Drakunov *et al.*, 1995] a model based approach is presented for hydraulic brakes. Here the maximum friction point is reached measuring the angular velocity of the wheel and the brake pressure. This approach uses sliding mode to reach and track the maximum friction during emergency braking. In [Liu and Sun, 1998], feedback linearization is used to design a slip controller and gain scheduling to handle variation with speed of the tire friction curve.

Most of the ABS control systems, including production ABS do not aim for control of tire slip at a given set-point, but they maximize the friction force between the tire and the surface by finding the peak of the friction curve. In the latest generation of brake-by-wire systems electro-mechanic actuators are used, which are capable of delivering continuously varying and different brake force on each of the four wheels. Set-point slip is supposed to be provided by a higher level in the hierarchy, such as an ESP system, and can be used for stabilizing the steering dynamics of the car while braking. This way the control objective shifts to maintain a specified tire slip for each of the four wheels. This might imply different reference values for the slip of each wheel. In [Johansen *et al.*, 2001], two model based hybrid approaches are presented. These controllers have been tested on the same vehicle as the one used in this thesis. One of the controllers is a Lyapunov function based adaptive controller. It is using Sontag's universal formula to obtain an optimal stabilizing control law. Independently of the set-point slip, the controller also returns an estimate of the maximum friction coefficient resulting from the adaptation. The other approach presented in [Johansen *et al.*, 2001] is a constrained LQ controller. To make it applicable for such fast processes, it does not rely on real-time optimization, but it evaluates the explicit solution to a suboptimal LQ problem. The controller is shown to be a piecewise linear controller. Additional gain-scheduling on tire slip and velocity is used. Test results for both approaches will be shown later, in comparison with

Figure 2.4 The $\mathcal{H}^2\mathcal{C}$ test vehicle. It is a modified Mercedes E220 passenger vehicle, fitted with an advanced brake-by-wire system and four state of the art electro-mechanical disc brakes.

results for the solution proposed in this thesis.

In [Jiang, 2000], different controllers have been proposed: a PID, a robust controller resulting from loop-shaping, and a nonlinear PID controller. In the latter the nonlinearity is a function that returns high gains for low errors and low gains for high errors. Simulation results are presented for a heavy vehicle.

2.4 The Test Vehicle

The test vehicle was a specially equipped Mercedes E220 passenger vehicle (see Figure 2.4). This vehicle was provided by DaimlerChrysler and it was used as test vehicle in the EU – Esprit project Heterogeneous Hybrid Control ($\mathcal{H}^2\mathcal{C}$). It was equipped with an advanced brake-by-wire system and four state of the art electro-mechanical disc brakes.

In addition, it was fitted with the following sensors:

- four wheel speed sensors,
- two accelerometers for longitudinal and lateral acceleration respectively,
- sensors for the position of the brake pedal and the force applied to the brake pedal,
- a sensor for the steering wheel angle,

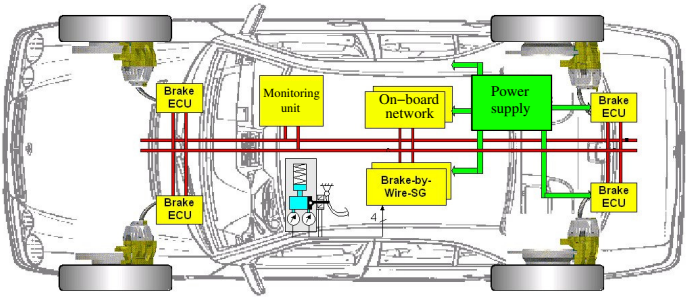

Figure 2.5 Test vehicle hardware architecture. It consists of four individually controlled electromechanical brakes, brake-by-wire control unit and a power supply unit. The control systems communicate on a TTP bus.

- a yaw rate sensor,
- hall sensors for measuring the clamping forces at each brake.

The ABS controllers are components of a complex brake-by-wire system. Figure 2.5 shows a block diagram of the hardware architecture of the test vehicle. It consists of four servo controllers for the brakes, a monitoring unit, a brake-by-wire control unit, and a power supply unit.

The electro-mechanical disc brakes are servo controlled by PID controllers. The brake-by-wire software, among other functions, gives access to sensor signals and command signals provided by the ABS controllers. The modules in the above shown architecture communicate on a synchronous TTP bus. This is advantageous from control point of view, in the sense that the time delay of the system is fixed.

2.5 The Control Problem

The control objective is, as mentioned above, to follow a reference trajectory for the tire slip on each of the four wheels while braking. The specifications include the following requirements [Kalkkuhl, 2001]:

- no wheel lock allowed to occur for speeds above 4 m/s
- wheel lock for a period of less than 0.2 seconds is allowed for speeds in the range of $0.8 \ldots 4$ m/s
- for speeds below 0.8 m/s the wheels are allowed to lock

- the control system should be robust with respect to other unmodeled dynamics:
  - actuator dynamics
  - suspension dynamics
- the control system should be robust to an additional time delay of 7 milliseconds due to communication

One of the most important signals in slip control is the velocity of the vehicle (v). This signal is not measurable and it has to be estimated. The measured signal that is used to obtain the velocity of the vehicle is the angular velocity of the wheels and an the output of an acceleration sensor.

In the same manner, any information about the tire friction curve has to be estimated. This later task can be challenging since the road surface conditions can change rapidly (e.g. a wet spot on a dry surface) and the estimate should converge rapidly inspite of the uncertain environment.

Thus already at this point, some of the robustness requirements can be identified due to:

- the feedback signal (λ) is not measurable but results from estimation and the quality of the signal is rather poor,
- time delay due to sampling and communication,
- high uncertainty in the tire-friction curve, especially in the nonlinear region.

In other words it is to avoid controllers with high gains, while robustness against modeling error has to be maintained (resulting especially from the friction curve). On the other hand fast response time is imperative, that is obviously contradictory to the above mentioned robustness requirements.

Thus, to have good control performance it is important to have precise estimate of the velocity of the car, a good estimate of the surface conditions and a not too long time delay in the control system. Naturally, the brake-actuator performance is also important. However, this work is focused on brake-by-wire systems equipped with electromechanical brakes, which guarantee high performance such that their limitations are not essential for the control system.

Another aim in the synthesis was to obtain a controller that is relatively easy to tune in the test vehicle and can easily be ported onto other vehicles.

As pointed out in the previous section, the proposed controller is model based, therefore, the quarter car model is a natural point to start with.

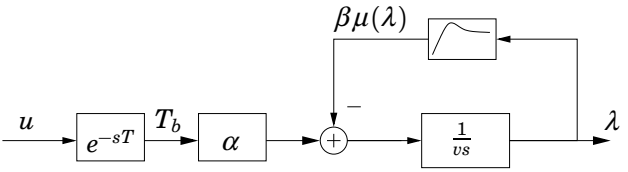

Figure 2.6 Proposed design model for an ABS. The nonlinearity is in feed-back with an integrator scaled by the linear velocity. Note that the system can have two equilibrium points. The one to the left of the peak of the friction curve is stable while the one to the right is unstable.

2.6 Proposed Design Model

From the equations of motion for the quarter car, taking into account that the velocity of the car varies much slower than the other variables involved, one obtains the dynamics of the tire slip:

$$\dot{\lambda} v = -\frac{r^2 F_z}{J}\mu + \frac{r}{J}T_b \tag{2.4}$$

Relation (2.4) is a first order nonlinear differential equation due to the tire friction coefficient function. Denoting $\beta \stackrel{\Delta}{=} r^2 F_z/J$, $\alpha \stackrel{\Delta}{=} r/J$ and adding a time delay T, the proposed design model (see Figure 2.6) can be synthesized in the following:

$$\dot{\lambda}(t) v = -\beta\mu(\lambda(t)) + \alpha u(t-T) \tag{2.5}$$

where v is considered constant but uncertain.

This model captures the main control difficulties of an anti-lock braking system. Notice that in addition to those pointed out at the beginning of this section, velocity dependence of the system is also included.

If the model (2.5) is linearized around an operating point, the resulting model is of the form:

$$\dot{\lambda}(t) v = -\beta(m_i \lambda(t) + \Psi) + \alpha u(t-T) \tag{2.6}$$

where m_i is the slope of the tire-friction curve at the considered operating point. Locally the slip dynamics is given by a first order system, stable or unstable depending on the sign of the slope m_i.

Fundamental Limitations

If the slope m_i resulting from the linearization is negative, one obtains locally an unstable system which in conjuncture with a time delay will give rise to fundamental limitations in control performance [Åström, 1997]. In the following a local analysis of the system in the mentioned situation will be carried out. Consider that there are no other unstable nor non-minimum phase dynamics in the system. Then the unstable pole is:

$$p = \beta \frac{|m_i|}{v}$$

with $m_i < 0$. According to rules of thumb in [Åström, 1997], satisfactory control performance with a phase margin $\varphi_m = \pi/4$ requires

$$pT \leq 0.3$$

where T is the time delay, and the resulting crossover frequency is:

$$\omega_c = p\sqrt{\frac{2}{pT} - 1}$$

Typical process parameters for a passanger vehicle are $\beta \approx 440$, a time delay of $T = 14$ ms, and a friction curve with local negative slope of -0.5 (that is a deflection from horizontal of -26^o). Satisfactory control performance can then be obtained until a velocity over ground is not less than $v = 10$ m/s. For a local negative slope of -0.05 (that is a deflection of approximately -3^o) the same performance can be obtained up to a velocity over ground not less than $v = 1$ m/s. The crossover frequency where this performance can be achieved is $\omega_c \approx 50$ rad/s.

Thus the time delay plays an important role in the investigated system.

2.7 Proposed Control Structure

As mentioned previously, many of the important signals used in the control unit are not directly measurable. The resulting control structure is of the form shown in Figure 2.7. The estimated variables are the tire slip (λ), velocity of the car (v) and the maximum friction coefficient (μ_H). In the design procedure these variables are considered to be measurable, i.e. no dynamics of the estimators are taken into account. This work is focused on the slip control loop based on given estimates of velocity and friction.

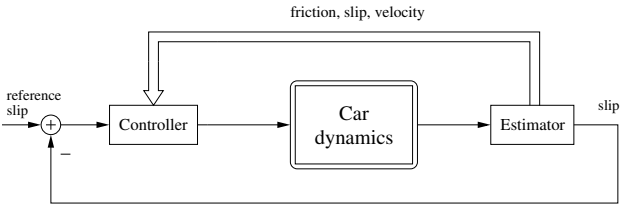

Figure 2.7 ABS control structure. The proposed controller is using information about friction, wheel slip, and linear velocity which are obtained through estimation.

Due to braking the car body will exhibit a pitching motion so there is a difference between the front and back wheels behavior. On the other hand, due to the position of the center of gravity of the car there is a difference between the left and right wheels even in case of straight line braking. In the design, only the simplified model (2.5) is be used. In this model none of the above mentioned phenomena are considered. The design is carried out based on the same model irrespective of the wheel location. Furthermore, no suspension dynamics are explicitly considered.

Estimation

The velocity of the car is estimated using information from the acceleration sensor and the wheel speed. An extended Kalman filter is used, that besides the velocity also estimates other states of the vehicle too. One of the estimated parameters is the maximum friction coefficient of the road (μ_H). However, the convergence of this estimate is too slow to be effectively used for control purposes. In [Kalkkuhl *et al.*, 2001] a multiple model observer structure is proposed. This hybrid observer can be used to obtain a fast estimate of the maximum friction coefficient for the slip curve. The idea is to construct a finite set of parallel observers, each being designed for a fixed parameter value of the nonlinear plant. Defining a performance index for each of the individual observers it is possible to quantify the parameter mismatch between each of these observers and the real plant. Then, a switching logic is used to select the observer with the best performance, this way obtaining an estimate for the unknown parameter. The transient behavior for the estimate of μ_H, is much faster than the one obtained from the extended Kalman filter. In the simulations and experiments in the test vehicle, an extended Kalman filter has been used to estimate the velocity v and the multiple model observer has been used to obtain an estimate of the maximum friction coefficient μ_H.

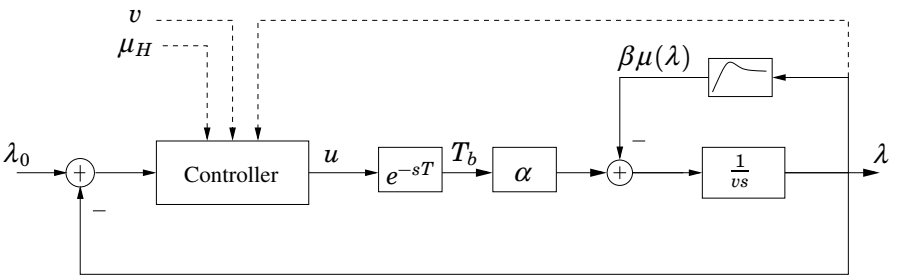

Figure 2.8 Block diagram for the proposed control scheme with the proposed design model. The controller uses a gain scheduling scheme based on the tire slip value λ, the velocity over ground v and the maximum friction coefficient μ_H.

Proposed Controller

The process is highly uncertain and nonlinear, mainly due to the tire friction characteristics. On the other hand, fast changes in operating conditions can appear (e.g. change in surface characteristics from wet to dry road-surface). An important limiting factor is time-delays due to sampling and communication.

In the following, a synthesis method is proposed that handles uncertainties induced mainly by the friction curve, while the system has to operate in a noisy environment. A simple static friction model is used. Based on this, we develop a gain-scheduled controller which switches between local controllers. The proposed control structure (Figure 2.8) is a gain scheduling scheme, based on the tire slip value λ, the velocity over ground (v) and the maximum friction coefficient μ_H (i.e. friction coefficient at the top of the friction curve).

The main idea behind the slip control design is to use a few local controllers that locally, robustly stabilize the system for different slopes of the friction curve and which tolerate the time variations due to the decreasing velocity over ground of the car (v). Switching between the local controllers is done according to the estimated friction and slip, which define the operating point on the friction curve.

Design of the Local Linear Controllers

Due to high uncertainty in the real process, it is natural to look for a simple robust controller which can easily be tuned in the test vehicle. Therefore, PI controllers are used and the gains are scheduled based on the three variables mentioned above.

Consider a linearized model as in (2.6). The bandwidth of this model

depends on v, i.e. the bandwidth is lower for high car velocities than for low car velocities. Therefore, it is natural to design the controller to counteract this variation. The controller is scaled by velocity (v) to ensure a higher gain for high velocities. In particular, when the system is operating at maximum friction, that is at the top of the friction curve, this scaling will theoretically remove the dependence on velocity over ground. The chosen local controllers are of the form:

$$u(t) = k\left(\lambda_0(t) - \lambda(t)\right)v(t) + \int k_i\left(\lambda_0(t) - \lambda(t)\right)v(t)dt \qquad (2.7)$$

and can be viewed as PI- controllers scaled by the velocity over ground.

As seen in (2.6), in stationarity the slip dynamics does not depend on v. Hence, in stationarity the control output should not be affected by the velocity scaling. This can be achieved by moving the velocity inside the integral, thus the integral term is kept constant as long as the slip error is zero. Also the gain k_i is inside the integral in order to obtain a smooth transition while switching between parameters [Åström and Hägglund, 1995].

Another important issue in ABS control is to prevent wheel-lock in case of changes in surface condition (e.g. a transition from dry to wet surface). Such a change will act as a load disturbance of magnitude $\beta(\Psi_1 - \Psi_2)/\alpha$ according to (2.6). Thus, it is important that the controller minimizes the effect of load disturbances on the system. On the other hand, as seen in relation (2.6), the slope of the approximating line (resulting from the linearization of the friction curve) affects the pole of the linear system. Furthermore this is scaled by the velocity as a consequence of (2.7).

The local control problem is to robustly stabilize the system while minimizing the effect of load a disturbance. The main uncertainty comes from one pole and the gain of the plant.

To synthesize a PI controller that minimizes the effect of load disturbances one can solve a constrained optimization problem as suggested in [Åström *et al.*, 1998]. To guarantee additional robustness against the uncertainty in the plant, it is possible to add a further inequality constraint based on the circle criterion as described in [Solyom and Ingimundarson, 2002; Ingimundarson and Solyom, 2003]. For improved accuracy, a model of the actuators was also introduced in the optimization.

PID controllers can be designed in the same way, with the arising design difficulties described in [Solyom and Ingimundarson, 2002]. The main potential advantage of using PID instead of PI controllers for the above described system is the ability to significantly increase the integral gain, while keeping the robustness constraints inactive. Simulations have been encouraging. More details about the design of the local controllers are given in Section 3.7.

The Scheduling

As described above, local robust controllers have been designed to handle different slopes on the friction curve at different velocities. By scheduling the gains k and k_i the controller can be adapted to the current operating mode/position on the estimated friction curve. In the results presented below, only two local PI controllers are used. Thus the resulting controller is a hybrid nonlinear PI respectively PID controller, abbreviated in the following as HPI and HPID.

The choice of two local controllers is based on the observation that usually there is a maximum on the friction curve, and to the left of this there is a positive slope region , while to the right of the top (tire slip values up to 0.5 are considered) there is a region with negative slope that tends to flatten out for higher slip values. Thus it is natural to have one of the scheduling variables depending on the slip value where the assumed maximum is located (λ_H). To the left of this, a controller is used which is tuned for relatively high positive slopes, while to the right a controller that can handle negative slopes is used.

The coordinate of the maximum, changes with the friction curve, thus a new scheduling variable is introduced, the maximum friction coefficient (μ_H) which is estimated. According to this a new λ_H is considered.

Due to the robustness of local designs, it is enough to use the same λ_H for a family of friction curves. This is a point where trade-off between robustness and performance will influence the complexity of the resulting controller.

This way, the scheduling scheme for the controller used in the simulations and experiments is the following:

If *low-friction* surface
- If *low slip*$_1$ use k_1, k_{i1}
- If *high slip*$_1$ use k_2, k_{i2}

If *high-friction* surface
- If *low slip*$_2$ use k_1, k_{i1}
- If *high slip*$_2$ use k_2, k_{i2}

Notice that the same parameters k, k_i are used for low and high friction surfaces, only the scheduling based on the tire slip is changing (λ_H). This is indicated by the subscripts 1 and 2 for the scheduling slip variable. Thus this controller has seven tunable parameters.

To have a fast response at the beginning of the braking action, an initial braking force is applied, by initializing the controller state at once as the ABS is switched on. In this way, fast response times are possible while the robustness of the controller is maintained.

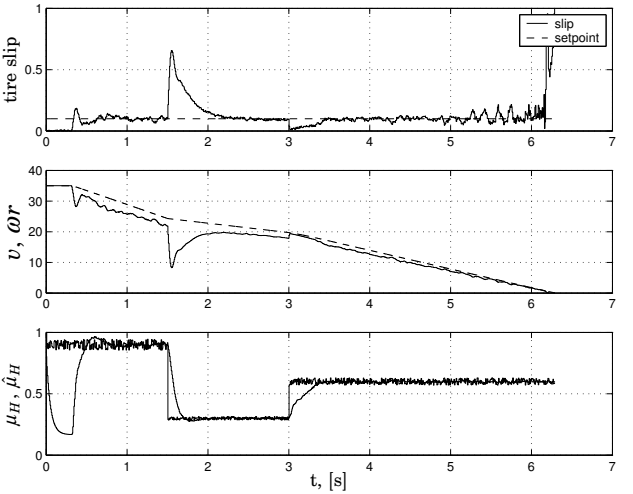

Figure 2.9 Simulation results for left front-wheel with a HPI controller. Controlled braking is initiated on a high friction surface, then surfaces with lower friction are encountered. The tire slip has to be controlled at a given set-point value.

2.8 Simulation and Experimental Results

Simulation Results

The simulator contains a four wheel model including pitch dynamics of the car body. This simulation environment has been written and provided by DaimlerChrysler. Ansi C has been used as programming language for the environment. The simulator also contains the estimators for μ_H and v, that is the Multi-Model Observer and the extended Kalman filter. The control software used in the simulator is designed such that it can be directly transferred onto the platform used in the test vehicle.

Figure 2.9 shows simulation results for the left front wheel during controled braking. Figures 2.14–2.16 in the Appendix show simulation results for the other wheels. As mentioned before, in the design procedure there is no information included regarding position of the wheel. That is, identical controllers are used on each of the four wheels. The first subplot shows the estimate of the controlled slip (λ) and its set-point. The second subplot shows the velocity of the car v (dashed line) and the linear velocity of the wheel ωr. The difference between these two is given by the tire slip scaled by the vehicles velocity v. The third subplot shows the estimate of the maximum friction, (denoted $\hat{\mu}_H$) and the maximum friction used in

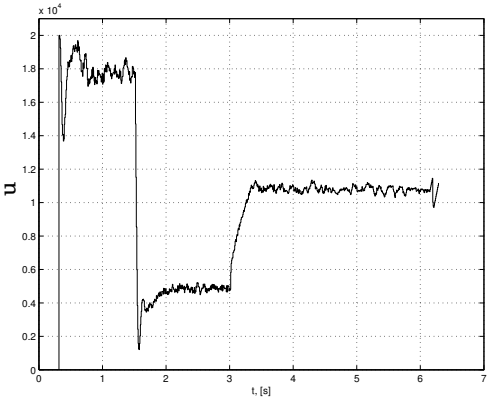

Figure 2.10 Control signal from the HPI controller on the left front-wheel in the simulation from Figure 2.9. Controlled braking is initiated on a high friction surface, then surfaces with lower friction are encountered. The braking torque is adjusted according to the surface conditions.

the simulation. Figure 2.10 shows the control signal during braking.

The plots show the tire slip control in a scenario where emergency braking is commenced on a high friction surface ($\mu_H = 0.9$) then a surface with low friction is encountered ($\mu_H = 0.3$) and finally the braking is finished on a high friction surface ($\mu_H = 0.6$). That means a scenario that would simulate braking on a dry surface with a wet or icy spot. Note the influence of the pitching dynamics which makes it harder to control the slip for the front wheel. The plot shows that in case of a change in the surface conditions, (transition from a high to a low-μ surface) the front wheels have a more pronounced tendency to lock than the rear wheels (see Figures 2.9 and 2.15). This phenomenon can be easily understood from (2.6). Pitching of the car body can be thought of as an increase of the mass acting on the front wheels, respectively decrease of the mass acting on the rear wheels. The mass is proportional to the term β in (2.6). A change in the surface characteristics, will act as a load disturbance on the system, as pointed out in the previous section. This load disturbance is proportional to β, which means that a change in the surface conditions will affect much more the front wheels than the back wheels. This is exactly the behavior noticed in the simulation results.

The same simulations have been performed using local PID controllers. The results are presented in Figures 2.17–2.20. It can be seen that the overall performance is better. In particular the influence of surface changes is significantly reduced.

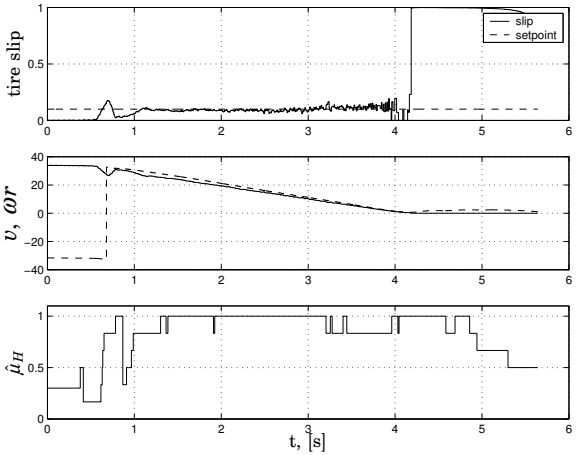

Figure 2.11 Experimental results for left front-wheel with HPI. Controlled braking is performed on dry asphalt. The tire slip has to be controlled at a given set-point value.

Experimental Results

The hybrid PI (HPI) controller has been tried out on the test vehicle with typical results as presented in Figure 2.11, and Figures 2.21 –2.23. Figure 2.11 presents the result for the left front-wheel. Here braking on dry surface with summer tires was tested. Summer tires present a prominent peek at the maximum friction coefficient, which will give rise to an unstable region for the slip dynamics.The third plot of the figure shows an estimate of the maximum tire friction coefficient, $\hat{\mu}_H$, obtained from the multi-model observer. Figure 2.12 shows the control signal during the experiment, for the left front-wheel. As shown in Figure 2.11, after an initial transient the slip is controlled very smoothly. It is to be noticed that for the back-wheels the performance is even better. The initial transient is not so pronounced.

In these tests the HPI controller had the best deceleration in comparison to the approaches in [Johansen *et al.*, 2001]. The braking distance for the HPI controller, from an initial velocity of 30 m/s was between $36-41$ meters, outperforming in this sense the controllers in [Johansen *et al.*, 2001] and the production ABS. A test result for the production ABS is shown in Figure 2.13. As mentioned before, the production ABS was not designed to track a reference slip trajectory, but to maximize the friction force. This explain the oscillatory behavior.

For the tests as well as the simulation a gain-scheduled controller

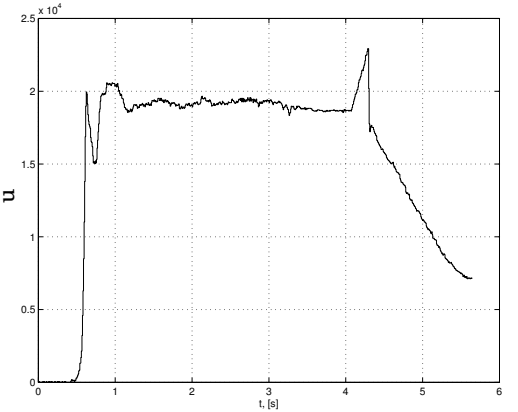

Figure 2.12 Control signal from the HPI controller on the left front-wheel in the tests from Figure 2.11. Controlled braking is initiated on dry asphalt. The braking torque is adjusted according to the surface condition.

has been used with two local controllers, one for the regions with high slopes in the tire-friction curve and one for regions with low slopes in the tire-friction curve. Hence for the HPI controller, seven parameters were tuned.

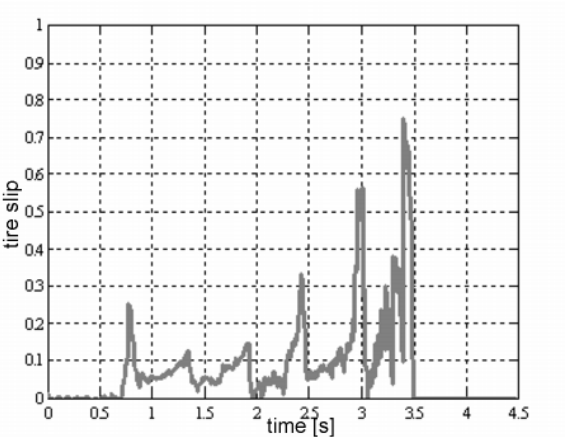

Figure 2.13 Test result for production ABS. Controlled braking is initiated on dry asphalt. The plot depicts slip versus time dependence. Notice the oscillatory behavior of the response, as the controller tries to maximize the friction force.

2.9 Conclusion

A simple but powerful design model for ABS control was presented. It was shown that this simple model captures the main control difficulties of the slip-control problem. Fundamental limitations on the control performance have been pointed out.

A gain-scheduled PI/PID design approach has been used for the controller. A controller with seven tunable parameters has been tested. The controller parameters have good, intuitive interpretations enabling a more straightforward tuning.

Simulations and experiments in a test vehicle were performed with satisfactory results proving the effectiveness of the proposed control scheme.

Appendix A – Additional Test and Simulation Results

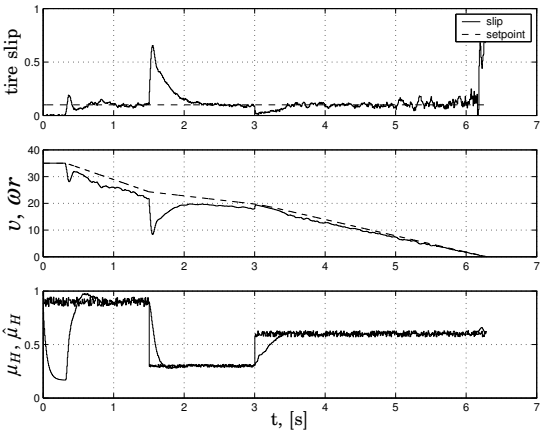

Figure 2.14 Simulation results for right front-wheel with HPI controller. Controlled braking is initiated on a high friction surface, then surfaces with lower friction are encountered. The tire slip has to be controlled at a given set-point value.

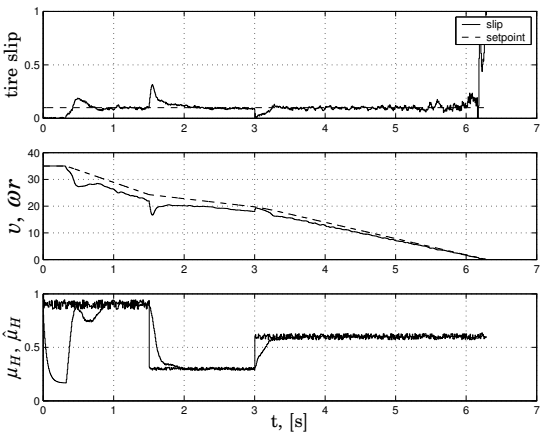

Figure 2.15 Simulation results for left back-wheel with HPI controller. Controlled braking is initiated on a high friction surface, then surfaces with lower friction are encountered. The tire slip has to be controlled at a given set-point value.

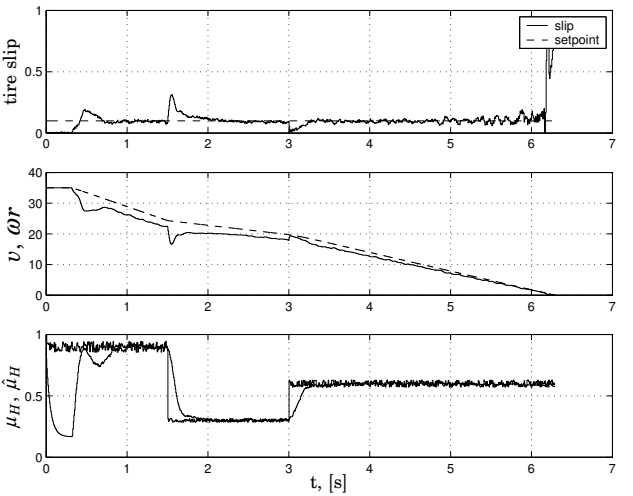

Figure 2.16 Simulation results for right back-wheel with HPI controller. Controlled braking is initiated on a high friction surface, then surfaces with lower friction are encountered. The tire slip has to be controlled at a given set-point value.

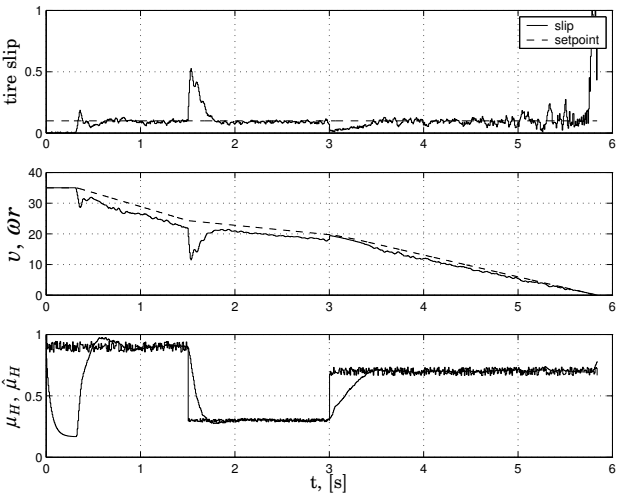

Figure 2.17 Simulation results for right front-wheel with HPID controller. Controlled braking is initiated on a high friction surface, then surfaces with lower friction are encountered. The tire slip has to be controlled at a given set-point value.

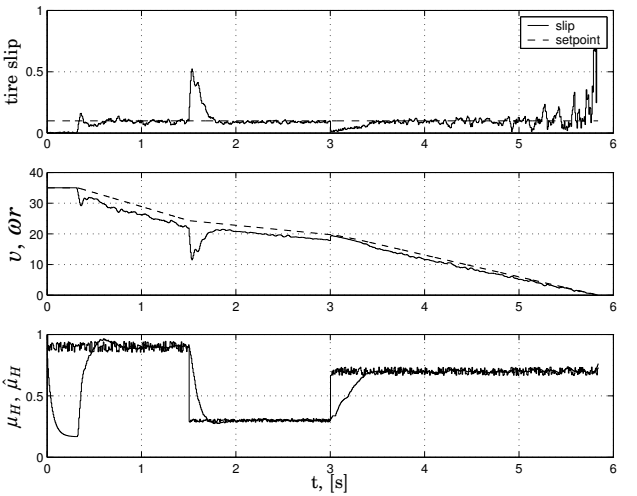

Figure 2.18 Simulation results for left front-wheel with HPID controller. Controlled braking is initiated on a high friction surface, then surfaces with lower friction are encountered. The tire slip has to be controlled at a given set-point value.

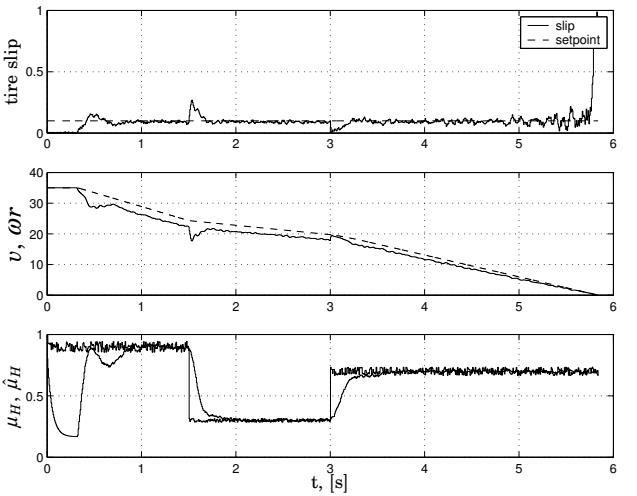

Figure 2.19 Simulation results for right back-wheel with HPID controller. Controlled braking is initiated on a high friction surface, then surfaces with lower friction are encountered. The tire slip has to be controlled at a given set-point value.

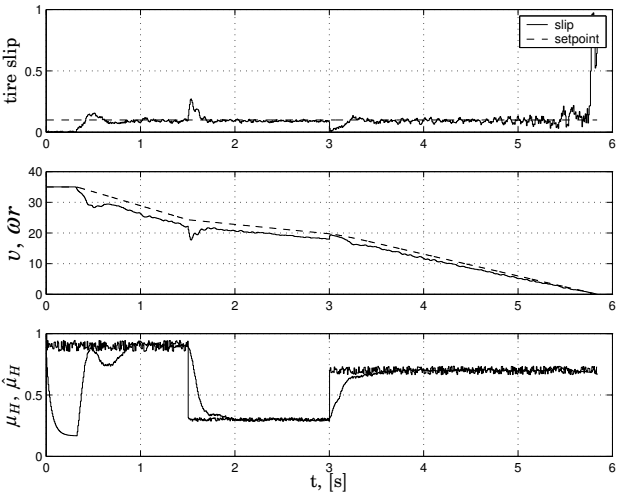

Figure 2.20 Simulation results for left back-wheel with HPID controller. Controlled braking is initiated on a high friction surface, then surfaces with lower friction are encountered. The tire slip has to be controlled at a given set-point value.

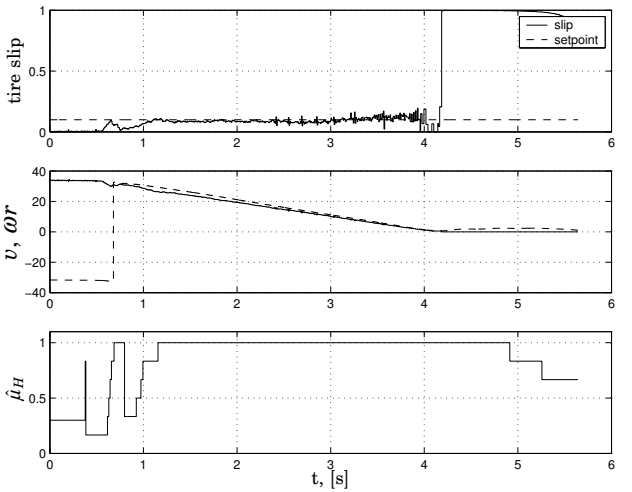

Figure 2.21 Experimental results for right front-wheel with HPI controller. Controlled braking is performed on dry asphalt. The tire slip has to be controlled at a given set-point value.

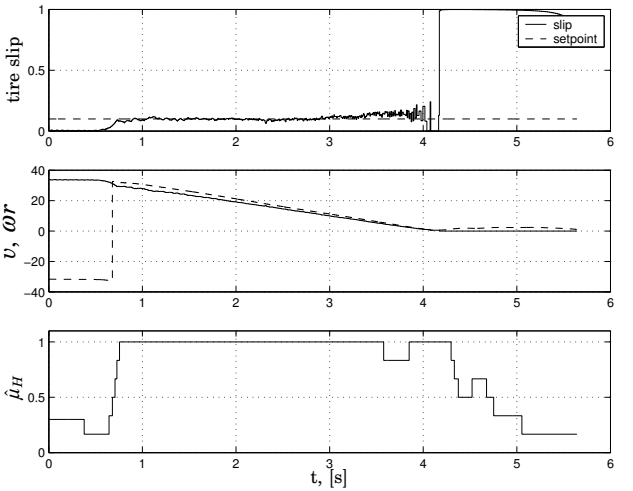

Figure 2.22 Experimental results for right back-wheel with HPI controller. Controlled braking is performed on dry asphalt. The tire slip has to be controlled at a given set-point value.

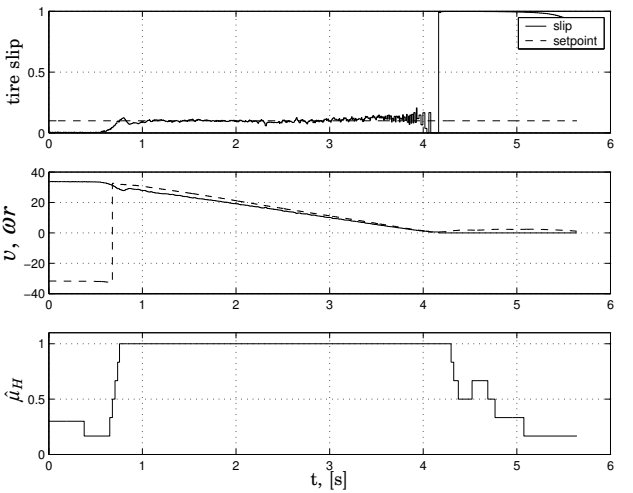

Figure 2.23 Experimental results for left back-wheel with HPI controller. Controlled braking is performed on dry asphalt. The tire slip has to be controlled at a given set-point value.

Appendix B – A Benchmark for Control of Anti-lock Braking Systems

The following is a simplified model of wheel dynamics subject to brake torque and ground contact forces.

$$\frac{d\omega(t)}{dt} = \alpha\mu\left(\lambda(t)\right) - \beta T_b(t-\tau)\mu_b(\omega(t)), \quad T_b \geq 0$$
$$\frac{dv(t)}{dt} = -\gamma\mu(\lambda(t))$$
$$\lambda(t) = \frac{v(t) - \omega(t)r}{v(t)}$$

where:

ω - angular velocity of the wheel

v - velocity over ground of the car

λ - longitudinal tire slip

T_b - brake torque. It is the input signal of the model.

μ - road-tire friction coefficient. Dependence on the longitudinal tire slip (λ) for four different surfaces is shown in Figure 2.24.

μ_b - friction coefficient in the brakes. This is used in the modeling of wheel lock. For simplicity use $\mu_b = \min(\omega/\varepsilon, 1)$, for some small $\varepsilon > 0$.

τ - time delay (an appropriate value is 14 milliseconds)

r - wheel radius (a suitable value for a passenger vehicle is 0.3 meters)

α, β, γ - positive constants, resulting from physical parameters of the vehicle (appropriate values for a passenger vehicle are respectively 1500, 1 and 10).

The following signals are available from the plant:

- ω - angular velocity of the wheel
- v - velocity over ground of the car
- μ_H - maximum road-tire friction coefficient

These are estimated or measured and available for feed-back in the control algorithm. In this benchmark, all of these signals can be considered as measurable.

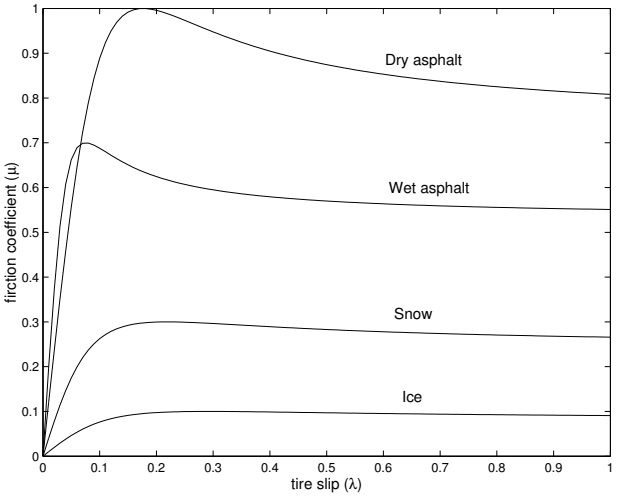

Figure 2.24 Tire friction curves

Specifications

The control objective is to maintain a desired tire slip level λ, by adjusting the brake torque (T_b). The ABS has to fulfill the following requirements [Solyom, 2002]:

- no wheel lock allowed to occur for speeds above 4 m/s
- wheel lock for a period of less than 0.2 seconds is allowed for speeds in the range of $0.8 \ldots 4$ m/s
- the control system should be robust with respect to other unmodeled dynamics, e.g. actuator dynamics. A reasonable model of the actuator dynamics, that can be used in the robust design is:

$$\frac{0.0091s + 3.9545}{0.0001s^2 + 0.0402s + 3.9545} .$$

It is of special importance that the above mentioned specifications are fulfilled in case of transition between different surface conditions while braking (e.g. transition from dry to wet surface).

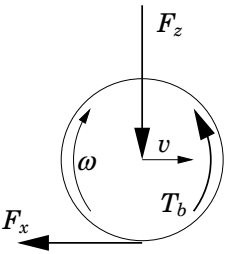

Figure 2.25 Quarter car. It consists of a mass attached to a wheel.

Comments on the Model

The benchmark model is derived from the well known quarter car model [Johansen *et al.*, 2001; Drakunov *et al.*, 1995]. This consists of a single wheel attached to a mass, as shown in Figure 2.25.

The benchmark describes the equations of motion of the quarter car in case of braking. The constants given in the model have the following physical interpretation:

$$\alpha = \frac{rF_z}{J}, \quad \beta = \frac{1}{J}, \quad \gamma = \frac{F_z}{m}$$

where,

m - mass of the quarter car

F_z - vertical force

r - wheel radius

J - wheel inertia

An additional time delay (τ) is added due to sampling and communication between the different modules of the system.

The longitudinal tire slip (λ) definition will imply that a locked wheel ($\omega = 0$) is described by $\lambda = 1$, while the free motion of the wheel ($\omega r = v$) is described by $\lambda = 0$.

The tire friction force, is given by $F_z\mu(\lambda, \mu_H, \alpha, F_z, v)$ where the term $\mu(\lambda, \mu_H, \alpha, F_z)$ is the road-tire friction coefficient. This is a nonlinear function with a typical dependence on the slip shown in Figure 2.24. The most common tire friction model used in the literature is the "Magic Formula" [Bakker *et al.*, 1989], or Pacejka model (other type of friction models can be found in [Bliman *et al.*, 1995; Canudas de Wit and Tsiotras, 1999; Svendenius, 2003]). This model uses static maps to describe dependence between slip and friction. This function depends also on the normal force

(F_z), steering angle (α), road surface (having different maximum values μ_H for different road conditions). For ease of writing, the model equations highlight only the dependence on the longitudinal tire slip (λ). In Figure 2.24 there are shown tire friction curves, generated by the Pacejka model, for four different kind of surfaces. The identification of such curves is not a trivial task. Some methods can be found in [Kalkkuhl *et al.*, 2001; Gustafsson, 1997].

Notice that this model contains a quite simple description of the slip dynamics for a wheel. It does not capture pitching motion of the car body while braking, suspension dynamics, actuator dynamics, tire dynamics nor camber angle (in the above given model, the tire is consider perpendicular on the road surface). However, it captures the major control challenges of the problem.

References

Åström, K. J. (1997): "Limitations on control system performance." In *European Control Conference*. Brussels, Belgium.

Åström, K. J. and T. Hägglund (1995): *PID Controllers: Theory, Design, and Tuning*. Instrument Society of America, Research Triangle Park, North Carolina.

Åström, K. J., H. Panagopoulos, and T. Hägglund (1998): "Design of PI controllers based on non-convex optimization." *Automatica*, **34:5**, pp. 585–601.

Bakker, E., H. B. Pacejka, and L. Lidner (1989): "A new tire model with application in vehicle dynamics studies." *SAE, 890087*.

Bliman, P. A., T. Bonald, and M. Sorine (1995): "Hysteresis Operators and Tire Friction Models: Application to vehicle simulation." In *Proceedings of ICIAM'95*.

Buckman, L. C. (1998): *Commercial Vehicle Braking Systems: Air Brakes, ABS and Beyond*. The 43rd L. Ray Buckendale Lecture. Society of Automotive Engineers, Inc.

Canudas de Wit, C. and P. Tsiotras (1999): "Dynamic Tire Friction Models." In *Proceedings of the IEEE Conference on Decision and Control*, pp. 3746–3751.

Drakunov, S., Ü. Özgüner, P. Dix, and B. Ashrafi (1995): "ABS control using optimum search via sliding mode." *IEEE Transactions on Control System Technology*, **3:1**, pp. 79–85.

Gustafsson, F. (1997): "Slip-based Tire-road Friction estimation." *Automatica*, **33:6**, pp. 1087– 1099.

Hattwig, P. (1993): "Synthesis of ABS hydraulic systems." *SAE, 930509*.

Ingimundarson, A. and S. Solyom (2003): "On a synthesis method for robust PID controllers for a class of uncertainties." In *Proceedings of the European Control Conference, ECC03*. Cambridge, UK.

Jiang, F. (2000): *A novel control approach to a class of Antilock Brake problems*. PhD thesis, Cleveland State University.

Johansen, T. A., J. Kalkkuhl, J. Lüdemann, and I. Petersen (2001): "Hybrid Control Strategies in ABS." In *Proceedings of the American Control Conference*.

Kalkkuhl, J. (2001): "Demonstrator Application Benchmark, Heterogeneous Hybrid Control: $\mathcal{H}^2\mathcal{C}$." Technical Report. DaimlerChrysler AG.

Kalkkuhl, J., T. A. Johansen, J. Lüdemann, and A. Queda (2001): "Nonlinear adaptive backstepping with estimator resetting using multiple observers." In *Proceedings of Hybrid Systems, Computation and Control, Rome*.

Kiencke, U. and L. Nielsen (2000): *Automotive Control Systems*. Springer Verlag.

Liu, Y. and J. Sun (1998): "Target slip tracking using gain-scheduling for braking systems." In *Proceedings of the American Control Conference*, pp. 1178–1182.

Maier, M. and K. Müller (1995): "ABS5.3: The new and compact ABS5 unit for passenger cars." *SAE, 930757*.

Maisch, W., W.-D. Jonner, R. Mergenthaler, and A. Sigi (1993): "ABS5 and ASR5: The new ABS/ASR family to optimize directional stability and traction." *SAE, 930505*.

Solyom, S. (2002): "Synthesis of a model-based tire slip controller." Technical Report Licentiate thesis LUTFD2/ TFRT--3228--SE. Department of Automatic Control, Lund Institute of Technology, Sweden.

Solyom, S. and A. Ingimundarson (2002): "A synthesis method for robust PID controllers for a class of uncertain systems." *Asian Journal of Control*, **4:4**, pp. 381–387.

Svendenius, J. (2003): "Tire models for use in braking applications." Technical Report Licentiate thesis ISRN LUTFD2/TFRT--3232--SE. Department of Automatic Control, Lund Institute of Technology, Sweden.

Wellstead, P. and N. Pettit (1997): "Analysis and redesign of an Anti-lock Brake System controller." *IEE Proceedings - Control Theory Appl.*, **144:5**, pp. 413–425.

3

A Synthesis Method for Robust PI(D) Controllers for a Class of Uncertainties

3.1 Introduction

Many optimal control synthesis methods result in controllers of order related to the order of the plant. However, it is desirable to design controllers with a restricted structure. Their performance can be often close to optimal performance while they remain substantially less complex.

The most common controller used today is the PID controller. Its popularity is mainly due to fact that despite of its simple structure, it provides some important functions such as: feedback, ability to eliminate steady state offsets through integral action, and can anticipate the future through derivative action [Åström and Hägglund, 1995].

This work presents a synthesis method for PID controllers in the case when a static nonlinearity is in feedback with the plant. For the PI case it is shown that the optimal controller can be easily found by visual inspection of constraints in the controller parameter space ($k - k_i$ plane). For the PID case, optimization routines are more suited for solving the problem.

The proposed synthesis method was succesfully applied to the tire slip control problem presented in Chapter 2.

3.2 Problem Statement and Previous Work

Robust PID control design has been considered by many authors. In the literature, there are several results on tuning methods of PID controllers with interval uncertainties in the plant [Ackermann and Kaesbauer, 2003; Ho *et al.*, 1998; Malan *et al.*, 1994]. These methods, essentially result in convex polygons in the parameter space of the controller, that robustly stabilize the considered plants. There have been reported results also on the parameterization of all stabilizing PID controller. In [Silva *et al.*, 2002] this is done for first order systems with time delays while in [Ho *et al.*, 1997] it is done for linear systems of any order. Both of these results are based on a generalization of the Hermite-Biehler Theorem for complex polynomials.

Also H_∞ synthesis of PID controllers has been reported [Ho, 2001]. The design procedure in this paper results in constraints in the controller parameter space. Similar approach can be found in [Saeki and Kimura, 1997] where graphical design method of robust PID controllers for three kinds of loop shaping problems and the H_∞ control problem is proposed. A CAD system for Matlab was also developed. The contribution of this paper in relation to the above mentioned articles is that the uncertainty is a cone bounded nonlinearity and the method is using the Circle Criterion to guarantee stability. The CAD system presented in the second article could be used as part of the synthesis procedure presented here.

The synthesis procedure presented in this chapter, is an extension to synthesis procedures presented in [Åström *et al.*, 1998; Panagopoulos *et al.*, 1999] which are collected in [Panagopoulos, 2000]. There, a design procedure for PI(D) controllers was presented which minimizes the effect of a load disturbance. This is achieved by maximizing the integral gain while making sure that the closed loop system is stable. Furthermore, it is guaranteed that the Nyquist curve of the loop transfer function is outside a circle with center $-C_s$ and radius R_s. This constraint can be expressed with the equations

$$\begin{array}{ll} \text{maximize} & k_i \\ \text{subject to} & l(k, k_i, k_d, \omega) \geq R_s^2 \qquad \forall \omega \geq 0 \end{array} \tag{3.1}$$

where l is the function:

$$l(k, k_i, k_d, \omega) = |C_s + C(i\omega)G(i\omega)|^2, \tag{3.2}$$

and $G(s)$ is a linear time invariant plant and $C(s)$ is the PID controller parameterized as

$$C(s) = k + \frac{k_i}{s} + k_d s \tag{3.3}$$

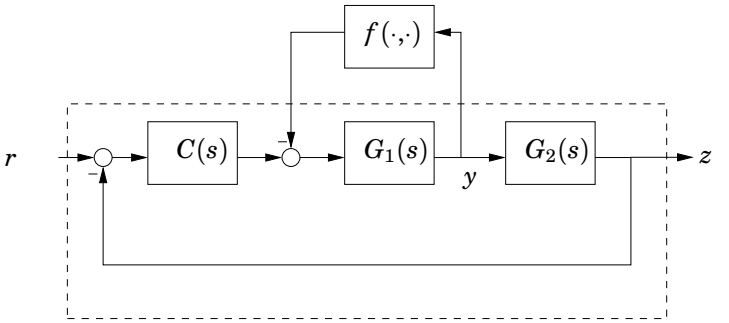

Figure 3.1 Block diagram showing nonlinearity, plant and controller.

By choosing $C_s = 1$ and R_s, the resulting controller will guarantee that the maximum of the sensitivity function equals $1/R_s$, i.e,:

$$\frac{1}{R_s} = \max_{\omega} |S(i\omega)|,$$

where $S(s) = 1/(1 + G(s)C(s))$. Controllers with constraints on the maximum complementary sensitivity function ($T(s) = 1 - S(s)$) could also be designed or a combination of these constraints. In the case of PID controllers, additional inequality constraints will be added regarding the curvature and phase change of $G(s)C(s)$.

In [Panagopoulos, 2000] the main design parameter was $M_s = 1/R_s$, with values typically between 1.4–2. The value of this parameter will influence the damping of the closed loop system. In the PID case, the above mentioned inequality constraints are supplemented. These will be reviewed later.

The extension presented in this chapter guarantees in addition asymptotic stability of the system when a cone bounded nonlinearity is present in feedback with part of the plant, as shown in Figure 3.1. Here, as well as in the rest of this chapter $C(s)$ represents the controller. The nonlinearity $f(\cdot,\cdot)$ is a memoryless, possibly time-varying nonlinearity within the cone given by $\alpha,\beta \in \mathbb{R}$, $\alpha < \beta$ and $\beta \neq 0$ (see Figure 3.2), that is:

$$\alpha y^2 \leq y f(y,t) \leq \beta y^2, \quad \forall y \in \mathbb{R}, \forall t \geq 0 \tag{3.4}$$

Furthermore, it is assumed that $f(y,t)$ is piecewise continuous in t and locally Lipschitz in y. The synthesis procedure is based on a frequency domain description of the system so it is easy to take into account dead time in the plant.

The synthesis procedure can be thought of as a nonlinear optimization problem with two families of constraints. One that ensures stability and performance for the closed loop system without the nonlinearity f, and another group of constraints that will guarantee stability of the closed loop system in presence of the nonlinearity f (as shown in Figure 3.1). From this point on the first family of constraints will be referred to as constraints for nominal performance, while the second group of constraints will be referred to as constraints for robust stability. Furthermore, it has to be mentioned that the constraints for nominal performance ensure robust stability against a cone-bounded nonlinearity in the control loop (see [Panagopoulos, 2000]).

The constraints for nominal performance can be considered those presented in [Panagopoulos, 2000]. This work will concentrate on the constraints for robust stability.

3.3 Sufficient Conditions for Stability

Consider the transfer functions $G(s)$ describing a linear plant. In feedback with a part of this plant, a cone bounded nonlinearity is present. Factorizing $G(s)$ as

$$G(s) = G_1(s)G_2(s), \tag{3.5}$$

the cone bounded nonlinearity is in feedback with $G_1(s)$, as shown in Figure 3.1. Consider the case with a PI controller first, i.e.:

$$C(s) = k + \frac{k_i}{s}. \tag{3.6}$$

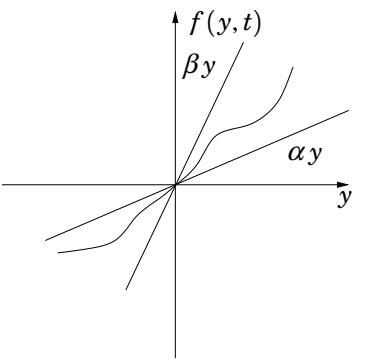

Figure 3.2 Sector bounded nonlinearity.

With $G(s)$, $G_1(s)$ and $G_2(s)$ as in (3.5) define

$$P(s) \stackrel{\Delta}{=} \frac{G_1(s)}{1 + C(s)G(s)} \tag{3.7}$$

Furthermore,

$$G(i\omega) = a(\omega) + ib(\omega) = r(\omega)e^{i\phi(\omega)} \tag{3.8}$$

and

$$G_1(i\omega) = a_1(\omega) + ib_1(\omega) = r_1(\omega)e^{i\phi_1(\omega)} \tag{3.9}$$

be the evaluations of the transfer functions $G(s)$ and $G_1(s)$ on the positive imaginary axis.

In the case that $P(s)$ is not strictly proper, the analysis involves additional test for the well posedness of the feedback connection. For simplicity, only the strictly proper case will be considered. Hence, a minimal realization of $P(s)$ is given by:

$$\begin{aligned} \dot{x} &= Ax + Bu \\ y &= Cx \end{aligned} \tag{3.10}$$

Then,

$$\begin{aligned} \dot{x} &= Ax - Bf(y,t) \\ y &= Cx \end{aligned} \tag{3.11}$$

describes the system in Figure 3.1 with $r = 0$.

First, some definitions will be quoted, that are necessary to state the main results.

Absolute stability [Khalil, 1992]: The system (3.11) is absolutely stable if the origin is globally uniformly asymptotically stable for any nonlinearity in the given sector. It is absolutely stable with a finite domain if the origin is uniformly asymptotically stable. □

Hurwitz transfer function [Khalil, 1992]: A transfer function $H(s)$ is Hurwitz, if all poles have negative real part. □

Positive real transfer function [Slotine and Li, 1991]: A transfer function $H(s)$ is positive real (PR) if

$$\mathrm{Re}\{H(s)\} \geq 0, \ \forall \, \mathrm{Re}\{s\} \geq 0.$$

It is said to be strictly positive real (SPR) if $H(s - \varepsilon)$ is positive real for some $\varepsilon > 0$. □

It is a well known result that a transfer function $H(s)$ is SPR if and only if $H(s)$ is Hurwitz and

$$\mathrm{Re}\{H(j\omega)\} > 0, \ \forall \omega \geq 0$$

Conditions for absolute stability of the system (3.11) can be obtained by applying the Circle Criterion, for the transfer function $P(s)$ as it is connected in a loop with the nonlinearity. Therefore the Circle Criterion for a scalar plant will be cited:

PROPOSITION 3.1—CIRCLE CRITERION [KHALIL, 1992]
Consider the system (3.11), where (A, B) is controllable, (A, C) is observable. $f(y,t)$ is locally Lipschitz in y, piecewise continuous in t and satisfies the sector condition (3.4) globally. Then, the system is absolutely stable if $A - \alpha BC$ is Hurwitz and

$$\frac{1+\beta P(s)}{1+\alpha P(s)}$$

is strictly positive real. □

In order to state the main results, some intermediary steps will be helpful.

LEMMA 3.1
Consider $P(s)$ as in (3.7) and $\alpha, \beta \in \mathbb{R}$. Then $\forall \omega \geq 0$

$$\mathrm{Re}\left\{\frac{1+\beta P(j\omega)}{1+\alpha P(j\omega)}\right\} > 0 \tag{3.12}$$

if and only if

$$r(\omega)^2 k^2 + p(\omega)k + \frac{r(\omega)^2}{\omega^2}k_i^2 + q(\omega)k_i + h(\omega) > 0 \tag{3.13}$$

with

$$\begin{aligned} p(\omega) &= (a(\omega)a_1(\omega) + b(\omega)b_1(\omega))(\alpha+\beta) + 2a(\omega) \\ q(\omega) &= \frac{1}{\omega}\left((a(\omega)b_1(\omega) - b(\omega)a_1(\omega))(\alpha+\beta) + 2b(\omega)\right) \\ h(\omega) &= (\alpha+\beta)a_1(\omega) + \alpha\beta r_1(\omega)^2 + 1 \end{aligned} \tag{3.14}$$

□

The proof of this lemma is based on elementary but tedious computations and it can be found in the Appendix of this chapter.

Lemma 3.1 states that since in the control structure (3.7) the controller $C(s)$ is a PI, the positivity constraint (3.12) can be checked in the parameter space of the controller, i.e. $k - k_i$ plane. The parametric curve in (3.13) is an ellipse in the $k - k_i$ plane, for a given frequency ω. This result is similar to those in [Åström *et al.*, 1998; Panagopoulos *et al.*, 1999; Saeki and Kimura, 1997].

Based on the Circle Criterion and the lemma above, the following theorem for absolute stability of system (3.11) can be stated:

THEOREM 3.1
Let A,B,C describe a minimal realisation of the system defined by (3.5)-(3.9). Consider $\alpha, \beta \in \mathbb{R}$ and a function $f(y,t)$ piecewise continuous in t and locally Lipschitz in y such that (3.4) holds.
If $A - \alpha BC$ is Hurwitz and (3.13) holds then the system of form (3.11) is absolutely stable.

□

Proof:
The circle criterion provides sufficient conditions for absolute stability of the system. The only condition left to prove is that $\frac{1+\beta P(s)}{1+\alpha P(s)}$ is SPR. All poles of $\frac{1+\beta P(s)}{1+\alpha P(s)}$ have strictly negative real part due to the fact that $A - \alpha BC$ is Hurwitz. By Lemma 3.1, $\forall \omega \geq 0$

$$\mathrm{Re}\left\{\frac{1+\beta P(j\omega)}{1+\alpha P(j\omega)}\right\} > 0$$

is equivalent to (3.13), and since $P(0) = 0$ the proof is complete. ◊

In many engineering applications it is of interest to look at other equilibrium points than the origin. This is natural since often the equilibrium point will change depending on the system input. Obviously any equilibrium point can be analyzed by shifting it to the origin. This would mean different tests for each equilibrium point. Therefore it is of special interest to derive a single test, that will give information about the stability of equilibrium points depending on the input signal. In this sense the following theorem gives a useful result.

THEOREM 3.2
Consider the system:

$$\begin{aligned} \dot{x} &= Ax - Bw + B_r r \\ w &= f(Cx) \end{aligned} \tag{3.15}$$

with A Hurwitz, (A,B), (A,C) controllable respectively observable pairs and f a continuous, memoryless scalar nonlinearity. Denote $P(s) = C(sI - A)^{-1}B$.
If there exist $\alpha, \beta \in \mathbb{R}$ such that

$$\alpha \leq \frac{f(y_1) - f(y_2)}{y_1 - y_2} \leq \beta, \quad \forall y_1, y_2 \in \mathbb{R}, \tag{3.16}$$

$$\mathrm{Re}\left\{\frac{1+\beta P(j\omega)}{1+\alpha P(j\omega)}\right\} > 0, \quad \forall \omega \geq 0 \tag{3.17}$$

and $A - \alpha BC$ is Hurwitz then every equilibrium point of (3.15) corresponding to some constant r, is a global uniformly asymptotically stable equilibrium point. □

Proof:
Consider the change of variable: $\xi = x - x_r$ with x_r given by

$$0 = Ax_r - Bf(Cx_r) + B_r r$$

for some constant r. If for a fixed r, the solution of the above equation exists, then it is unique. (see Lemma 3.2 in the Appendix)
Consider the system:

$$\dot{\xi} = A\xi - B\varphi(C\xi)$$

with the new nonlinearity $\varphi(C\xi) = f\left(C(\xi + x_r)\right) - f(Cx_r)$. According to (3.16) this is a cone bounded nonlinearity.
Using the circle criterion for this system, it can be concluded that $\xi = 0$ is a global uniformly asymptotically stable equilibrium point. Hence x_r is a global uniformly asymptotically stable equilibrium point of (3.15), for the considered $r \in \mathbb{R}$. ◊

Consider now the system defined by (3.5) - (3.9) in feedback with a nonlinearity f. This system is shown in Figure 3.1. The system equations are given by:

$$\begin{aligned} \dot{x} &= Ax - Bf(y) + B_r r \\ y &= Cx \\ z &= C_r x \end{aligned} \tag{3.18}$$

where (A, B), (A, C) are controllable respectively observable pairs and f is a continuous, memoryless scalar nonlinearity. This system has a special structure, in the sense that it uses a PI controller. The problem is to investigate the equilibrium points with respect to r. Hence, for the system (3.18) Theorem 3.2 can be applied. Since the controller is a PI, the positivity condition (3.17) can be checked, according to Lemma 3.1, in the parameter space of the controller ($k - k_i$ plane). Then the following proposition can summarize the result for the case of PI controllers.

PROPOSITION 3.2
Let A,B,C describe a minimal realization of the system defined by (3.5) - (3.9). If there exist $\alpha, \beta \in \mathbb{R}$ such that (3.13), (3.16) hold and $A - \alpha BC$ is Hurwitz then every equilibrium point of (3.18) corresponding some constant r, is a global uniformly asymptotically stable equilibrium point. □

Thus in the case of PI controllers, the constraints that guarantees nominal performance, robust stability as well as solution for the servo problem in case of a constant input can be easily drawn in the parameter space of the controller ($k - k_i$ plane). In this way the optimization problem of finding the maximum k_i such that these constraints hold can be solved by visual inspection.

Systems with time delays In most of the text books the Circle Criterion is proved for systems without time delays. By using the small gain theorem one can show that the theorem holds also for systems with time delays.

Nevertheless, for plants with time delays a slight modification of the above theorems is required. In case of infinite dimensional systems it is more convenient to use the transfer function description. This way, in the theorems one should check that $P(s)/(1+\alpha P(s))$ is assymptotically stable instead of $A-\alpha BC$ being Hurwitz and that $P(s)$ is asymptotically stable instead of A being Hurwitz.

3.4 Other Design Issues

PID controllers

In the case of PID controllers the synthesis procedure is similar to the PI case presented above. The above presented results hold with minor changes. The easiest way to migrate the results to the case of PID controllers is by replacing the parameter k_i with $k_i - \omega^2 k_d$. This way the parameter space becomes three dimensional (k, k_i, k_d) making the synthesis procedure more complex.

Furthermore, in the case of PID controllers it was found in [Panagopoulos, 2000] that the sensitivity constraint alone was not sufficient to guarantee a nice, well-damped response. Condition ensuring negative curvature of the loop gain and the monotonicity of the phase function of the loop gain were added to the optimization problem. In the case of integrating processes only the second condition is imposed.

Thus in contrary to the PI case, where the optimization problem could be easily solved by visual inspection, for the case of PID controllers a similar approach is significantly more difficult. Therefore an optimization routine is more adequate to solve this problem.

3.5 Optimization

Using the results presented in the previous section the synthesis problem can be stated as the following optimization problem.

$$\begin{aligned} \max \quad & k_i \\ \text{subject to} \quad & f(k, k_i, k_d, \omega_1) \geq R_s^2 \quad \forall \omega_1 \geq 0 && (3.19) \\ & g(k, k_i, k_d, \omega_2) \geq 0 \quad \forall \omega_2 \geq 0 && (3.20) \\ & k > 0, k_i > 0, k_d > 0 && (3.21) \end{aligned}$$

Constraint (3.21) guarantees that the controller will not have an unstable zero. The two frequency dependent inequalities define the exterior of two ellipses for a fixed frequency. For $0 \leq \omega < \infty$ these ellipses generate envelopes that define the boundaries of the set of parameters which satisfy the constraints.

The constraints can be visualized by plotting the ellipses for a tight griding of frequencies, enabling to visually identify the optimizer. This graphical approach is suitable when PI design is considered but is more difficult in case of PID controllers. However it is possible to plot the ellipses for a grid of k_d values. Here it is of more interest to have a numerical optimization procedure that can give the desired result. For most numerical optimization procedures it is important to have good starting values. The problem of finding good starting values is related to determining if the problem has any feasible solution. But a quick view of the constraints for a few values of k_d should be sufficient to obtain good starting values and to see if the problem is feasible.

Automating the synthesis procedure

So far the synthesis procedure that has been presented would need much manual intervention. It is of interest to automate the synthesis procedure so that only the process and the parameters characterizing the uncertainties would need to be specified. This is in principle to automate the checking of feasibility and finding a good start value for the numerical optimization procedure. For ideas about this issue see [Panagopoulos, 2000].

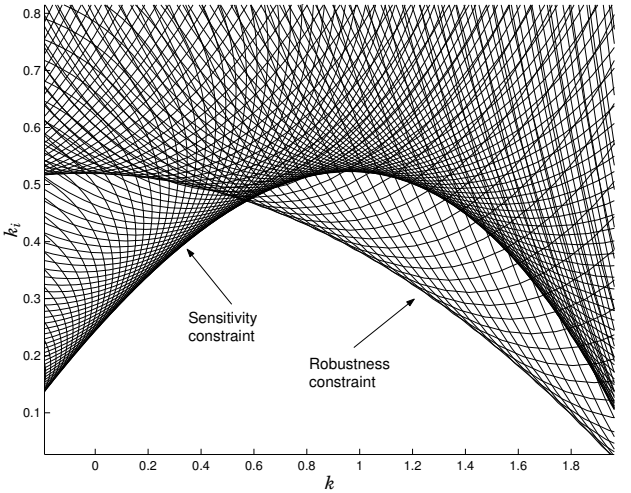

Figure 3.3 Constraints in the $k - k_i$ plane in Example 3.1.

3.6 Examples

Two examples of PI controller design will now be given followed by one example for PID design.

EXAMPLE 3.1
Consider the system in Figure 3.1 with

$$G_1(s) = \frac{1}{(s+1)^3} \qquad G_2(s) = 1$$

and a static, time varying nonlinearity $f(y_1, t) : \alpha \leq f(y,t)/y \leq \beta$ with $\alpha = 1,\ \beta = 4$. In particular if the cone bounded uncertainty would be an uncertain gain the transfer function would be given by

$$G(s) = \frac{1}{(s+1)^3 + \Delta}$$

where $\Delta \in [1, 4]$. The two constraints, equations (3.19) and (3.20), will give rise to constraint surfaces as shown in Figure 3.3. As seen in the figure, in this case, the optimizer considering the stability constraints for the linear system (in the figure indicated as "sensitivity constraint") will not guarantee stability of the nonlinear system with cone bounded uncertainty as considered above. The stability constraint for the nonlinear

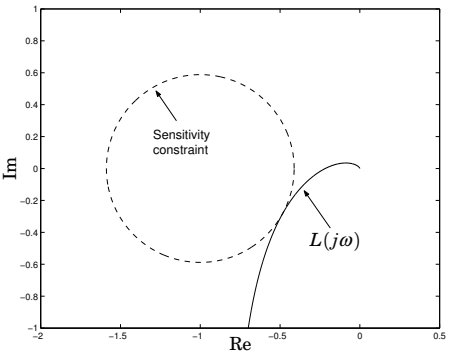

Figure 3.4 Nyquist plot of the loop transfer function $L(s)$ in Example 3.1.

system is indicated in the figure as "robustness constraint". Choosing the maximum k_i that falls below both constraint surfaces and a corresponding k, Theorem 3.1 guarantees absolute stability of the nonlinear system.

The Nyquist plots of the loop transfer function and the transfer function defined by equation (3.7), shown in the Figures 3.4 respectively 3.5, confirm that the constraints are not violated. In both cases the Nyquist plot is outside the constraint circle (dashed line). □

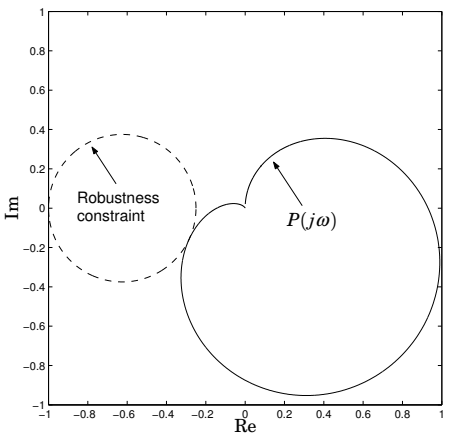

Figure 3.5 Nyquist plot of $P(s)$ in Example 3.1.

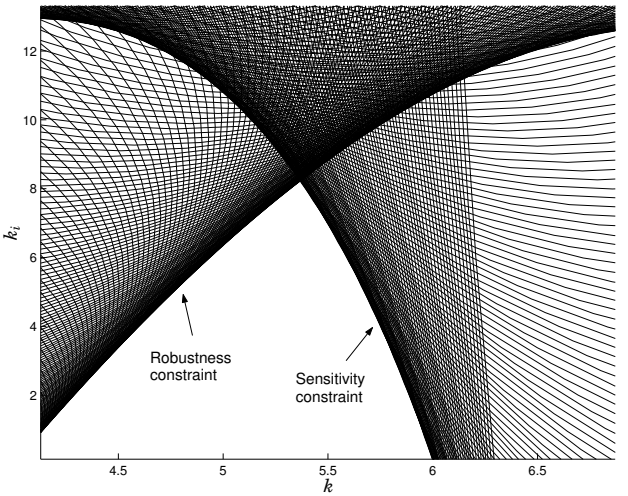

Figure 3.6 Constraints in the $k - k_i$ plane in Example 3.2.

EXAMPLE 3.2
Consider the system in Figure 3.1 with

$$G_1(s) = \frac{1}{s+1} \qquad G_2 = e^{-0.1s}$$

and a static, time varying nonlinearity $f(y,t) : \alpha \leq f(y,t)/y \leq \beta$ with $\alpha = -5,\ \beta = 5$. In particular, if $f(y,t)$ is an uncertain gain, the transfer function would be given by: $G_1(s) = 1/(s+\Delta)\, e^{-0.1s}$ where $\Delta \in [-4, 6]$. Constraints (3.19) and (3.20) give rise to constraint surfaces as shown in Figure 3.6.

From this figure follows that neither in this case the "optimum", considering only the stability constraints for the linear system, will guarantee stability of the nonlinear system. Choosing the maximum k_i that falls below both constraint surfaces and a corresponding k, Theorem 3.1 guarantees absolute stability of the nonlinear system. The Nyquist plots of the loop transfer function and (3.7), shown in Figure 3.7 respectively 3.8, confirm that the constraints are not violated.

Consider now the case when a reference signal r is present at the control system input. This will modify the equilibrium point of the system. Assume that the considered nonlinearity f satisfies the condition $\alpha \leq (f(y_1) - f(y_2))/(y_1 - y_2) \leq \beta, \forall y_1, y_2$. Then Theorem 3.2 guarantees stability of the arising equilibrium point.

□

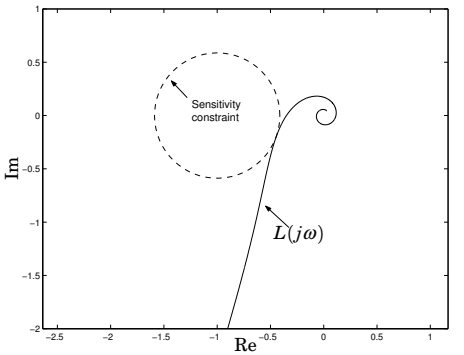

Figure 3.7 Nyquist plot of the loop transfer function $L(s)$ in Example 3.2.

EXAMPLE 3.3
Assume a PID controller is wanted for the process in Example (3.2). The maximum integral gain was $k_i = 8.0$ when only a PI controller was used. By plotting the ellipses for a selection of k_d values the following solution could be obtained.

$$[k\ k_i\ k_d] = [6.7\ 22.5\ 0.2]$$

The envelopes that the ellipses generated for these parameters can be seen in Figure 3.9. A substantial increase in integral gain could be achieved

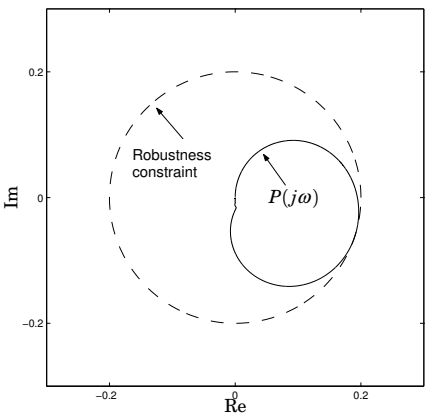

Figure 3.8 Nyquist plot of $P(s)$ in Example 3.2.

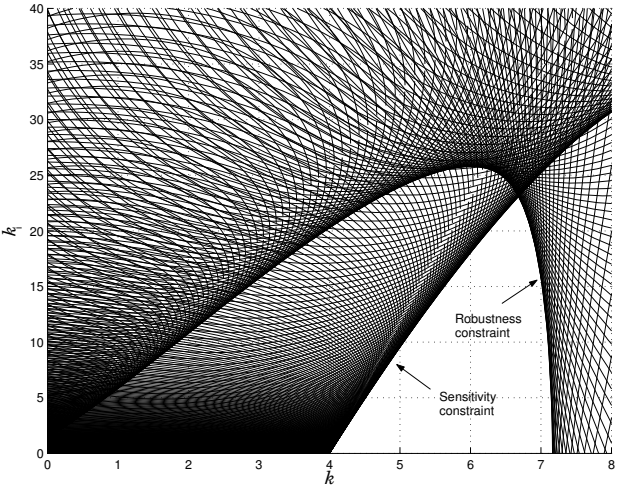

Figure 3.9 Ellipses for $k_d = 0.2$ in Example 3.3.

with the PID design. The process on the other hand is simple so this could be expected. The Nyquist plots of the loop transfer function and (3.7), shown in Figure 3.10 respectively 3.11, confirm that the constraints are not violated. Notice that the constraints shown in Figure 3.9 do not contain any extra constraints on the curvature nor the phase lead of the

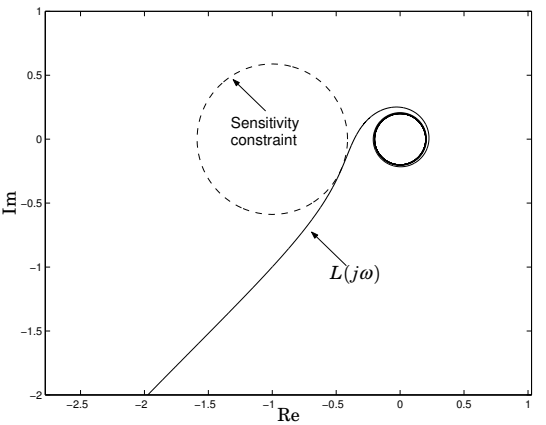

Figure 3.10 Nyquist plot of the loop transfer function $L(s)$ in Example 3.3.

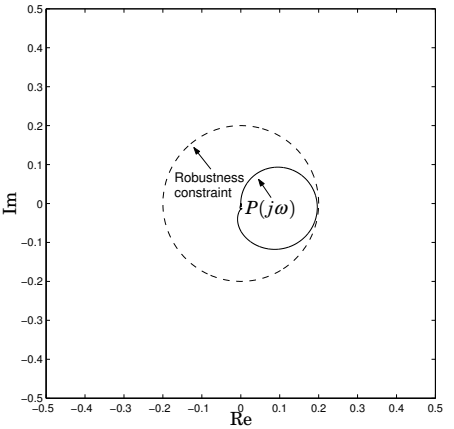

Figure 3.11 Nyquist plot of $P(s)$ in Example 3.3.

loop transfer function as suggested in Section 3.4. However, in this case, the Nyquist curve of the loop transfer function ($L(j\omega)$) has a satisfactory behavior. Naturally, for more complicated systems this might not be the case. □

3.7 Controller Synthesis for an Anti-lock Braking System

In this section an application of the above described synthesis method to an Anti-lock Braking System (ABS) will be presented. The synthesis method will be used to design local PI(D) controllers for a gain scheduled scheme as presented in Chapter 2 and [Solyom and Rantzer, 2003; Solyom *et al.*, 2004]. The proposed design model from chapter one will be used to design the local controllers.

According to (2.5) the plant can be written as:

$$\dot{\lambda}(t)v = -\beta\mu(\lambda(t)) + \alpha u(t-T)$$

As pointed out before $\mu(\lambda)$ is a nonlinear function of λ, and possibly time varying (e.g. as result of a change in surface conditions). Moreover, v is the traveling velocity of the car, which is obviously time varying, however, it has a slower dynamics than the tire slip λ.

The tire friction curve, $\mu(\lambda)$, is highly uncertain. It depends on many variables, as described in Chapter 2. However, it is safe to assume that is cone bounded. Furthermore, we assume that it is locally Lipschitz in

λ. Then Theorems 3.1 and 3.2 can be used to design optimal controllers that are robust against a cone bounded nonlinearity, which in this case is the tire friction curve.

Applying the synthesis method for a cone that contains the entire friction curve will give rise to difficulties. In case that all equilibrium points are considered (Theorem 3.2) it is very likely that the optimization problem turns out infeasible. This can be due to a potentially large cone while the degrees of freedom in the controller are restricted. On the other hand, as pointed out in Section 2.6, limitations on the control performance arise due to time delay and unstable dynamics. Even if it would be possible to stabilize the system at any point on the entire friction curve, the resulting controller would be very conservative and it would not satisfy the performance requirements on the ABS.

A way around this problem is to design controllers for different smaller cones and then switch between them according to some scheduling variables. These cones are supposed to describe different regions of a typical friction curve. Using Theorem 3.2, one would look at regions on the friction curve with slopes in a given cone. The resulting controllers will stabilize any equilibrium point on the considered cone bounded nonlinearity. Considering all possible slopes of the friction curves, by Theorem 3.2 one is able to stabilize any point on a friction curve by its appropriate controller. Then by switching between these controllers, it will be possible to stabilize points on any friction curve that are contained in the considered cone and has its slope confined to the same cone.

The scheduling variable is supposed to be able to determine the operating point on the friction curve. This was presented in Chapter 2 of this work.

Furthermore, scaling the controller by velocity over ground (v) as suggested in Section 2.7, will in turn scale the relative uncertainty caused by the friction curve by v^{-1}. This scaled uncertainty remains in feedback with a nominal plant as shown in Figure 2.6. Considering the uncertainty as being cone bounded, this scaling will "tighten" the cone with increasing velocity.

As pointed out in Section 2.7, to prevent wheel lock in case of sudden change in the surface conditions, it is important that the controller minimizes the effect of load disturbances.

Thus the synthesis methods proposed in this chapter can be directly applied to this problem, resulting in optimal controllers that stabilize the system for a family of friction curves.

Furthermore, to obtain a better performance, the actuator dynamics have been also considered. These are incorporated in $G_2(s)$ and can be easily handled by the proposed design method.

It is worth mentioning that during the field tests, diagrams of the kind

shown in Figure 3.3, showing the constraint surfaces in the k–k_i plane, has been proven to be helpful in retuning the controllers.

3.8 Conclusions

The synthesis method presented deals with design of robust controllers with restricted structure, in particular PID controllers. The uncertainty in the plant is described by a cone bounded nonlinearity, which is in feedback with part of the plant. To obtain a "good" controller, maximum sensitivity is limited as well. The synthesis method presented requires much manual intervention but it is the belief of the author it can be automated significantly. The design method was successfully used to tune local controllers for an Anti-lock Braking System.

Appendix

Proof of Lemma 3.1:

$$\begin{aligned}
&\mathrm{Re}\left\{\frac{1+\beta P(s)}{1+\alpha P(s)}\right\} = \mathrm{Re}\left\{\frac{1+C(s)G(s)+\beta G_1(s)}{1+C(s)G(s)+\alpha G_1(s)}\right\} \\
&\mathrm{Re}\left\{\frac{1+(k-j\frac{k_i}{\omega})(a(\omega)+jb(\omega))+\beta(a_1(\omega)+jb_1(\omega))}{1+(k-j\frac{k_i}{\omega})(a(\omega)+jb(\omega))+\alpha(a_1(\omega)+jb_1(\omega))}\right\} > 0 \iff \\
&\mathrm{Re}\left\{\left(1+\left(k-j\frac{k_i}{\omega}\right)(a(\omega)+jb(\omega))+\beta(a_1(\omega)+jb_1(\omega))\right)\right. \\
&\qquad \left.\left(1+\left(k+j\frac{k_i}{\omega}\right)(a(\omega)-jb(\omega))+\alpha(a_1(\omega)-jb_1(\omega))\right)\right\} > 0
\end{aligned} \tag{3.22}$$

which represents a region outside some ellipses (depending on ω) in the $k-k_i$. By identifying the coefficients of k and k_i in (3.22), one obtains inequality (3.13) with parameters as in (3.14). ◊

LEMMA 3.2
Consider the system:

$$\begin{aligned}
\dot{x} &= Ax - Bw + B_r r \\
w &= f(Cx)
\end{aligned} \tag{3.23}$$

with A Hurwitz, (A,B), (A,C) controllable respectively observable pairs and f a continuous, memoryless scalar nonlinearity. Denote $P(s) = C(sI - A)^{-1}B$.
Assume that there exist $\alpha, \beta \in \mathbb{R}$ such that

$$\alpha \leq \frac{f(y_1) - f(y_2)}{y_1 - y_2} \leq \beta, \quad \forall y_1, y_2 \in \mathbb{R},$$

$$\text{Re}\left\{\frac{1 + \beta P(j\omega)}{1 + \alpha P(j\omega)}\right\} > 0, \quad \forall \omega \geq 0. \tag{3.24}$$

If for a given $r_0 \in \mathbb{R}$, (3.23) has an equilibrium point then it is unique. □

Proof
An equilibrium point x_e corresponding an $r_0 \in \mathbb{R}$ satisfies the equation:

$$0 = Ax_e - Bf(Cx_e) + B_r r_0 \tag{3.25}$$

Assume there exist $x_{e1} \neq x_{e2}$ satisfying (3.25) for the same r_0. Since A is Hurwitz, one obtains:

$$x_{ei} = A^{-1}Bf(Cx_{ei}) - A^{-1}B_r r_0, \quad i = 1,2$$

then

$$x_{e1} - x_{e2} = A^{-1}B(f(Cx_{e1}) - f(Cx_{e2}))$$

hence

$$\alpha \leq \frac{f(Cx_{e1}) - f(Cx_{e2})}{Cx_{e1} - Cx_{e2}} = \frac{1}{CA^{-1}B} \leq \beta \tag{3.26}$$

Furthermore, (3.24) is equivalent to:

$$\text{Re}\left\{(1 + \beta P(j\omega))\overline{(1 + \alpha P(j\omega))}\right\} > 0, \quad \forall \omega \geq 0$$

thus in particular

$$\text{Re}\left\{(1 + \beta P(0))(1 + \alpha P(0))\right\} > 0$$

i.e.

$$(1 - \beta CA^{-1}B)(1 - \alpha CA^{-1}B) > 0$$

or

$$\left(\frac{1}{CA^{-1}B} - \beta\right)\left(\frac{1}{CA^{-1}B} - \alpha\right) > 0$$

which contradicts (3.26), completing the proof. ◊

References

Ackermann, J. and D. Kaesbauer (2003): "Stable polyhedra in parameter space." *Automatica*, **39:1**, pp. 937–943.

Åström, K. J. and T. Hägglund (1995): *PID Controllers: Theory, Design, and Tuning*. Instrument Society of America, Research Triangle Park, North Carolina.

Åström, K. J., H. Panagopoulos, and T. Hägglund (1998): "Design of PI controllers based on non-convex optimization." *Automatica*, **34:5**, pp. 585–601.

Ho, M.-T. (2001): "Synthesis of H_∞ PID controllers." In *Proceedins of the 40th Conference on Decision and Control*, pp. 255–260.

Ho, M.-T., A. Datta, and B. S.P. (1997): "A linear programming characterization of all stabilizing PID controllers." In *Proceedins of the American Control Conference*, pp. 3922–3928.

Ho, M.-T., A. Datta, and B. S.P. (1998): "Design of P, PI, and PID controller for interval plants." In *Proceedins of the American Control Conference*, pp. 2496–2501.

Khalil, H. K. (1992): *Nonlinear Systems*. MacMillan, New York.

Malan, S., M. Milanese, and M. Taragna (1994): "Robust tuning for PID controllers with multiple performance specifications." In *Proceedins of the 33rd Conference on Decision and Control*, pp. 2684–2689.

Panagopoulos, H. (2000): *PID Control, Design, Extension, Application*. PhD thesis, Lund Institute of Technology, Department of Automatic Control.

Panagopoulos, H., K. J. Åström, and T. Hägglund (1999): "Design of PID controllers based on constrained optimization." In *Proc. 1999 American Control Conference (ACC'99)*, pp. 3858–3862. San Diego, California.

Saeki, M. and J. Kimura (1997): "Design method of robust PID controller and CAD systems." In *11th IFAC Simposium on System Identification*, pp. 1587–1593.

Silva, G., A. Datta, and B. S.P. (2002): "New results on the synthesis of PID controllers." *IEEE Transcations on Automatic Control*, **47:2**, pp. 241–252.

Slotine, J. J. and W. Li (1991): *Applied Nonlinear Control*. Prentice Hall, Englewood Cliffs, New Jersey.

Solyom, S. and A. Rantzer (2003): "ABS control—a design model and control structure." In *Nonlinear and Hybrid Systems in Automotive Control*, pp. 85–96. Springer Verlag.

Solyom, S., A. Rantzer, and J. Lüdemann (2004): "Synthesis of a model-based tire slip controller." *Vehicle System Dynamics*, **41:6**, pp. 477–511.

4

The Servo Problem for Piecewise Linear Systems

4.1 Introduction

Behavior of trajectories for piecewise linear systems, in presence of an input signal, is an important issue from a control theoretic point of view. Most analysis results on piecewise linear systems are oriented towards stability of the origin for the unforced system [DeCarlo *et al.*, 2000; Hassibi and Boyd, 1998; Johansson and Rantzer, 1998].The convergence of trajectories of the *unforced piecewise linear system* as defined in [Johansson and Rantzer, 1998] is not sufficient, in general, to guarantee good behavior when input signals are applied to the system. Even if the unforced system is proved to be *stable*, applying an input might change the equilibrium point in such a way that the system behavior becomes unsatisfactory. Moreover, stability for constant input signals is not sufficient to imply input-output stability of the system.

The servo problem for a general nonlinear system can be analyzed in a framework such as presented in Figure 4.1. The problem is to estimate the differences between the system trajectory (x) and a predetermined trajectory x_r in presence of an input signal r. The trajectory x_r is defined such that each x_r is the value at rest of the system trajectory x corresponding to a constant reference signal r. The exogenous input considered in this framework will be the time derivative of r. Choosing $\mathcal{L}_2$ norm as a measure for the signals, it is natural to use the $\mathcal{L}_2$ gain to characterize the system behavior. Thus by computing the $\mathcal{L}_2$ gain from the derivative of the input signal $(\dot{r})$ to the "distance" between system trajectory (x) and reference trajectory (x_r), one obtains information relating the convergence

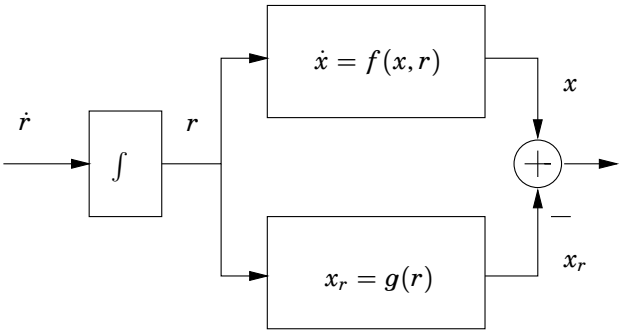

Figure 4.1 This chapter derives computable bounds on the map from the time derivative $\dot{r}$ of the reference signal to the magnitude $|x - x_r|$ of the state error.

of the system trajectory. Then an inequality of the form:

$$\int_0^T |x - x_r|^2 \mathrm{dt} \leq \gamma^2 \int_0^T |\dot{r}|^2 \mathrm{dt}\,. \tag{4.1}$$

describes how a disturbance in form of variations in r, will affect the system trajectory in comparison to its value at rest. Note that this relation gives information also about the input-output stability of the system.

In the literature on nonlinear systems, there exist qualitative results [Khalil, 1992; Rugh and Shamma, 2000], of the following type: if an autonomous nonlinear system depending on some parameter, is stable for different fixed values of this parameter, then slow variations of the parameter between these fixed values, result in a non-autonomous system that will stay in the neighborhood of the equilibria defined by the fixed parameters. The contribution of this work is to give a quantitative bound on the neighborhood of the equilibria when the variation of the parameter is a continuous function. For piecewise linear systems a computational method using convex optimization is proposed.

Application of this theory in the field of anti-windup compensation is studied in some detail.

This chapter contains the work of [Solyom and Rantzer, 2002; Solyom, 2003]. The outline of the chapter is as follows: Section 4.2 presents the analogous problem for a linear system while Section 4.3 generalizes the problem for a nonlinear system. Section 4.4 treats the case of piecewise linear systems. In Section 4.5 the results are applied for anti-windup compensation. Finally, some conclusions are presented in Section 4.6.

4.2 The Linear Case

The $\mathcal{L}_2$ gain for a linear system is given by well known formulas. One approach is to solve a Riccati inequality, by means of convex optimization [Zhou and Doyle, 1998]. Theorem 4.1 uses this approach for the computation of $\mathcal{L}_2$ gain between the derivative of the reference signal and the difference $x - x_r$.

THEOREM 4.1
Consider the linear system:

$$\dot{x} = Ax + Br, \; x(0) = 0 \tag{4.2}$$

such that A^{-1} exists. Furthermore, define

$$x_r \stackrel{\Delta}{=} -A^{-1}Br \tag{4.3}$$

then the following statements are equivalent:

i) There exist $\gamma > 0, P > 0$ such that

$$\begin{bmatrix} A^T P + PA + I & PA^{-1}B \\ (A^{-1}B)^T P & -\gamma^2 I \end{bmatrix} < 0. \tag{4.4}$$

ii) For each solution of (4.2) with $r \in \mathcal{C}^1$ and $r(0) = 0$ the following inequality holds:

$$\int_0^\infty |x - x_r|^2 \mathrm{dt} \leq \gamma^2 \int_0^\infty |\dot{r}|^2 \mathrm{dt} \tag{4.5}$$

□

Proof:
Defining $\tilde{x} \stackrel{\Delta}{=} x - x_r$, the following linear system is obtained:

$$\dot{\tilde{x}} = A\tilde{x} + A^{-1}B\dot{r}\,.$$

The $\mathcal{L}_2$ gain of this system can be found using standard results [Zhou and Doyle, 1998], which will result in the relations (4.4) and (4.5). ◊

4.3 The Generic Nonlinear Case

In case of a general nonlinear system with a time varying input, it is more difficult to draw conclusions about trajectory convergence. Still, it is possible to find an upper bound on the $\mathcal{L}_2$ gain from the derivative of the input to the state deviation.

THEOREM 4.2
Let $f : \mathbb{R}^n \times \mathbb{R}^m \to \mathbb{R}^n$ be locally Lipschitz. For every $r \in \mathcal{R} \subset \mathbb{R}^m$ let $x_r \in \mathbb{R}^n$ be a unique solution to $0 = f(x_r, r)$.

If there exists $\gamma > 0$ and a non-negative $\mathcal{C}^1$ function V, with $V(x_r, r) = 0$ for all $r \in \mathcal{R}$ and

$$\begin{bmatrix} \frac{\partial V}{\partial x} f(x,r) + |x - x_r|^2 & \frac{1}{2}\frac{\partial V}{\partial r} \\ \frac{1}{2}\left(\frac{\partial V}{\partial r}\right)^T & -\gamma^2 I \end{bmatrix} < 0 \tag{4.6}$$

for all $(x, r) \in \mathcal{S}$, then for each solution to

$$\dot{x} = f(x,r),\ x(0) = x_{r_0},\ r(0) = r_0 \tag{4.7}$$

such that $r(t) \in \mathcal{R}$ and $(x(t), r(t)) \in \mathcal{S}$ for all t, it holds that

$$\int_0^T |x - x_r|^2 \mathrm{d}t \leq \gamma^2 \int_0^T |\dot{r}|^2 \mathrm{d}t \tag{4.8}$$

□

Proof:
Multiplying (4.6) from left and right with $[\mathbf{1} \quad \dot{r}^T]$ one obtains:

$$\frac{\partial V}{\partial x} f(x,r) + |x - x_r|^2 + \frac{\partial V}{\partial r}\dot{r} - \gamma^2 |\dot{r}|^2 < 0$$

that is

$$\frac{dV}{dt} + |x - x_r|^2 - \gamma^2 |\dot{r}|^2 < 0$$

which in turn by integration on $[0,\ T]$ gives

$$V(x(T), r(T)) + \int_0^T |x - x_r|^2 \mathrm{d}t - \gamma^2 \int_0^T |\dot{r}|^2 \mathrm{d}t < 0$$

and inequality (4.8) results since $V(x, r) \geq 0$. ◊

Remark Consider a linear system as in (4.2) with x_r defined by (4.3). Furthermore, consider a Lyapunov function of the form $V(x, r) = (x - x_r)^T P (x - x_r)$. Then

$$\frac{\partial V}{\partial x} f(x,r) \overset{(4.3)}{=} (x - x_r)^T (A^T P + PA)(x - x_r)$$
$$\frac{\partial V}{\partial r} = 2(x - x_r)^T P A^{-1} B$$

and the matrix in (4.6) becomes:

$$\begin{bmatrix} x-x_r & 0 \\ 0 & \mathbf{1} \end{bmatrix}^T \begin{bmatrix} A^TP+PA+I & PA^{-1}B \\ (A^{-1}B)^TP & -\gamma^2 I \end{bmatrix} \begin{bmatrix} x-x_r & 0 \\ 0 & \mathbf{1} \end{bmatrix}$$

which negative definiteness is given by (4.4).

Remark The matrix inequality (4.6) using Schur complement can be written as

$$\frac{\partial V}{\partial x} f(x,r) + \frac{1}{2\gamma^2}\frac{\partial V}{\partial r}\left(\frac{\partial V}{\partial r}\right)^T + \frac{1}{2}(x-x_r)^T(x-x_r) \leq 0$$

which is the Hamilton-Jacobi inequality for the system

$$\begin{cases} \begin{bmatrix} \dot{x} \\ \dot{r} \end{bmatrix} = \begin{bmatrix} f(x,r) \\ 0 \end{bmatrix} + \begin{bmatrix} 0 \\ 1 \end{bmatrix} u \\ \quad y = \ x - x_r \end{cases} \tag{4.9}$$

(see Theorem 6.5 in [Khalil, 1992]).

Similarly to Theorem 4.2, an upper bound on the instantaneous value of $|x-x_r|$ can be obtained. The following result is analogous to the one in Theorem 4.2.

THEOREM 4.3
Let $f : \mathbb{R}^n \times \mathbb{R}^m \to \mathbb{R}^n$ be locally Lipschitz. For all $r \in \mathcal{R} \subset \mathbb{R}^m$, let $x_r \in \mathbb{R}^n$ be a unique solution to $0 = f(x_r, r)$.
If there exist $\gamma, c, p, \lambda > 0$ and a $\mathcal{C}^1$ function V with $V(x,r) \geq c|x-x_r|^p$, $V(x_r,r) = 0$ and

$$\begin{bmatrix} \frac{\partial V}{\partial x} f(x,r) + \lambda V & \frac{1}{2}\frac{\partial V}{\partial r} \\ \frac{1}{2}\left(\frac{\partial V}{\partial r}\right)^T & -\gamma^2 I \end{bmatrix} < 0 \tag{4.10}$$

for all $(x,r) \in \mathcal{S}$, then for each solution to

$$\dot{x} = f(x,r), \ x(0) = x_{r_0}, \ r(0) = r_0 \tag{4.11}$$

such that $r(t) \in \mathcal{R}$ and $(x(t), r(t)) \in \mathcal{S}$, it holds that

$$|x(T) - x_r(T)|^p \leq \frac{\gamma^2}{c}\int_0^T |\dot{r}|^2 e^{-\lambda(T-t)} \mathrm{d}t \tag{4.12}$$

□

Proof:
Multiplying (4.6) from left and right with $[\mathbf{1} \quad \dot{r}^T]$ one obtains:

$$\frac{\partial V}{\partial x} f(x,r) + \frac{\partial V}{\partial r}\dot{r} + \lambda V - \gamma^2 |\dot{r}|^2 < 0$$

thus on $\mathcal{S}$ yields that:

$$\frac{dV}{dt} + \lambda V - \gamma^2 |\dot{r}|^2 < 0$$

which by multiplication with $e^{-\lambda(T-t)} > 0$ gives

$$\begin{aligned} &\frac{dV}{dt} e^{-\lambda(T-t)} + \lambda V e^{-\lambda(T-t)} - \gamma^2 |\dot{r}|^2 e^{-\lambda(T-t)} < 0 \\ \Leftrightarrow &\frac{d}{dt} V e^{-\lambda(T-t)} - \gamma^2 |\dot{r}|^2 e^{-\lambda(T-t)} < 0 \end{aligned}$$

then by integrating on $[0,\ T]$ and using that $V(x(0), r(0)) = 0$, gives

$$c|x(T) - x_r(T)|^p \leq V(x(T), r(T)) < \gamma^2 \int_0^T |\dot{r}|^2 e^{-\lambda(T-t)} \mathrm{dt}$$

thus inequality (4.12) holds. ◊

Remark Consider a linear system as in (4.2) with x_r defined by (4.3) and $\mathcal{S} = \mathbb{R}^n \times \mathbb{R}^m$. Furthermore, consider a Lyapunov function of the form $V(x,r) = (x - x_r)^T P (x - x_r)$ and $p = 2$. By using Schur complement, the positivity condition of the Lyapunov function in Theorem 4.3 translates to:

$$P - c^2 I > 0 \Leftrightarrow \begin{bmatrix} P & I \\ I & \frac{1}{c^2} I \end{bmatrix} > 0$$

while (4.10) becomes:

$$\begin{bmatrix} A^T P + PA + \lambda P & PA^{-1}B \\ (A^{-1}B)^T P & -\gamma^2 I \end{bmatrix} < 0$$

Obviously, for a generic nonlinear system as considered in (4.7) it might be difficult to find a $V(x,r)$ such that (4.6) or (4.10) is fulfilled. In case of piecewise linear systems, however, LMIs can be used. This will be presented next.

4.4 Piecewise Linear System

Consider now a particular kind of nonlinear systems, a piecewise linear system, of the form:

$$\dot{x} = A_i x + B_i r, \quad x(t) \in X_i \tag{4.13}$$

with $\{X_i\}_{i \in I} \subseteq \mathbb{R}^n$ a partition of the state space into a number of convex polyhedral cells with disjoint interior. Suppose that $A_i x + B_i r, x \in X_i$ is locally Lipschitz and for any constant $r \in \mathcal{R}$, the piecewise linear system has a unique equilibrium point.

Furthermore, consider symmetric matrices S_{ij} that satisfy the inequality:

$$\begin{bmatrix} x - x_r \\ r \end{bmatrix}^T S_{ij} \begin{bmatrix} x - x_r \\ r \end{bmatrix} > 0, \ x \in X_i, \ \in \mathcal{R} \tag{4.14}$$

Define

$$\bar{B}_j \triangleq \begin{bmatrix} A_j^{-1} B_j \\ 1 \end{bmatrix}, \qquad \bar{I} \triangleq \begin{bmatrix} I & 0 \\ 0 & 0 \end{bmatrix} \tag{4.15}$$

$$\bar{A}_{ij} \triangleq \begin{bmatrix} A_i & -A_i A_j^{-1} B_j + B_i \\ 0 & 0 \end{bmatrix} \tag{4.16}$$

The following proposition is useful for application of Theorem 4.2 and Theorem 4.3.

PROPOSITION 4.1
Let $f(x,r) = A_i x + B_i r, \ x \in X_i$, and $x_r = -A_j^{-1} B_j r, \ x_r \in X_j$ with $x(0) = x_r(0)$, $r(0) = r_0$. If there exist $\gamma > 0$, $P > 0$ such that $\bar{P} = \text{diag}\{P, 0\}$ satisfies

$$\begin{bmatrix} \bar{A}_{ij}^T \bar{P} + \bar{P} \bar{A}_{ij} + S_{ij} + \bar{I} & \bar{P} \bar{B}_j \\ \bar{B}_j^T \bar{P} & -\gamma^2 I \end{bmatrix} < 0, \ i \neq j \tag{4.17}$$

$$\begin{bmatrix} A_j^T P + P A_j + I & P A_j^{-1} B_j \\ (A_j^{-1} B_j)^T P & -\gamma^2 I \end{bmatrix} < 0 \tag{4.18}$$

then $V(x,r) = (x - x_r)^T P (x - x_r)$ satisfies (4.6) for all $x \in X_i$, $r \in \mathcal{R}$. □

In particular, in the case when $\dot{r}(t) = 0$, for $t > T$, by finding a finite $\gamma > 0$ it is shown that all trajectories of the nonlinear system (4.13) will converge to x_r.

The conservatism of the theorems can be reduced by considering piecewise quadratic Lyapunov function. In this case the Lyapunov function will be piecewise $\mathcal{C}^1$ instead of $\mathcal{C}^1$. Imposing that it is non-increasing at

the points of discontinuity, the results hold (see [Johansson and Rantzer, 1998]).

Remark When the local linear systems contain affine terms the argument vector of the Lyapunov function will be extended to $[\tilde{x} \quad r \quad 1]$. Similarly, when partitions that do not contain the origin are to be described, the vector of variables will be extended. Then the definitions in (4.15), (4.16) become:

$$\bar{B}_j \triangleq \begin{bmatrix} A_j^{-1}B_j \\ 1 \\ 0 \end{bmatrix}, \tag{4.19}$$

$$\bar{A}_{ij} \triangleq \begin{bmatrix} A_i & -A_iA_j^{-1}B_j + B_i & a_i \\ 0 & 0 & 0 \end{bmatrix} \tag{4.20}$$

Remark The variation in the affine term due to r, can be viewed as parametric uncertainty in the system. Thus the theorem can be used to prove robust stability for a piecewise linear system, with uncertain affine terms in the local linear systems.

A Unifying View

In Section 4.2, in the case of linear systems, it has been shown that the proposed method is equivalent to finding the $\mathcal{L}_2$ induced gain of a system expressed in the coordinates $x - x_r$. It is natural to ask if the same type of recasting is possible in the case of piecewise linear systems. That is, is it possible to find a piecewise linear system which $\mathcal{L}_2$ induced gain gives an equivalent characterization of the servo problem in (4.1) for system (4.13)?

In [Johansson, 1999] a method has been developed for estimating an upper bound on the $\mathcal{L}_2$ induced gain of a piecewise linear system. This result is cited below:

THEOREM 4.4
Suppose there exist symmetric matrices T, U_i and W_i such that U_i and W_i have non-negative entries, while $P_i = F_i^T T F_i$ and $\overline{P}_i = \overline{F}_i^T T \overline{F}_i$ satisfy

$$0 > \begin{bmatrix} P_iA_i + A_i^TP_i + C_i^TC_i + E_i^TU_iE_i & P_iB_i \\ B_i^TP_i & -\gamma^2 I \end{bmatrix} \quad \text{for } i \in I_0$$

$$0 > \begin{bmatrix} \overline{P}_i\overline{A}_i + \overline{A}_i^T P_i + \overline{C}_i^T\overline{C}_i + \overline{E}_i^T U_i\overline{E}_i & \overline{P}_i\overline{B}_i \\ \overline{B}_i^T\overline{P}_i & -\gamma^2 I \end{bmatrix} \quad \text{for } i \in I_1$$

Then every trajectory $x(t)$ of (4.13) with $x(0) = 0$, $\int_0^\infty (|x|^2 + |u|^2)\mathrm{d}t < \infty$ satisfies

$$\int_0^\infty |y|^2 \mathrm{d}t \leq \gamma \int_0^\infty |u|^2 \mathrm{d}t.$$

The best upper bound on the $\mathcal{L}_2$ induced gain is achieved by minimizing γ subject to the constraints defined by the inequalities. □

In the above theorem, I_0 denotes the index set of the cells that contain the origin and I_1 is the index set of the cells that do not contain the origin.

In light of this theorem, one can characterize the servo problem for piecewise linear system by finding the $\mathcal{L}_2$ induced gain for the piecewise linear system:

$$\begin{cases} \begin{bmatrix} \dot{\tilde{x}} \\ \dot{r} \end{bmatrix} = \begin{bmatrix} A_i & -A_i A_j^{-1} B_j + B_i \\ 0 & 0 \end{bmatrix} \begin{bmatrix} \tilde{x} \\ r \end{bmatrix} + a_i + \begin{bmatrix} A_j^{-1} B_j \\ 1 \end{bmatrix} \dot{r} \\ \tilde{y} = \tilde{x} \end{cases} \quad x \in X_i,\ r \in \mathcal{R}$$

$$\begin{cases} \dot{\tilde{x}} = A_j \tilde{x} + A_j^{-1} B_j \dot{r} \\ \tilde{y} = \tilde{x} \end{cases} \quad x \in X_j,\ r \in \mathcal{R}$$

which is equivalent to the result in Proposition 4.1.

Polyhedral Cell Boundings and Continuity Matrices

In the LMIs from the above theorems, the S-procedure is used to specify the region where the analysis is carried out. One way to describe the regions of the state space is by using polyhedral cell boundings [Johansson, 1999]. Using compact matrix representation, the polyhedral cell boundings E_i have the property:

$$E_i x \succeq 0 \quad \text{for } x \in X_i$$

It basically contains information about the hyperplanes bounding the cell in question.

In case of continuous piecewise quadratic Lyapunov functions, continuity can be automatically imposed by parameterizing the Lyapunov functions as:

$$F_i^T T F_i \quad \text{for } x \in X_i$$

where T is a positive definite matrix and F_i are constrain matrices. Each F_i contains information about the hyperplanes bounding the cell in question.

It is obvious from the above, that in order to construct the polyhedral cell boundings and the constraint matrices, one has to provide the hyperplanes bounding the cell.

In the case of the servo problem, the argument of the Lyapunov function includes also the reference signal r. Still it is rather straightforward to describe the bounding hyperplanes. On the other hand, in the LMIs one has to describe the regions in the coordinates $[x - x_r \; r \; 1]^T$. One easy way to overcome this problem is by specifying the hyperplanes $[x \; r \; 1]^T$ coordinates and then use the coordinate transformation:

$$\begin{bmatrix} x - x_r \\ r \\ 1 \end{bmatrix} = \begin{bmatrix} I & A_j^{-1}B_j & 0 \\ 0 & I & 0 \\ 0 & 0 & 1 \end{bmatrix} \begin{bmatrix} x \\ r \\ 1 \end{bmatrix}$$

where $x_r = -A_j^{-1}B_j r$.

Computational Example

Consider the system of the form:

$$\dot{x} = Ax + B(r - \varphi(Cx))$$

where A is a stable matrix. The nonlinearity is defined as:

$$\varphi(z) = \begin{cases} z, \; z < 1 \\ 1, \; z \geq 1 \end{cases}$$

This system can be described by the following piecewise linear system.

$$\dot{x} = \begin{cases} Ax - B + Br, \; Cx \geq 1 \\ (A - BC)x + Br, \; Cx < 1 \end{cases} \tag{4.21}$$

Here the two partitions are $X_1 = \{x | Cx \geq 1\}$ and $X_2 = \{x | Cx < 1\}$. The numerical values are:

$$A = \begin{bmatrix} -0.5 & 1 \\ -1 & 0 \end{bmatrix}, \; B = \begin{bmatrix} 1 \\ 3 \end{bmatrix}, \; C = \begin{bmatrix} 1 & 0 \end{bmatrix}.$$

The state space partitions of such a system is shown in Figure 4.2. Then the sets $\mathcal{R}_1 = (\frac{4}{3}, \infty)$ and $\mathcal{R}_2 = (-\infty, \frac{4}{3})$ follow from simple computations.

Consider first the case when $r(t) \in \mathcal{R}_2$ for all t, i.e. $x_r(t) \in X_2$ for all t. The LMIs resulting from Theorem 4.2 turn out to be infeasible, suggesting that a quadratic Lyapunov function might be too conservative. Therefore, a piecewise quadratic Lyapunov function is tried:

$$V(x, r) = \begin{cases} \begin{bmatrix} x - x_r \\ r \\ 1 \end{bmatrix}^T P_1 \begin{bmatrix} x - x_r \\ r \\ 1 \end{bmatrix}, \; x \in X_1 \\ (x - x_r)^T P_2 (x - x_r), \; x \in X_2 \end{cases}$$

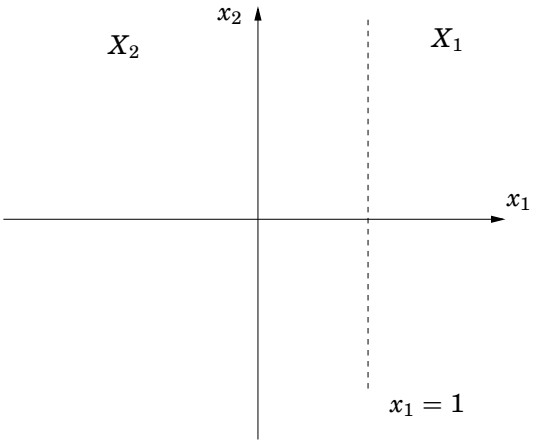

Figure 4.2 State space partitions in the computational example.

Minimizing γ subject to the LMI constraints, one obtains the Lyapunov function's matrices:

$$P_1 = \begin{bmatrix} 5.0749 & -0.8930 & -6.6918 & 8.9351 \\ -0.8930 & 5.1082 & 0.0703 & 0.2583 \\ -6.6918 & 0.0703 & -12.1141 & 16.2238 \\ 8.9351 & 0.2583 & 16.2238 & -2.2493 \end{bmatrix}$$

$$P_2 = \begin{bmatrix} 20.69 & -0.63 \\ -0.63 & 5.1 \end{bmatrix}$$

and $\gamma = 7.182$.

Consider now the case when $r(t) \in \mathcal{R}_1$ for all t, i.e. $x_r(t) \in X_1$ for all t and consider the Lyapunov function:

$$V(x,r) = \begin{cases} (x - x_r)^T P_1 (x - x_r), \ x \in X_1 \\ \begin{bmatrix} x - x_r \\ r \\ 1 \end{bmatrix}^T P_2 \begin{bmatrix} x - x_r \\ r \\ 1 \end{bmatrix}, \ x \in X_2 \end{cases}$$

Solving the constrained minimization problem, one obtains a Lyapunov function with the matrices:

$$P_2 = \begin{bmatrix} 18.36 & -2.55 & 47.17 & -68.64 \\ -2.55 & 4.22 & -13.32 & 8.21 \\ 47.17 & -13.32 & 146.8 & -173.34 \\ -68.64 & 8.21 & -173.34 & 317.36 \end{bmatrix}$$

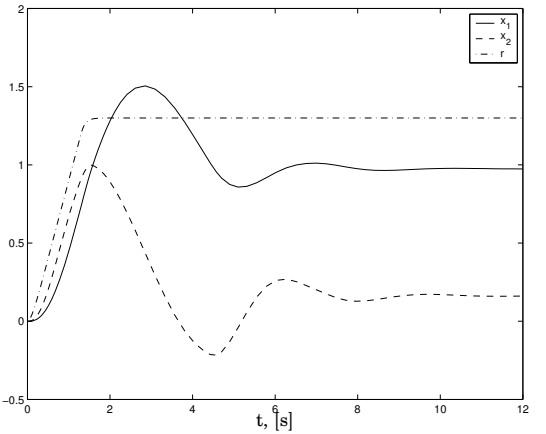

(a) System trajectories and input signal.

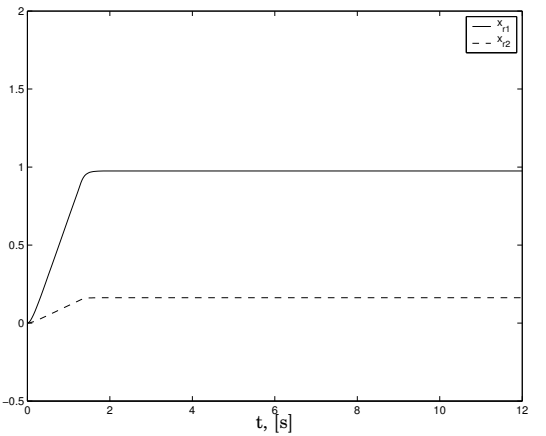

(b) Reference trajectories.

Figure 4.3 Simulation results for the computational example.

$$P_1 = \begin{bmatrix} 3.874 & -0.503 \\ -0.503 & 4.225 \end{bmatrix}$$

and $\gamma = 8.3221$. Thus, for every (x, r) starting in $X_1 \times \mathcal{R}_1$ respectively in $X_2 \times \mathcal{R}_2$, trajectory convergence, in the sense of Theorem 4.2, is guar-

anteed by the finite γ's. In Figure 4.3 state trajectories x_1 and x_2 are presented when $r \in \mathcal{R}_2$. Notice that x_1 is passing through region X_1.

It is of interest to derive lower bounds on the $\mathcal{L}_2$ gain to verify the conservativeness of the result. A natural lower bound is obtained by Theorem 4.1. This way for the case when $x_r \in X_2$ a lower bound of 1.12 is obtained, while in the case $x_r \in X_1$ a lower bound of 8.318 is computed. For the case when $x_r \in X_1$ the resulting bounds turned out to be very tight. However, it can be noticed that the lower bound when $x_r \in X_2$ is rather small in comparison to the upper bound. This could be refined by finding a "worst case disturbance" for the nonlinear system.

As seen above, *S-procedure* is used (S_{ij}) to describe the state-space partition of (4.13), and in the same time describe the set of considered r's. More details on how to find such matrices can be found in [Johansson, 1999]. The used matrices are:
for X_1

$$S_{12} = \begin{bmatrix} 0 & 0 & -8.562 & 11.772 \\ 0 & 0 & 0 & 0 \\ -8.562 & 0 & -12.844 & 16.259 \\ 11.772 & 0 & 16.259 & -20.528 \end{bmatrix}$$

and for X_2

$$S_{21} = \begin{bmatrix} 0 & 0 & -52.66 & -34.957 \\ 0 & 0 & 0 & 0 \\ -52.66 & 0 & -315.965 & 100.217 \\ -34.957 & 0 & 100.217 & -336.966 \end{bmatrix}$$

4.5 A Synthesis Method for Static Anti-Windup Compensators

Figure 4.4 shows the studied system. A linear plant with saturation-type limitations on the input, is to be controlled by a linear controller.

The usual way to handle this kind of nonlinear systems is by using a two-stage design approach. First, design the linear controller without taking into account the nonlinearity at the plant input. Second, design a compensator that will ensure a graceful decay of the control performance once the system enters saturation. The latter is the so called anti-windup compensator.

It is customary to use linear filters for anti-windup compensation. Both static and dynamic compensators are reported in the literature. In this work, static anti-windup compensators are to be designed, i.e. the static

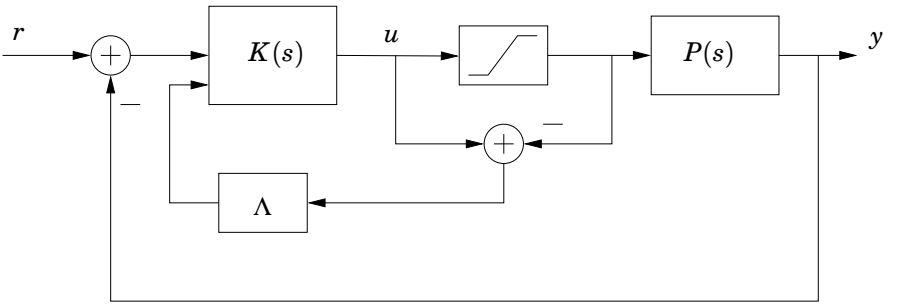

Figure 4.4 The anti-windup scheme considered.

compensator block Λ is to be found, according to some appropriate performance criterion.

In [Teel and Kapoor, 1997] the problem of anti-windup compensation has been recognized as being that of returning the system to linear behavior. That is, return of the system output to the one that would have been without saturation. Thus it is clear that the anti-windup problem can naturally be posed as a servo problem for a nonlinear system (i.e. the closed-loop piecewise linear system). The goal is to return to the behavior of the linear system as fast as possible.

The use of a $\mathcal{L}_2$ performance criterion in the synthesis of anti-windup compensator is well established (see [Teel and Kapoor, 1997; Mulder and Kothare, 2001; Weston and Postlethwaite, 1998; Grimm *et al.*, 2001]). However, to the best of the author's knowledge, posing the anti-windup problem as a servo problem with the performance criterion as proposed in this work has never been presented.

Return of the system output to the linear region is imposed as a goal in [Turner and Postlethwaite,]. However, this method does not allow the kind of variations of the input signal as in the here proposed theory.

Anti-Windup and the Servo Problem

The description of the system in Figure 4.4, as a piecewise linear system is similar to that presented in [Mulder and Kothare, 2000].

The linear plant $P(s)$ has a state-space description given by the matrices A_p, B_p, C_p, D_p. The state-space description of the linear controller $K(s)$ is given by A_c, B_c, C_c, D_c. It is assumed that $P(s)$ is stable and $K(s)$ has been designed such that the closed loop linear system is stable.

The saturation function is defined as

$$\text{sat}(u) = \begin{cases} u_m, & u < u_m \\ u, & u_m \leq u \leq u_M \\ u_M, & u > u_M \end{cases}$$

The saturation nonlinearity will give rise to a partitioned state-space for the system, obtaining a piecewise linear system. The three resulting regions will be denoted as follows X_2 – the linear region, X_1 – the region where $u < u_m$ and X_3 denotes the region where $u > u_M$.

The anti-windup compensation block Λ enters the controller as follows:

$$\begin{aligned} \dot{x}_c &= A_c x_c + B_c e + \Lambda_1(u - \text{sat}(u)) \\ u &= C_c x_c + D_c e + \Lambda_2(u - \text{sat}(u)) \end{aligned}$$

where $\Lambda = \begin{bmatrix} \Lambda_1 \\ \Lambda_2 \end{bmatrix}$ and $e = r - y$. Thus, in the three partitions the dynamics will be given by:

$$\begin{cases} \dot{\bar{x}} = A_1\bar{x} + a_1 + B_1 r \\ y = C_1\bar{x} + D_1 r \end{cases}, \bar{x} \in X_1$$

$$\begin{cases} \dot{x} = A_2 x + B_2 r \\ y = C_2 x + D_2 r \end{cases}, x \in X_2$$

$$\begin{cases} \dot{\bar{x}} = A_3\bar{x} + a_3 + B_3 r \\ y = C_3\bar{x} + D_3 r \end{cases}, \bar{x} \in X_3$$

Here the matrices A_i, B_i depend linearly on the parameter $\Lambda_1(I + \Lambda_2)^{-1}$. The matrices used in the representation are the same as in [Mulder and Kothare, 2000] (for details see Appendix 4.6).

The anti-windup problem can naturally be posed as a servo problem for the nonlinear system (i.e. the closed-loop piecewise linear system). The goal is to return to the behavior of the linear system as fast as possible. In this context, x_r introduced in the previous section can be used to define a trajectory that describes the behavior of the system in the linear region. That is, define

$$x_r = -A_2^{-1} B_2 r \tag{4.22}$$

Computing the $\mathcal{L}_2$ gain from the derivative of the input signal to $x - x_r$, gives a measure on the behavior of the system trajectories with respect to x_r. Notice that the input signal is smoothly time varying.

It is reasonable to assume that the reference signals have such a magnitude that they can be achieved by the system output without violating

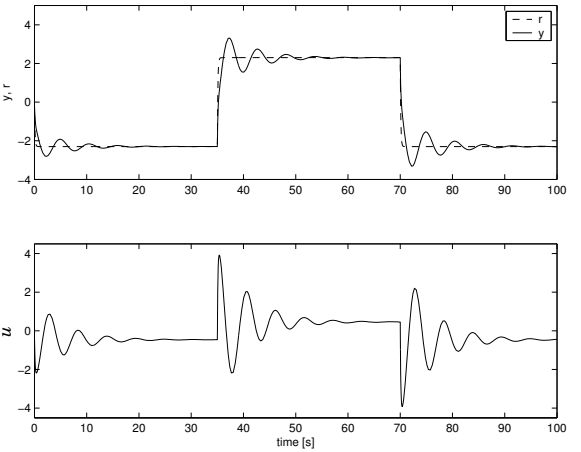

Figure 4.5 Output and control signal when no saturation is present.

the saturation constraints in stationarity. This way all the equilibrium points of the system remain in the linear region. Using this assumption, it is enough to use only the x_r defined by (4.22) in the synthesis.

Thus, a solution to the considered anti-windup problem is given by Proposition 4.1, with $i = 1, 3$ and $j = 2$ using the definition in (4.19) and (4.20). Unfortunately, if one is searching also for the parameters Λ_1, Λ_2 in the same time as solving for P, the matrix inequality becomes a BMI (bilinear matrix inequality). Iterative approaches can be used to solve this kind of problems, however no guarantee for convergence exists. The iteration scheme could contain the following steps:

- fix Λ and search for T, S_{ij}, while minimizing γ,
- fix T and search for Λ, S_{ij}, while minimizing γ.

These steps are repeated, passing the optimal T, respectively Λ from one step to the other until they converge to a constant value.

EXAMPLE 4.1
To demonstrate the method, a simple SISO example with a PI controller will be used. This example has been studied also in [Mulder and Kothare, 2000; Turner and Postlethwaite,]. The plant and controller are:

$$P(s) = \frac{0.5s^2 + 0.5s + 1}{s^2 + 0.2s + 0.2}$$

$$K(s) = 2\left(1 + \frac{1}{s}\right)$$

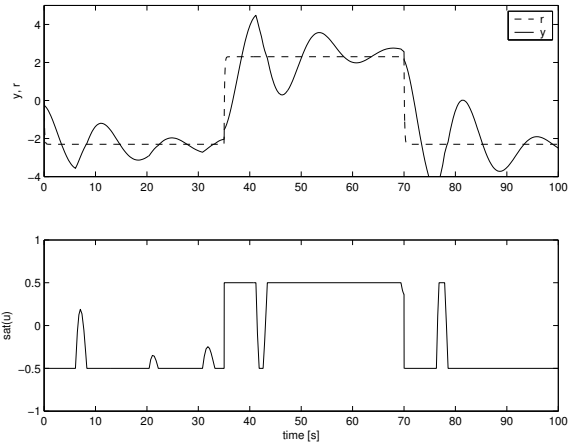

Figure 4.6 Output and control signal when saturation is acting on the control signal.

The saturation on the control signal is set to ± 0.5. The output in the case when there is no saturation acting on the plant is shown in Figure 4.5, while in the case of saturation acting on the control output the performance deteriorates considerably (see Figure 4.6). The reference signal in both cases is a square wave filtered by a first order linear system with a time constant of 0.1 seconds.

Due to the integrator in the controller the LMIs are not strictly feasible as long there is no anti-windup compensation. In this case, where the compensator is a scalar, it is easy to choose an initial guess for the anti-windup compensator, to start with. However, in case the compensator is in form of a matrix (e.g. multivariable systems), this choice is no longer straightforward. In those cases a "forgetting factor" can be introduced in the controller, that is the controller pole in the origin can be slightly moved to the left complex half-plane.

In the scalar case, no iteration is necessary for solving the BMI. Instead, one can grid all Λ for which the LMIs are feasible and then pick the optimal.

Applying this method, a static compensator of the form $\Lambda_1 = -0.41$, $\Lambda_2 = 0$ is found. Piecewise quadratic Lyapunov functions are used in the algorithm. The best upper bound found on the $\mathcal{L}_2$ gain from $\dot{r}$ to $x - x_r$ is 5.0691. For a lower bound on this $\mathcal{L}_2$ gain, a local analysis in the linear region can be carried out. This way, a lower bound of 3.8639 is obtained. The output of the compensated system is shown in Figure 4.7. Notice the significant improvement in the performance of the control system.

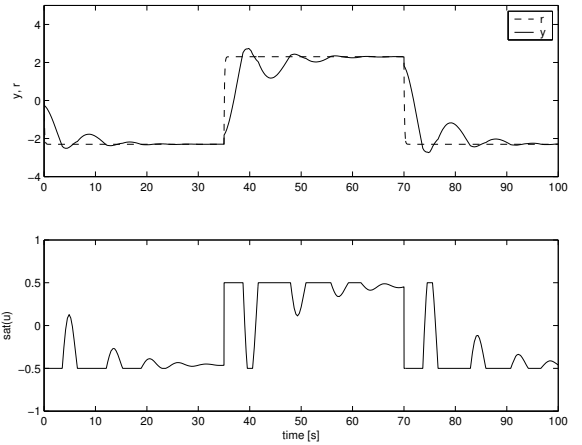

Figure 4.7 Output and control signal when saturation is acting on the control signal. Anti-windup compensation is applied on the control system.

It is interesting to notice that the anti-windup tracking-time constant $T_r = -1/\Lambda_1 = 2.439$, is in this case higher than the well-known heuristic choice $T_r = T_i = 1$ (see [Åström and Wittenmark, 1997]). □

4.6 Conclusions

Trajectory convergence in presence of constant and time varying inputs has been studied. Quantitative result has been established for a sufficient condition regarding trajectory convergence for a class of nonlinear systems, where one of the parameters (r) is time varying. This result has been used for piecewise linear systems, where Proposition 4.1 in combination with Theorem 4.2, give a tool for computing an upper bound on the $\mathcal{L}_2$ gain from $\dot{r}$ to $x - x_r$, characterizing the servo problem for such systems.

The theory can be naturally applied to anti-windup compensation. An example is presented for a scalar system. The theory provides scalability, so that the same method can be applied for systems with multiple saturations. However, this will result in combinatorial increase of the number of analysis regions.

Appendix – Anti-Windup Compensated System

System matrices

$$\bar{A}_1 = \begin{bmatrix} A_p & 0 & B_p u_m \\ -B_c C_p & A_p & -B_c D_p u_m \\ 0 & 0 & 0 \end{bmatrix}, \quad \bar{B}_1 = \begin{bmatrix} 0 \\ B_c \\ 0 \end{bmatrix} - \bar{\Lambda} \begin{bmatrix} 0 \\ D_c \\ 0 \end{bmatrix},$$

$$\bar{C}_1 = \begin{bmatrix} C_p & 0 & D_p u_m \end{bmatrix}, \quad \bar{D}_1 = 0,$$

$$A_2 = \begin{bmatrix} A_p - B_p J_2 D_c C_p & B_p J_2 C_c \\ -B_c C_p + B_c D_p J_2 D_c C_p & A_c - B_c D_p J_2 C_c \end{bmatrix},$$

$$B_2 = \begin{bmatrix} B_p J_2 D_c \\ B_c - B_c D_p J_2 D_c \end{bmatrix},$$

$$C_2 = \begin{bmatrix} -C_p + D_p J_2 D_c C_p & -D_p J_2 C_c \end{bmatrix}, \quad D_2 = -D_p J_2 D_c,$$

$$\bar{A}_3 = \begin{bmatrix} A_p & 0 & B_p u_M \\ -B_c C_p & A_p & -B_c D_p u_M \\ 0 & 0 & 0 \end{bmatrix}, \quad \bar{B}_3 = \begin{bmatrix} 0 \\ B_c \\ 0 \end{bmatrix} - \bar{\Lambda} \begin{bmatrix} 0 \\ D_c \\ 0 \end{bmatrix},$$

$$\bar{C}_3 = \begin{bmatrix} C_p & 0 & D_p u_M \end{bmatrix}, \quad \bar{D}_3 = 0,$$

$$\bar{\Lambda} = \begin{bmatrix} 0 & 0 & 0 \\ 0 & \Lambda_1 (I + \Lambda_2)^{-1} & 0 \\ 0 & 0 & 0 \end{bmatrix}$$

$$\bar{J}_1 = \begin{bmatrix} 0 & 0 & 0 \\ D_c D_p & -C_c & u_m + D_c D_p u_m \\ 0 & 0 & 0 \end{bmatrix}$$

$$J_2 = (I + D_c D_p)^{-1}$$

$$\bar{J}_3 = \begin{bmatrix} 0 & 0 & 0 \\ D_c D_p & -C_c & u_M + D_c D_p u_M \\ 0 & 0 & 0 \end{bmatrix}$$

The Obtained Piecewise Quadratic Lyapunov Function

$$\bar{P}_1 = \begin{bmatrix} 27.1175 & -7.8885 & -69.9081 & 1.0217 & 2.5541 \\ -7.8885 & 13.5924 & 65.9505 & 2.6048 & 6.5120 \\ -69.9081 & 65.9505 & 439.1050 & -2.2092 & -5.5230 \\ 1.0217 & 2.6048 & -2.2092 & -0.5597 & -1.3992 \\ 2.5541 & 6.5120 & -5.5230 & -1.3992 & -3.4979 \end{bmatrix}$$

$$P_2 = \begin{bmatrix} 28.9654 & -3.1184 & -73.8381 \\ -3.1184 & 25.7025 & 55.5776 \\ -73.8381 & 55.5776 & 447.2053 \end{bmatrix}$$

$$\bar{P}_3 \begin{bmatrix} 27.1175 & -7.8885 & -69.9081 & 1.0217 & -2.5541 \\ -7.8885 & 13.5924 & 65.9505 & 2.6048 & -6.5120 \\ -69.9081 & 65.9505 & 439.1050 & -2.2092 & 5.5230 \\ 1.0217 & 2.6048 & -2.2092 & -0.5597 & 1.3992 \\ -2.5541 & -6.5120 & 5.5230 & 1.3992 & -3.4979 \end{bmatrix}$$

References

Åström, K. J. and B. Wittenmark (1997): *Computer-Controlled Systems*. Prentice Hall.

DeCarlo, R. A., M. S. Branicky, S. Pettersson, and B. Lennartson (2000): "Perspectives and results on the stability and stabilizability of hybrid systems." In *Proceedings of IEEE*, pp. 1069 – 1082.

Grimm, G., I. Postlethwaite, A. Teel, M. Turner, and L. Zaccarian (2001): "Linear Matrix Inequalities for full and reduced order anti-windup synthesis." In *Proceedings of the American Control Conference*, pp. 4134–4139.

Hassibi, A. and S. Boyd (1998): "Quadratic Stabilization and Control of Piecewise-Linear Systems." In *Proceedings of the American Control Conference*, pp. 3659 – 3664.

Johansson, M. (1999): *Piecewise Linear Control Systems*. PhD thesis ISRN LUTFD2/TFRT--1052--SE, Department of Automatic Control, Lund Institute of Technology, Sweden.

Johansson, M. and A. Rantzer (1998): "Computation of piecewise quadratic Lyapunov functions for hybrid systems." *IEEE Transactions on Automatic Control*, **43:4**, pp. 555 –559.

Khalil, H. K. (1992): *Nonlinear Systems*. MacMillan, New York.

Mulder, E. F. and M. Kothare (2000): "Synthesis of stabilizing anti-windup controllers using piecewise quadratic lyapunov functions." In *Proceedings of the Amercian Control Conference*.

Mulder, E. F. and M. Kothare (2001): "Multivariable anti-windup controller synthesis using Linear Matrix Inequalities." *Automatica*.

Rugh, W. J. and J. S. Shamma (2000): "Research on gain scheduling." *Automatica*, pp. 1401 – 1425.

Solyom, S. (2003): "A synthesis method for static anti-windup compensators." In *Proceedings of the European Control Conference, ECC03*. Cambridge, UK.

Solyom, S. and A. Rantzer (2002): "The servo problem for piecewise linear systems." In *Proceedings of the Fifteenth International Symposium on Mathematical Theory of Networks and Systems*. Notre Dame, IN.

Teel, A. R. and N. Kapoor (1997): "The $\mathcal{L}_2$ anti-windup problem: Its definition and solution." In *Proceedings of the European Control Conference*.

Turner, M. C. and I. Postlethwaite "A new perspective on static and low order anti-windup synthesis." *To be published*.

Weston, P. F. and I. Postlethwaite (1998): "Analysis and design of linear conditioning schemes for systems containing saturating actuators." In *IFAC Nonlinear Control System Design Symposium*.

Zhou, K. and J. C. Doyle (1998): *Essentials of Robust Control*. Prentice Hall.

5

Voltage Stability Control in Power Systems

This chapter aims at the study of voltage stability in power systems. A simple model of a power system will be considered and analyzed. In addition, a hybrid control law will be derived that is shown to improve the stability properties of the considered power grid.

5.1 Power Systems

Modern day society requires a large amount of electrical energy. It is the backbone of our technological society.

A power system consists of several electrical components (e.g. generators, transmission lines, loads) connected together, its purpose being generation, transfer and usage of electrical power. Power systems are referred to as the largest machines built by man. Geographically they stretch over entire continents including hundreds of generators and millions of consumers.

Currently, most of the electrical energy is obtained from fossil fuels (e.g. coal, oil). Renewable energy resources such as hydro, solar, wind are used to lesser extent. However, environmental issues force a continuously growing use of the latter resources.

An important feature of electrical energy is that it cannot easily be stored in large quantities. This basically means that at any instant in time the energy demand has to be met by corresponding generation. This is a difficult task if no prediction of the consumption is available. Although the connected users, loads, are of different types and capacity, and some can vary quite rapidly and unpredictably, the combined load pattern of a power system normally changes in a relatively predictable manner. This predictable demand governs the daily generation schedule [Machowski

et al., 1997].

In case of special events in the network such as faults or sudden increase of power demand, the balance between the generation and consumption can be easily disturbed. Such disturbances can lead to catastrophic consequences, such that major parts of the grid can be lost. In the year 2003 the US, Sweden and Italy suffered major blackouts.

The Structure of a Power System

Conventionally, the basic structure of a power system consists of three parts: generation, transmission, and distribution [Machowski *et al.*, 1997].

- *Generation:* electrical energy is obtained by converting mechanical energy from the output shaft of a turbine. The mechanical energy is obtained from fossil or non-fossil fuels. The generator produces energy at 10–20 kV. However, this voltage is increased by an order of magnitude before transmission.
- *Transmission:* The produced electrical energy is usually transmitted on long distances to the load centers. The energy losses are proportional to the current squared, and to minimize the losses, the transmission lines operate at high or very high voltages ($100-1000$ kV). The transmission network is usually connected in a meshed structure such that many possible routes are available from a generating point to a costumer. This structured adds to the flexibility and redundancy of the grid.
- *Distribution:* As the electrical energy is getting closer to the load center, it is taken over by the distribution network. This network has usually a radial structure as opposed to the transmission system. Finally, before the end-user is connected to the network, the voltage is transformed to lower values as requested by the consumer.

Usually, 8% of the produced energy is lost through the transmission and distribution systems from the generator to the consumer.

Transformers

One of the most important components in power networks is the transformer. It is used to connect different parts of the network that are operating at different voltage levels. The transformers are equipped with taps, in order to adjust the transformation ratio. Moreover, since the power demands of the load are continuously changing, the transformers are equipped with *tap changers* to adjust the transformed voltages. The tap changing at distribution level is typically automatic and it aims to keep the voltage at a desired level.

The tap changing facilities can be made to operate either off-load or on-load. That is, the off-load tap changer requires the transformer to be de-energized while the tap changing takes place. The *on-load tap changer (OLTC)* can change the taps while the transformer is energized. OLTCs are one of the control elements used in a power network.

The Load

In a mature power system there can be millions of loads connected to the grid simultaneously. These loads have different characteristics and capacities. In addition, some loads will connect and disconnect in an unpredictable manner (e.g. household consumers).

These factors make it difficult to build a good model of the aggregate load connected to the grid. Within the power system community, there is a considerable effort put into modeling of aggregate loads and identification of existing models.

Load models are important both for analysis and synthesis of power systems. One of the major research areas where load modeling is important is that of voltage stability of power systems.

5.2 Stability of Power Systems

Due to the complexity of a power system, instabilities can be manifested in different ways. In general, *power system stability* can be defined as the property of the power system that enables it to remain in a state of equilibrium under normal operating conditions and to regain an acceptable state of equilibrium after being subject to a disturbance [Kundur, 1993].

Power system stability can be categorized in *angle stability* and *voltage stability*.

Angle Stability

The generation of electrical power in a power system relies on synchronous machines. A necessary condition for satisfactory system operation is that all synchronous machines in the network remain in synchronism. Traditionally, the stability of power system treated the problem of maintaining synchronous operation. This is the so called angle stability problem. An important factor in angle stability problems is the relationship between the power interchange and angular position of the rotors of synchronous machines. This relationship is highly nonlinear being most of the time the principal cause for this kind of instabilities.

Voltage Stability

Instability in power system may also appear without loss of synchronism. One such instability scenario is the collapse of load voltage.

Voltage at the load end of a power system has to be controlled within prescribed tolerances, to guarantee a satisfactory voltage for the consumers. Even in case of normal operation, this task is not trivial due to the ever-changing load conditions. Moreover, in case of emergencies this task can be very difficult and sometimes impossible.

Voltage stability of a power system is defined by the IEEE Power System Engineering Committee as being *the ability of the system to maintain voltage such that when load admittance is increased, load power will increase so that both power and voltage are controllable*. A voltage collapse is defined as being the process by which voltage instability leads to a very low voltage profile in a significant part of the system [IEEE, 1990; Begovic *et al.*, 2001].

Voltage stability in power networks is a widely studied problem. Several voltage collapses resulting in system-wide blackouts made this problem of major concern in the power system community.

The voltage dynamics in power systems appear on two time scales. The short-term dynamics act on a time scale of seconds or shorter (e.g. effect of generator excitation control). The long-term dynamics are on a scale of minutes (e.g. effect of recovery dynamics in heating loads, effect of tap changers). In the latter category falls the effects of the OLTC, the main control tool considered in this work, for improving stability of the power system.

It is accepted that voltage instability is caused by the load characteristics, as opposed to the angular instability, which is caused by the rotor dynamics of the generators [Begovic *et al.*, 2001]. It is also known that voltage instability is closely related to the maximum loadability of the transmission network [Julian *et al.*, 2000]. The closer the power transmitted by the system is to its maximum transferable power, the risk of voltage collapse increases. However, it has been established that voltage instability can not be attributed solely to such static arguments. Voltage instability is a dynamic phenomenon [Hill, 1993].

The major concern of this work is the situation when in stationarity the load power request does not exceed the maximum loadability of the network. However, voltage collapse occurs due to some dynamic effects in the load and tap-changer. This phenomenon will be presented in more detail in Section 5.4.

Although it is natural to call this instability phenomenon *dynamic instability*, the author refrains from this designation. The reason is that in the power system community, the term dynamic instability has been used

in the context of angle stability. In addition, the term has been used quite inconsistently denoting for different authors different aspects of the angle stability, causing much confusion. Therefore, whenever the instability phenomenon in question arises, it will be designated as *instability due to dynamic effects*.

5.3 Previous and Related Work

By now there is an extensive literature on analysis of voltage stability in power systems. There exist both static and dynamic approaches which are more or less mathematically involved.

As the load characteristics is important for voltage stability studies, considerable effort has been put into developing aggregate load models.

In the following some of the most well known models and analysis approaches will be summarized [Machowski *et al.*, 1997].

Load Models

Due to high diversity of the existing loads and the purpose of their modeling, several alternatives of load models have been proposed. Generically they can be split in two groups, static models and dynamics models.

Static Load Models A traditional way of describing aggregate loads is by static models. In the following, two of the most popular static load models will be presented.

- **ZIP model.** This model is a linear combination of three sub-models: constant impedance (**Z**), constant current (**I**), and constant power (**P**). For a constant impedance load, the load power changes proportionally with the square of the voltage. A constant current model gives a power demand that is linearly dependent on the voltage. In the case of a constant power load, the model is voltage independent and describes a system with power demand that does not depend on voltage (so called *stiff load*).

$$P = P_0 \left(a_1 \left(\frac{V}{V_0} \right)^2 + a_2 \left(\frac{V}{V_0} \right) + a_3 \right)$$

$$Q = Q_0 \left(a_4 \left(\frac{V}{V_0} \right)^2 + a_5 \left(\frac{V}{V_0} \right) + a_6 \right)$$

  P_0, Q_0, V_0 are values at initial operating conditions and a_{1-6} are model parameters.

- **Exponential load model.** These models are of the form:

$$P = P_0 \left(\frac{V}{V_0} \right)^{n_p}$$
$$Q = Q_0 \left(\frac{V}{V_0} \right)^{n_q}$$

where n_p, n_q are parameters of the model. Notice that by setting the parameters to 2, 1, and 0, one obtains constant impedance, constant current, and constant power models, respectively.

Dynamic Load Models In most of the voltage stability studies, static load models can not capture, explain the behavior of the power system. In these situations, dynamic load models are required.

One of the most popular load models for voltage stability studies is an exponential dynamic load model of the form:

$$\begin{aligned}
\dot{x}_p &= -\frac{x_p}{T_p} + P_0 \left(\left(\frac{V}{V_0} \right)^{a_s} - \left(\frac{V}{V_0} \right)^{a_t} \right) \\
\dot{x}_q &= -\frac{x_q}{T_q} + Q_0 \left(\left(\frac{V}{V_0} \right)^{b_s} - \left(\frac{V}{V_0} \right)^{b_t} \right) \\
P &= \frac{x_p}{T_p} + P_0 \left(\frac{V}{V_0} \right)^{a_t} \\
Q &= \frac{x_q}{T_q} + Q_0 \left(\frac{V}{V_0} \right)^{b_t}
\end{aligned} \tag{5.1}$$

where in addition to the static exponential load model the following variables are introduced: x_p, x_q are the active and reactive power recovery, T_p, T_q are time constants of the dynamic model, a_s, b_s are the steady state active and reactive load-voltage dependence, a_t, b_t are the transient active and reactive load-voltage dependence. This model has been introduced in [Karlsson and Hill, 1994], together with an identification method for the variables in question.

Voltage Stability in Power Networks

The analysis methods used in voltage stability studies can be classified in two groups: static methods and dynamic methods. In the static methods, the analysis is carried out using steady state models. This problem is closely related to the ability of the network to transfer the power demand of the load [Schlueter *et al.*, 1990]. Here can be included the work done on the VIP (voltage instability predictor) method [Begovic and Novosel,

2002], [Julian *et al.*, 2000]. This method devises a measure for critical operation of the power system. In [Vu and Novosel, 2001] this method is used for devising control actions when the system arrives in a critical operating regime.

The other approach for stability analysis is dynamic, where also the dynamic evolution of the voltage is examined. In [Zaborszky and Baohua, 1989] dynamic analysis together with bifurcation theory is used to analyze the behavior of a simple power system. This article models the power system with a differential-algebraic equation (DAE).

An illustrative use of both static and dynamic analysis approaches is given in [Morison *et al.*, 1993].

In [Vu and Liu, 1992], dynamic analysis is carried out using a simple dynamic reactive-load model. For this model, the region where the power system is guaranteed to maintain voltage stability is explicitly given. Based on this stability region, control actions are also proposed.

Bifurcation theory is a popular tool in the analysis of power systems. In [Rosehart and Cañizares, 1999] it is used for the analysis of different load models. Bifurcation theory is used also for control synthesis. In [Shahrestani and Hill, 2000] a multilevel nonlinear control scheme is proposed. Here the state space is divided in operating regions. Bifurcation analysis is used for establishing the bounds of the regions with different control requirements.

In [Guo *et al.*, 2000], robust backsteping is used for the synthesis of decentralized controllers for a large scale power systems.

5.4 Problem Description

The considered power system is shown in Figure 5.1. It is a radial system containing a generator E, a transmission line with impedance $\tilde{Z}_{LN}$, a transformer with an on-load tap changer (OLTC) and a load with impedance $\tilde{Z}_{LD}$. The system can be thought of as having two nodes, generation (i.e. the generator source) and consumption (i.e. the load). The on-load tap changer regulates the voltage on the load side at a desired value V_{ref}. In a power system, the loads have a built-in control system that tries to achieve some control objective. Usually this control objective is to keep the absorbed power at a given value. In turns this means that the load will dynamically change its impedance.

For ease of reference a list of used variables is compiled below:

- $\tilde{Z}_{LD} = Z_{LD}e^{j\Phi}$ – load impedance,
- $\tilde{Y}_{LD} = 1/\tilde{Z}_{LD}$ – load admittance,

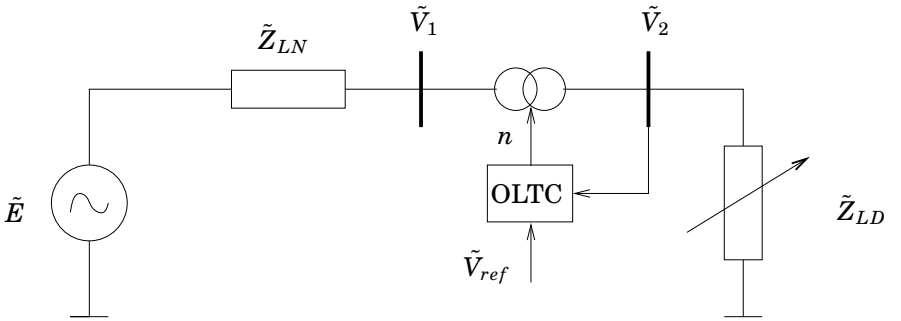

Figure 5.1 The considered two-node system with generator, transmission line, transformer, and load.

- $\tilde{Z}_{LN} = Z_{LN}e^{j\Theta}$ – transmission line impedance,
- $\tilde{E} = Ee^{j0}$ – generator voltage,
- $\tilde{V}_1$ – voltage on the primary side of the transformer,
- $\tilde{V}_2$ – voltage on the secondary side of the transformer,
- n – transformer ratio,
- V_{ref} – reference voltage,
- $\tilde{I}_1$ – current in the primary winding of the transformer,
- $\tilde{I}_2$ – current in the secondary winding of the transformer

The system in Figure 5.1 models a very simple power system. Nevertheless, it will be shown that the system captures some of the major instability behaviors of a power system.

Mathematical Modeling – The Two-Node System

In the following, mathematical models will be developed for the study of voltage stability in power systems.

Consider at first a system without dynamics in the load and without the OLTC control system.This simplification is useful to understand the underlying structure and behavior of the system.

Using basic circuit theory, the following relations can be stated [Kun-

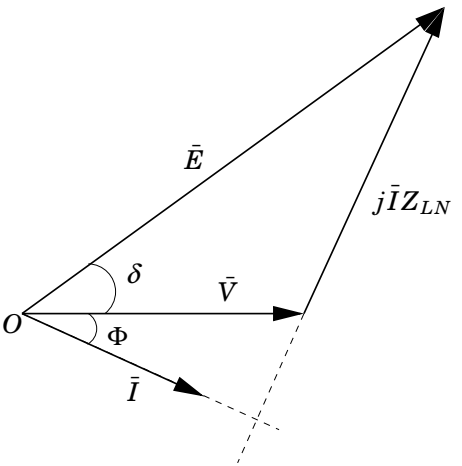

Figure 5.2 Phasor diagram for the considered power system.

dur, 1993]:

$$\frac{\tilde{V}_2}{\tilde{V}_1} = \frac{\tilde{I}_1}{\tilde{I}_2} = n \tag{5.2}$$

$$\tilde{E} = \tilde{I}_1\tilde{Z}_{LN} + \tilde{V}_1 = \tilde{I}_2\left(n\tilde{Z}_{LN} + \frac{1}{n}\tilde{Z}_{LD}\right) \tag{5.3}$$

$$P = |\tilde{I}_2^2\tilde{Z}_{LD}|\cos\Phi = E^2\underbrace{\frac{Z_{LD}/n^2}{\left|\tilde{Z}_{LN} + \tilde{Z}_{LD}/n^2\right|^2}}_{f(Z_{LD}/n^2)}\cos\Phi \tag{5.4}$$

$$Q = |\tilde{I}^2\tilde{Z}_{LD}|\sin\Phi = E^2\underbrace{\frac{Z_{LD}/n^2}{\left|\tilde{Z}_{LN} + \tilde{Z}_{LD}/n^2\right|^2}}_{f(Z_{LD}/n^2)}\sin\Phi \tag{5.5}$$

$$V_2 = |\tilde{I}_2\tilde{Z}_{LD}| = E\frac{Z_{LD}/n}{\left|\tilde{Z}_{LN} + \tilde{Z}_{LD}/n^2\right|} \tag{5.6}$$

To further simplify the studied problem, consider at first only the case when $n = 1$. This will imply $\tilde{V}_2 = \tilde{V}_1 = V$ and $\tilde{I}_2 = \tilde{I}_1 = I$.

Using phasor representation, the considered system is described by the phasor diagram shown in Figure 5.2. The angle between the voltage and the current on the load side is Φ, while the angle between the voltage at the generation node and the load is δ.

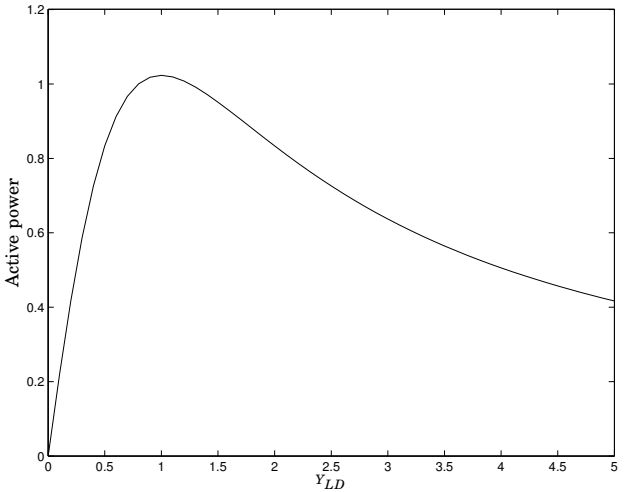

Figure 5.3 Active power with respect to load impedance. For a particular impedance the transfered active power reaches a maximum.

The function $f(Z_{LD})$ is a nonlinearity with a particular structure. This nonlinearity gives the typical shape of the active power with respect to the load admittance (see Figure 5.3). It is predominantly linear for small load admittance and will increase up to a value where the transfered active power reaches its maximum. For higher load admittance the transfered active power will gradually decrease.

By further algebraic manipulations, the function f can be expressed as:

$$f(Z_{LD}) = \frac{Z_{LD}}{Z_{LD}^2 + 2Z_{LD}Z_{LN}\cos(\Theta - \Phi) + Z_{LN}^2}$$

Taking the derivative of f with respect to Z_{LD}, gives the expression:

$$f'(Z_{LD}) = \frac{Z_{LN}^2 - Z_{LD}^2}{\left(Z_{LD}^2 + 2Z_{LD}Z_{LN}\cos(\Theta - \Phi) + Z_{LN}^2\right)^2}$$

This gives that the maximum active power transfer (i.e. the top of the function f) is obtained for

$$Z_{LD} = Z_{LN}. \tag{5.7}$$

Thus the value of the maximum transferable active power is,

$$P_{max} = \frac{E^2}{2Z_{LN}(1 + \cos(\Theta - \Phi))}\cos\Phi. \tag{5.8}$$

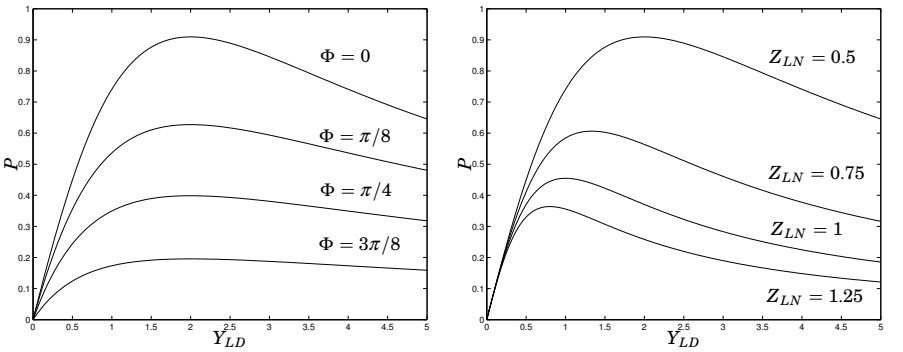

Figure 5.4 Active power with respect to load impedance. In the left plot the power factor $\cos\Phi$ is varied and $Z_{LN} = 0.5$. Notice that the bigger the power factor is, the higher the transferable maximum active power becomes. In the right plot, the line impedance is varied while $\cos\Phi = 1$. Observe that the smaller the line impedance is the higher the transferable maximum active power becomes.

Similarly, the maximum reactive power to be transmitted through the line is

$$Q_{max} = \frac{E^2}{2Z_{LN}(1+\cos(\Theta-\Phi))}\sin\Phi. \tag{5.9}$$

It is interesting to notice that the argument of the load (Φ) will influence only the value of the maximum active power and not the actual admittance for which this will happen. However, Φ will change also the function f, that is the dependence of the active power with respect to the load. Figure 5.4 shows the active power for different Φ in a system with $E = 1$, $\Theta = 10$, $Z_{LN} = 0.5$. The plot clearly shows that the maximum active power that can be transfered is proportional to the power factor $\cos\Phi$. Notice that the maximum active power is achieved at $Y_{LD} = 1/Z_{LN} = 2$, in each of the four cases of the power factor. In the right plot of Figure 5.4 the line impedance is varied. The behavior of the curve is similar to that of varying $\cos\Phi$. However, in this case the higher the line impedance is the smaller the transferable active power becomes.

From voltage stability point of view it is of increasing interest to study the relation between the voltage on the load side and the transfered power. From (5.6) the load admittance is obtained as:

$$Y_{LD} = \frac{-V\cos(\Theta-\Phi) \pm \sqrt{V^2\left(\cos(\Theta-\Phi)^2-1\right)+E^2}}{Z_{LN}V},$$

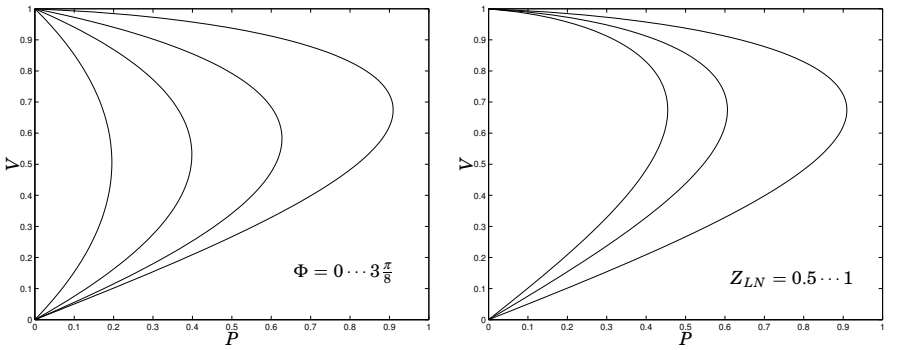

Figure 5.5 Active power with respect to load voltage. In the left plot Φ is varied taking the values $0, \pi/8, \pi/4, 3\pi/8$. The bigger the power factor is, the higher the transferable maximum active power becomes. In the right plot, the line impedance takes the values $Z_{LN} = 0.5, 0.75, 1$.The bigger the line impedance is, the smaller the transferable maximum active power becomes.

and thus:

$$P = \frac{-V^2 \cos(\Theta - \Phi) \pm V\sqrt{V^2\left(\cos(\Theta - \Phi)^2 - 1\right) + E'^2}}{Z_{LN}} \cos\Phi.$$

The positive, real values of P give an important connection betwen the active power and the load voltage. This relationship is commonly used in the power system community, under the name of P-V curve or "nose curve" (see Figure 5.5). The power factor has an important influence on this relationship, i.e. the higher the power factor is the higher the maximum active power becomes. This maximum point can be further increased for lead power factors, by injecting reactive power into the system (i.e. using capacitor banks). However, this will make the system more sensible to disturbances.

The P-V curve reveals another important property, from the graphical representation. It can be easily seen that a given power can be transfered at two different voltages. This property will have an increased importance when dynamic loads will be considered.

In a similar fashion, variations of Z_{LN} will result in changes in the P-V curve and the maximum transferable power. The larger Z_{LN} becomes, the smaller the maximum transferable power is (see Figure 5.5).

The transformation ratio n introduces another degree of freedom in the system that helps to deliver the requested power at a specific voltage. The above presented analysis can be carried out in a similar fashion. An easy way to introduce the transformer ratio in the analysis is by interpreting

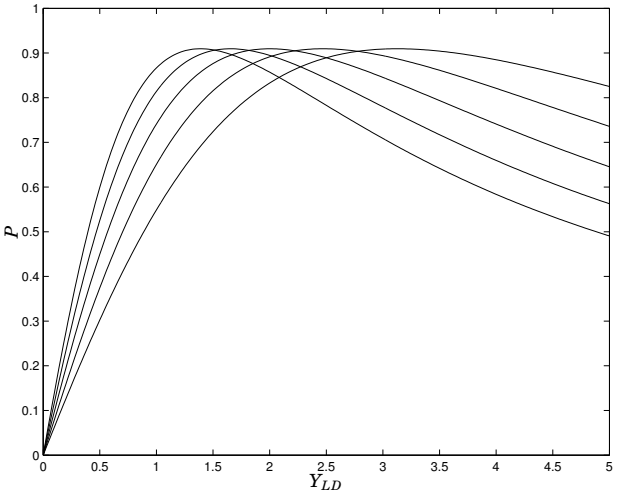

Figure 5.6 Active power with respect to load impedance for transformer ratios n ranging between 0.8 and 1.2 with an increment of 0.1. Notice that the maximum active power remains constant while the coordinate of maximum power transfer $Y_{LD} = 1/(n^2 Z_{LN})$ changes.

Z_{LD}/n^2 as an apparent load impedance as seen through the transformer. This gives:

$$f(Z_{LD}/n^2) = \frac{Z_{LD}}{Z_{LD}^2/n^2 + 2Z_{LD}Z_{LN}\cos(\Theta - \Phi) + Z_{LN}^2 n^2} \tag{5.10}$$

and the maximizer of this function is:

$$Z_{LN} = \frac{Z_{LD}}{n^2} \tag{5.11}$$

However, the maximum transmitted power remains the same as in (5.8) and (5.9). Figure 5.6 shows the active power for transformer ratios n between 0.8 and 1.2 with an increment of 0.1. The system parameters are $E = 1$, $\tan\Theta = 10$, $Z_{LN} = 0.5$, $\cos\Phi = 1$. Notice that the coordinate of the maximum active power changes according to equation (5.8).

The load voltage V_2 also has an interesting dependence on the load impedance and the transformer ratio n. Figure 5.7 is obtained from equation (5.6) for $n = 0.8, 1, 1.2$. The point of intersection for two curves with transformer ratios n_1 and n_2 can be found by equating:

$$f(Z_{LD}/n_1^2) = f(Z_{LD}/n_2^2) \tag{5.12}$$

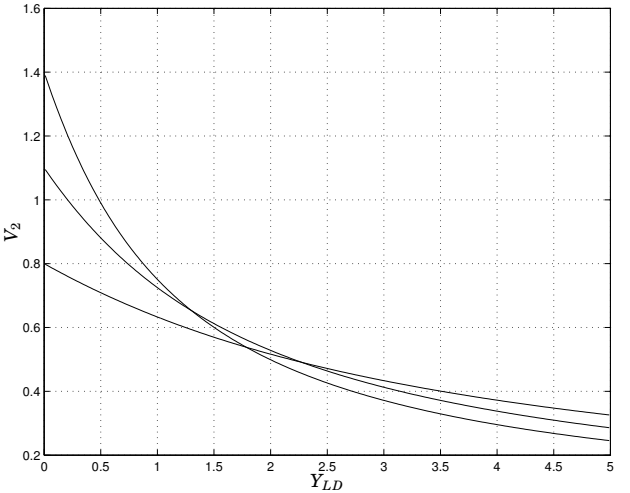

Figure 5.7 Load voltage with respect to load impedance for transformer ratios $n = 0.8, 1, 1.2$. For two curves with transformer rations n_i and n_j the intersection point is given by $n_i n_j Y = 1/Z_{LN}$. After this value of the load admittance the effect of increasing n is reversed.

which gives the second order equation:

$$Y_{LD}^2(n_1^2 - n_2^2)Z_{LN}^2 + \frac{1}{n_1^2} - \frac{1}{n_2^2} = 0$$

with the positive solution satisfying:

$$n_1 n_2 Y_{LD} = \frac{1}{Z_{LN}} \tag{5.13}$$

As Figure 5.7 reveals, after the point of intersection of two curves the effect of increasing n is reversed. This means that if the load admittance is greater then $1/(Z_{LN}n_1n_2)$ then increasing the transformer ratio from n_1 to n_2 will have inverse effect (i.e. the load voltage will be decreased). Naturally, this behavior has a major impact on control of load voltage as it will be shown later. This phenomenon is the so called "reverse action" and has been discussed also in [Ohtsuki *et al.*, 1991].

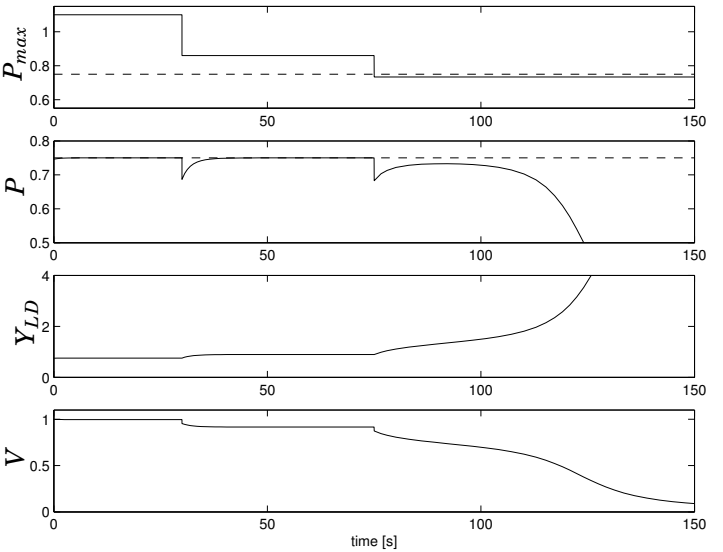

Figure 5.8 Simulation of a two-node system with recovery mechanism in the load. A fault is simulated at $t = 30$ by increasing the line impedance. The load is trying to achieve the desired active power 0.75 (dashed line) by decreasing its impedance. Since the maximum achievable active power is greater than 0.75, the system can achieve a stable equilibrium. At $t = 75$ the line impedance is further increased such that the achievable active power is just below 0.75. The system becomes unstable and the voltage collapses.

Two-Node system with Recovery in the Load

Consider now a time varying load. This variation is due to recovery mechanism embedded in the load. The simplest example for such dynamics is:

$$\dot{Y}_{LD} = P_{ref} - P = P_{ref} - E^2 \frac{Z_{LD}}{\left|\tilde{Z}_{LN} + \tilde{Z}_{LD}\right|^2} \cos\Phi. \tag{5.14}$$

That is, the load tries to absorb a desired active power by modifying its own impedance. Y_{LD} is the absolute value of the load admittance, i.e. $Y_{LD} = 1/Z_{LD}$. According to this adaptation law, the load will decrease its impedance at an increase in power demand or load voltage drop.

Simulation results for the above model are shown in Figure 5.8. The variables in the plot are the maximum transferable active power, the transfered active power, the load admittance and the load voltage. The simulation starts when the system is at rest, with transfered active power at 0.75 and load voltage at nominal value.

In this scenario the load is trying to absorb an active power of 0.75 (dashed line). The initial value for the line impedance is 0.5. At $t = 30$ a fault is simulated in the line by changing its impedance to 0.75. As shown in the figure, this implies that the maximum power that can be transferred through the line will drop to a value above 0.75. The load tries to absorb the desired active power by reducing its impedance. After a transient the system will attain a new equilibrium point at a lower voltage level. At $t = 75$ the line impedance is further increased to 0.75. This will have as effect the decrease of P_{max} to a value just below 0.75. Thus the load tries to absorb an active power that can not be maintained by the network and the system ends up in a voltage collapse. The other system parameters used in the simulation are $E = 1.1$, $\tan\Theta = 10$, and $\cos\Phi = 1$.

The load considered up to now controls the power to the requested level independently of the load voltage. These types of load are called *stiff loads*. These type of loads exert an increased stress on the power system and voltage instability phenomena can arise much easier.

Consider now a voltage dependent load. In particular consider a load that has its power reference depending on the load voltage. Take first the case of a quadratic dependence on the load voltage. Then the model becomes:

$$\dot{Y}_{LD} = P_{ref}V^2 - P = E^2 \frac{Z_{LD}}{\left|\tilde{Z}_{LN} + \tilde{Z}_{LD}\right|^2} \left(P_{ref}Z_{LD} - \cos\Phi\right) \tag{5.15}$$

Figure 5.9(a) shows simulation results for such loads, in the same scenario as before. At $t = 30$ a primary fault arises which will result in a voltage and active power drop. Since the load is not stiff, it will not demand the same power as before the fault. At $t = 75$ when $Z_{LN} = 0.75$ the stability of this system is maintained, however, the load voltage is further decreased.

It is apparent from the structure of equation (5.15) that once in stationarity, the load impedance is insensitive to line faults. On the other hand, there is no dynamic recovery of the active load power. This can be modeled by introducing constant current, constant power terms or both in the load, similarly to the ZIP model.

$$\begin{aligned}\dot{Y}_{LD} =& P_{ref}\left(a_1V^2 + a_2V + a_3\right) - P \\ =& E^2 \frac{Z_{LD}}{\left|\tilde{Z}_{LN} + \tilde{Z}_{LD}\right|^2} \left(a_1P_{ref}Z_{LD} - \cos\Phi\right) \\ &+ a_2E\frac{Z_{LD}}{\left|\tilde{Z}_{LN} + \tilde{Z}_{LD}\right|}P_{ref} + a_3P_{ref}\end{aligned} \tag{5.16}$$

Simulation results are shown in Figure 5.9(b). The simulation scenario

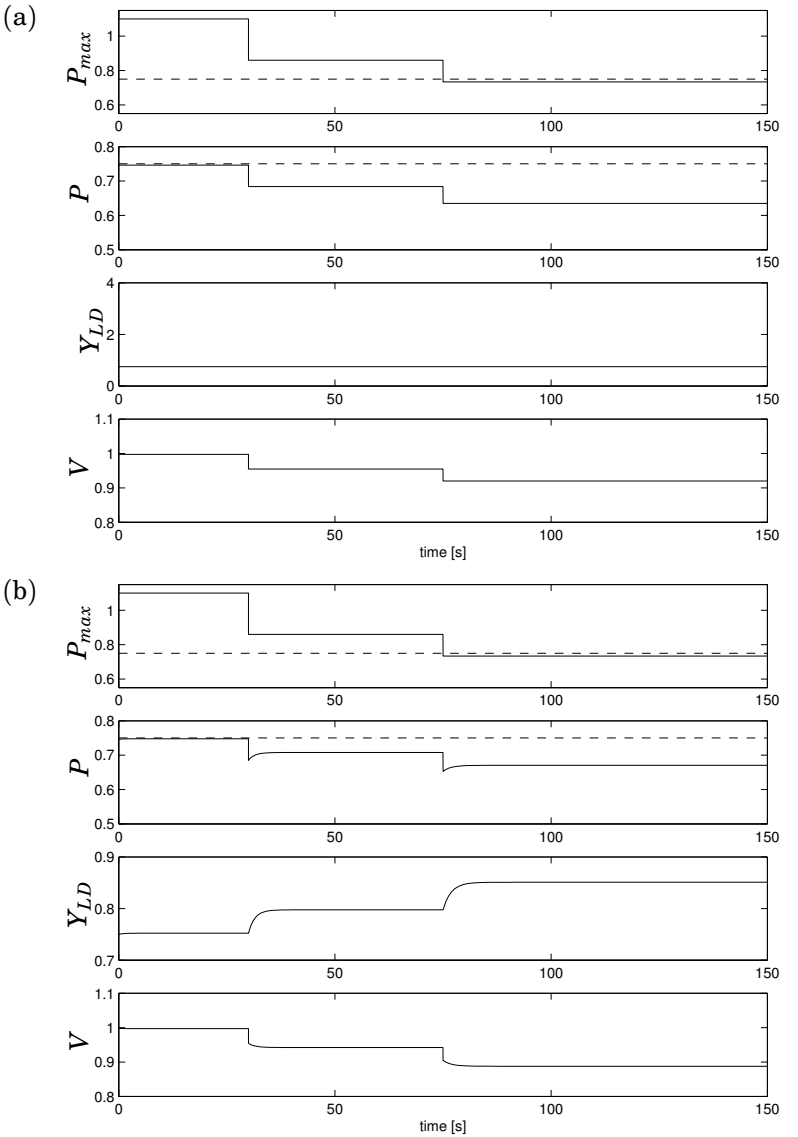

Figure 5.9 Simulation of a two-node system with recovery mechanism in the load. The load model is voltage dependent according to equation (5.15) in plot (a) respectively (5.16) in plot (b). A fault is simulated at $t = 30$ and $t = 75$ by increasing the line impedance. The load is trying to attain an active power equal to $P_{ref}V^2$ in (a) respectively $0.5(P_{ref}V^2 + P_{ref})$ in (b). Stability is maintained at load voltage levels below the nominal value.

is identical to those presented before. Notice the dynamic recovery of the active power at each simulated line fault. This type of behavior is similar to those obtained from experiments and measurements as reported in [Hill, 1993].

Two-Node System with Recovery in the Load and OLTC

Consider now also the OLTC control system dynamics included in the model. A common way to approximate the OLTC dynamics is by an integrator. Thus, for a constant Φ the model that describes our system becomes:

$$\begin{cases} \dot{Y}_{LD} = P_{ref} - P = P_{ref} - E^2 \dfrac{Z_{LD}/n^2}{\left|\tilde{Z}_{LN} + \tilde{Z}_{LD}/n^2\right|^2} \cos\Phi \\ \dot{n} = V_{ref} - V_2 = V_{ref} - E \dfrac{Z_{LD}/n}{\left|\tilde{Z}_{LN} + \tilde{Z}_{LD}/n^2\right|} \end{cases} \tag{5.17}$$

The OLTC will try to keep the load voltage at the desired level V_{ref}. Simulation results are shown in Figure 5.10. In this scenario the system is at rest with $E = 1.1$, $n = 1$, $V_2 = 1$, $Y_{LD} = 0.45$, $Z_{LN} = 1$. In plot (a) the reference active power is $P_{ref} = 0.45$ while in plot (b) $P_{ref} = 0.46$. At 10 seconds, a fault in the transmission network is simulated, increasing Z_{LN} by 20%. In plot (a), after a transient the requested power is restored as well as the load voltage is restored to its reference value. Notice that during the transient the $n^2 Y_{LD}$ had a significant increase, however it did not exceed $1/Z_{LN} \approx 0.83$, and the system recovers to a stable operating regime. In Figure 5.10(b), the same simulation had been carried out except that the desired active power was set to $P_{ref} = 0.46$. Before the fault to occur, the system is at equilibrium where both the desired power and the desired load voltage are achieved. However, following the fault in the transmission line, after an initial recovery, the system loses stability and voltage collapse occurs.

The same behavior can be observed for voltage dependent loads as long the OLTC is forcing the system back to the nominal voltage. However, in case there is a dead zone on the voltage control error, the voltage dependent loads can exhibit a “milder stress” on the network. Moreover, in case of real life systems, the tap changer has a limited number of steps, which bounds the achievable load voltage.

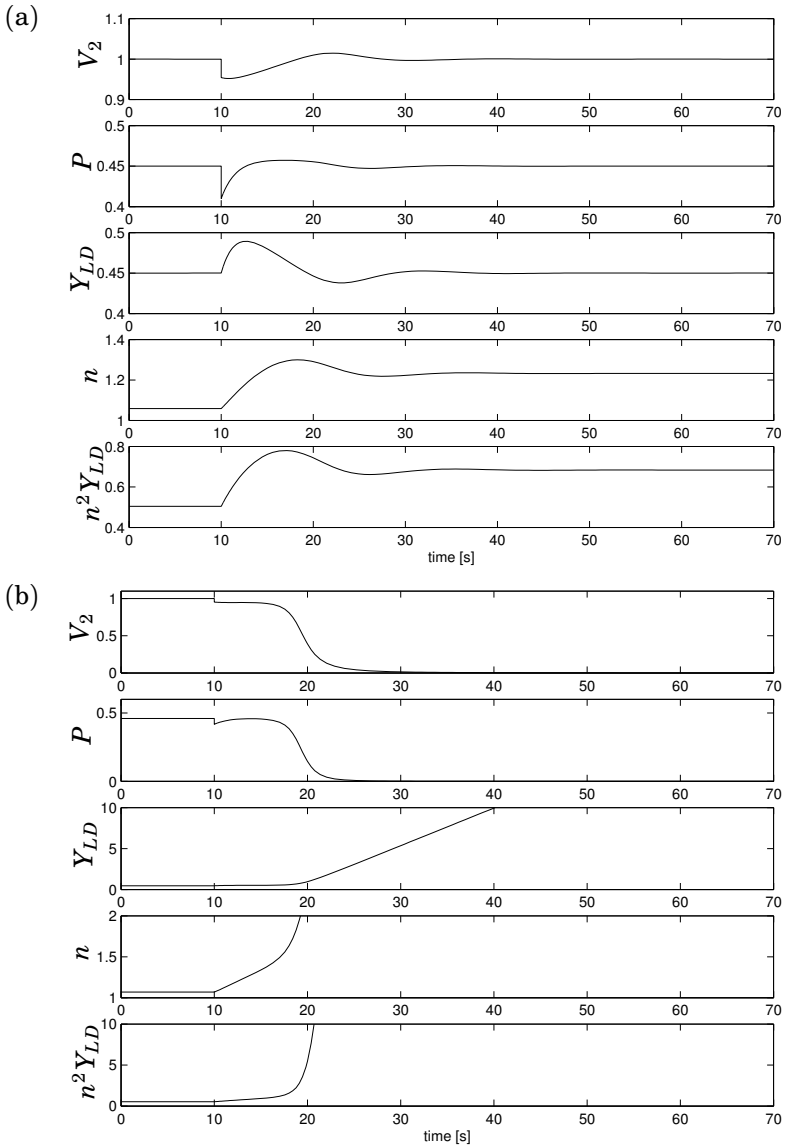

Figure 5.10 A two-node system with recovery mechanism in the load and OLTC. A fault is simulated at 10 seconds by increasing the line impedance by 20%. The load is trying to achieve the desired active power by decreasing its impedance. Without the OLTC system, the voltage V_2 would decrease. The OLTC system increases the voltage in the secondary side of the transformer. In plot (a) the desired active power is 0.45 and stability is maintained. In plot (b) the desired active power 0.46. After an initial recovery the system loses stability and voltage collapse occurs.

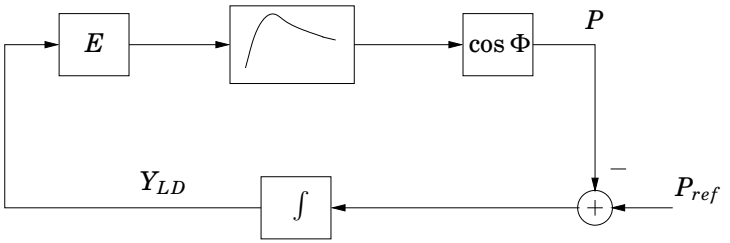

Figure 5.11 Block diagram for the model in equation (5.14). It is easily seen that the system can have multiple equilibria.

Stability of the Two-Node System

Consider first a two-node system without the OLTC but with dynamics in the load. The model in equation (5.14) can also be represented using the block diagram in Figure 5.11. It can be easily seen from the block diagram that the system can have multiple equilibria, one or no equilibrium point depending on the operating point.

Consider the scenario simulated in the previous section (Figure 5.8), in particular the case when the line impedance has been increased to 0.75. This lead to instability and voltage collapse. Figure 5.12 shows the active power with respect to load admittance respectively load voltage. In both plots the dashed line represents the desired active power. It is clear from the figure that there is no equilibrium point satisfying the system equations. This will clearly lead to instability. Such instability scenarios are commonly studied in the literature. They can be analyzed by static arguments and have clear connection to the maximum loadability of the network.

In case of voltage dependent load, the analysis is carried out in a similar manner. However, since $P_{ref}V^2$ is quadratic in V, in case of a line fault, the equilibrium point will change its location in a different manner (see Figure 5.13). The loci of the equilibrium point is now a quadratic function of V as in contrast to the stiff load where the equilibria are found on a line parallel to the voltage axis. This explains the "milder" behavior of the non-stiff loads.

As shown in the previous section, the tranformer ratio n does not change the total transferable active power. Thus the conclusions of the stability analysis will not change significantly when the dynamics of the OLTC is included in the system.

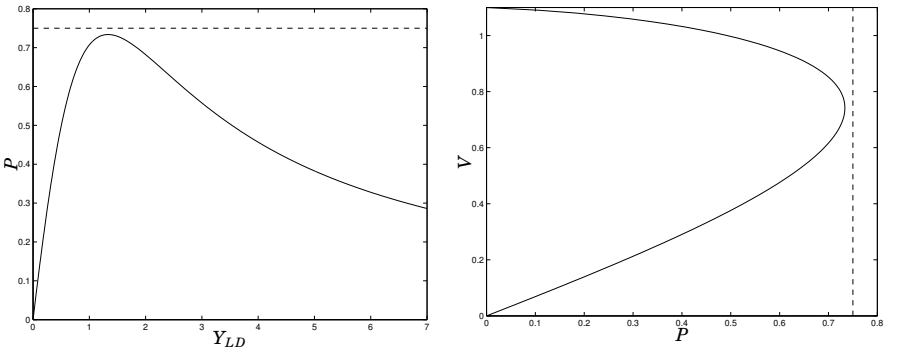

Figure 5.12 Active power with respect to load admittance (left) respectively normalized load voltage with respect to active power (right). There are no intersection points between the desired active power (dashed line) and the power characteristics, that is there are no real equilibrium points of the system. This will result in instability and voltage collapse.

Instability due to Dynamic Effects In the simulations in Figure 5.8, after the line fault occures, equilibrium is regained. This means that at least one stable equilibrium point exists. Figure 5.14 shows that there are two equilibrium points. In the active power vs. load admittance char-

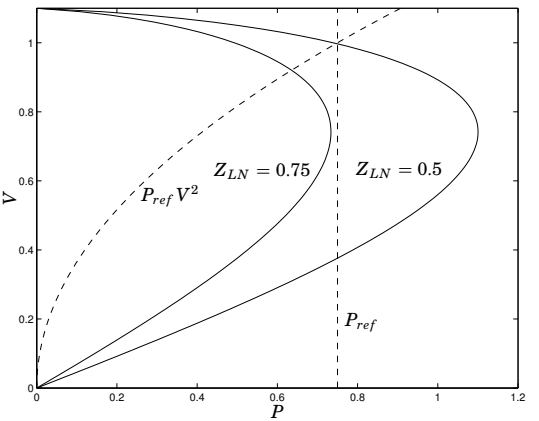

Figure 5.13 Active power with respect to load voltage for various line impedances. The quadratic characteristics $P_{ref}V^2$ corresponds to a voltage dependent load. Such loads will achieve a stable equilibrium point even when a stiff load will be unstable (dashed line).

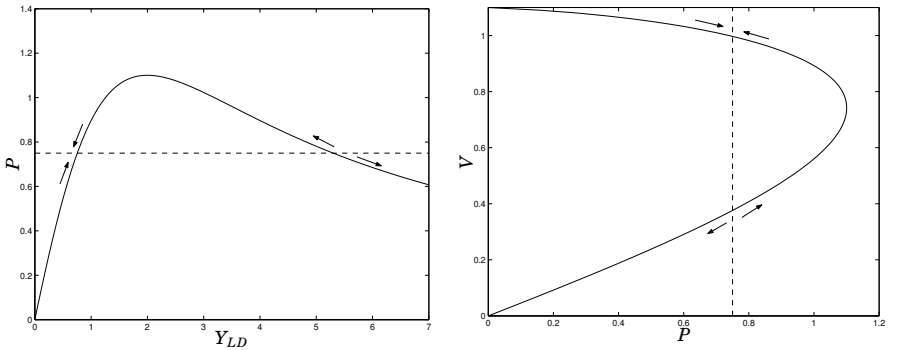

Figure 5.14 Active power with respect to load admittance (left) respectively load voltage (right). The intersection points between the desired active power (dashed line) and the power characteristics, gives the equilibrium points of the system. The equilibrium to the left of (respectively above) the peak of the characteristics is stable. The other is unstable.

acteristics the equilibrium point to the left of the peak is stable (this corresponds to the equilibrium point above the peak of the P-V curve). The other equilibrium point is unstable (the arrows in the figure indicate the derivative of the load admittance). One way to rigorously show this has been presented in Section 2.6. This structure, naturally give rise to situations when instabilities occur due to transients in the load admittance. If th load admittance increases such that the unstable equilibrium point is surpassed, the system ends up in voltage collapse. In this work, this phenomenon is referred to as *instability due to dynamic effects*.

Consider now the two-node system having dynamics both in the load and the OLTC. A convenient way to investigate the stability properties of this system is by inspecting the phase plot (see Figure 5.15). The qualitative behavior of this system is similar to the scalar case. Figure 5.15 shows the vector field near the two equilibrium points (marked with asterisks). The dashed line is given by the curve $n^2 Y_{LD} Z_{LN} = 1$, i.e. the loci of maximum power transfer (this happens if the line impedance and the load impedance are equal). As in the scalar case, one of the equilibrium points are stable (the one to the left of the dashed line) while the other one is unstable. A region of attraction of the stable equilibrium point, obtained by simulation is the shaded region in the figure.

Notice the unstable behavior to the right of the loci of maximum power transfer. From this point on, the region to the left of this curve is referred to as the stable region and the region to the right will be referred to as the unstable region. Obviously there is an abuse of language in these designations since from some small area of the unstable region the sys-

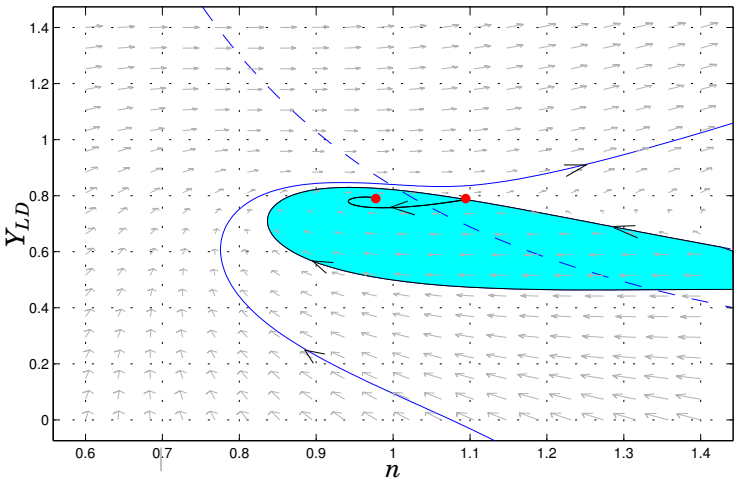

Figure 5.15 Vector field for the model (5.17). The dots mark the two equilibrium points. The dashed curve is the loci for maximum power transfer, $n^2 Y_{LD} Z_{LN} = 1$.

tem will return to the stable equilibrium point. Similarly from an area of the stable region the trajectories will escape to infinity. However, it is considered to be useful to differentiate between the region that contains the stable respectively unstable equilibrium point. This will be especially convenient in the controller synthesis section, where the loci of maximum power transfer will act as a natural switching surface between qualitatively different control actions.

In case of voltage dependent loads (Figure 5.16), the region of attraction of the stable equilibrium point can be considerably larger than in case of stiff loads. In such systems, dynamic instabilities can be compensated for much easier.

As shown above, even when the power network could, in stationarity, deliver the requested power, the system can still become unstable. The phenomenon that occurs is most suggestively shown in the phase-plot (Figure 5.15). Although a stable equilibrium point exists, some trajectories starting in the stable region, will escape to infinity. This practically means that there will be an overshoot in the equivalent load admittance $n^2 Y_{LD}$ such that the unstable equilibrium point on the nonlinear curve f is passed.

The main contribution of this chapter is a compensator that will reduce the risk for such instabilities to appear.

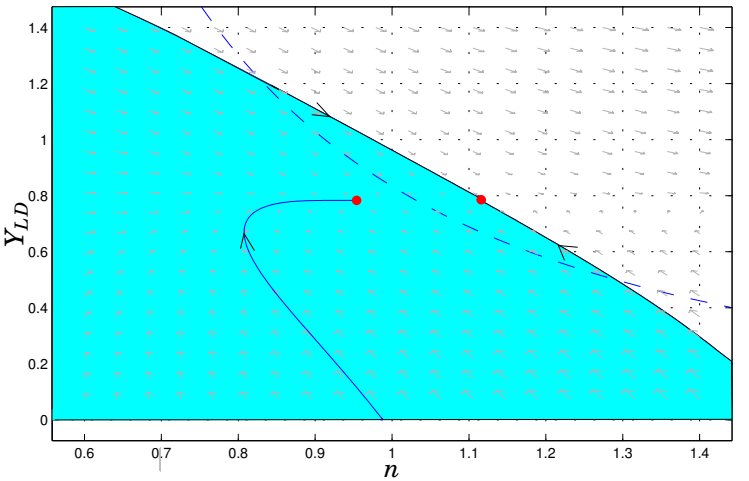

Figure 5.16 Vector field for the model (5.16), with $a_1 = 1$, $a_2 = a_3 = 0$. The dots mark the two equilibrium points. The dashed curve is the loci for maximum power transfer, $n^2 Y_{LD} Z_{LN} = 1$. Notice that the region of attraction of the stable equilibrium point is larger than for the stiff load.

5.5 Synthesis of an Emergency Load-Voltage Controller

As shown in the previous section, there are two main type of voltage instabilities:

1. The system is not able to transfer the requested active power. This corresponds to the situation when the system has no real equilibrium points.
2. Another instability scenario is when a stable equilibrium point exists, but where the system ends up in instability due to some transients.

In today's state-of-the-art practice it is mainly the first type of instability that is accounted for. The actions taken by the power company is usually one or both of the following:

1. Locking of tap-changers. It is typical to lock the tap-changer when the load voltage achieves a given lower threshold. This measure can in some cases restore stability of the power system. However, usually the operating point is at an unacceptable load voltage level [Larsson, 2000].
2. Connect capacitor banks, to increase the active power that can be

consumed by the load. If this is done in time, a voltage collapse can sometimes be avoided. A disadvantage of this method is that it makes the network more sensible to load variations.

3. Disconnect certain amounts of load (load shedding). This is a *very "expensive"* measure, and therefore avoided for as long as possible by the power company. However, this measure can prevent the whole power net from collapsing.

In the method proposed in this chapter, both types of instabilities are addressed. The proposed control scheme is supposed to act as an emergency controller that is activated in case of potentially dangerous situations.

Detection of Instabilities

An important part of a successful emergency-control strategy is detection of the potentially dangerous situations. In todays practice, the following methods are used to detect that the system is close to voltage instability:

1. As too much power is requested by the load, the generators will start using their rotational energy, implying that the frequency of the voltage (50/60 Hz) will start to decrease. Detecting a low frequency has been a too slow measure to stop the voltage collapse in for example Eastern US in 2003. On the other hand, as mentioned in the introduction, it is not always the case that significant frequency variations occur at the early stage of a voltage collapse phenomenon.

2. Another sign of instability is that the load voltage drops. However, it has been shown that neither this is a good measure for the instability of the grid. This can be specially misleading in case of a networks that have significant reactive compensation. Such situations are typical to occur when capacitor banks are connected to the load end of the system in order to increase the active power transfer limit. Figure 5.17 shows variations in the P-V curve when the aparent power factor is increased. The shaded region depicts typical, acceptable deviation limits from the nominal voltage. The distance from the tip of the curve to the peak of the P-V curve can be considered as a measure of the system robustness. In case of overcompensation, the lead power factor will move the tip of the curve closer to the normal operating region. This way the system is brought to a potentially dangerous operating regime.

It has been shown in the previous section that the loci of maximum active power (i.e. when $Z_{LD}/n^2 = Z_{LN}$) acts as a natural barrier between two qualitatively different behaviors of the system. Since the load

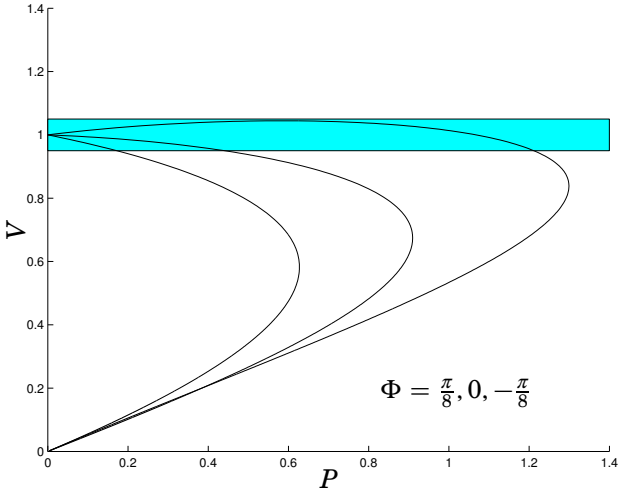

Figure 5.17 P-V curve for $\Phi = \pi/8, 0, -\pi/8$. The shaded region shows typical, acceptable deviation limits from the nominal voltage. Notice that in case of lead power factors, the normal operating region is close to the tip of the curve. This is a dangerous operating regime.

impedance can be computed from the measurements and the equivalent line impedance can also be considered measurable, it is natural to use the distance $Z_{LD}/n^2 - Z_{LN}$ as a measure of stability for the power network. This distance has been proposed as measure for stability in a power system also in [Julian *et al.*, 2000].

Structure of the Proposed Controller

As mentioned above, the proposed controller will deal with both instabilities caused by dynamics phenomena and also the inability of the network to transfer the power demand of the load. This way the controller can be split in two parts:

- **Compensation for dynamic effects**, is the part of the controller that compensates for dynamic instabilities.
- **Compensation for static effects**, increases the steady state transfer capability of the network by various methods (i.e. capacity bank coupling, load shedding).

The main contribution of this section is the compensator for dynamics effects. The two controllers can act both independently or in synchronization with each-other, that is either or both of the controllers can be added

to existing, state-of-the-art voltage control systems.

Compensation for Dynamic Effects

As mentioned before, this control structure is meant to operate in case of dynamic instabilities. This means that after a line and/or load impedance change (for example due to a line failure or an increase of power request from the load) the power grid is still statically capable of transferring the load power request.

A general method will be proposed that momentarily, changes the behavior of the OLTC when the line and/or load impedance changes such that the system is driven into the critical operation regime. Thus the used control variable is the transformation ration n.

As can be seen in Figure 5.15, it is desirable to move the system away from the unstable region above the stability limit marked by the dashed curve (by stability limit is meant that the stability measure $Z_{LD}/n^2 - Z_{LN} = 0$). Since the load dynamics cannot be changed (except by load shedding), the proposed method suggests to *momentarily alter the transformer ratio n so as to avoid the unstable region*. However, the transformation ratio n is not directly accessible for control purposes. Nevertheless, it is indirectly controllable by changing the voltage reference signal V_{ref}, that is accessible in the standard OLTC.

The compensator consists of two subsystems. The first subsystems is a feed-forward compensator and the second is a feedback controller. A block diagram over the structure of the proposed compensator is shown in Figure 5.18. As seen in the figure, the informations used for control are: the line impedance Z_{LN}, the load impedance Z_{LD}, and the actual transformation ratio n.

The following sections describe how to obtain these regulator subsystems, and outlines some suitable tuning rules. It is interesting to notice that also these two subsystems can be used separately or both together. They can be implemented as an upgrade unit to existing OLTC systems.

Subsystem 1: Feed-Forward The goal of the feed-forward compensation is to improve the convergence ratio of the system in case of a fault in the transmission line. In other words, the compensator will drive the system to the stable equilibrium point in case of a line fault. However, this method works only if, after the fault, the system is still the stable region (i.e. $n^2 Y_{LD} Z_{LN} < 1$).

The idea of using such compensation is suggested by the structure of the presented simplified model. It is rather straightforward to show that the line impedance Z_{LN} acts as a load disturbance on the system, similarly to P_{ref}. This can be shown rigorously in a similar way as in Section 2.6. There the surface conditions acted as a load disturbance on the system

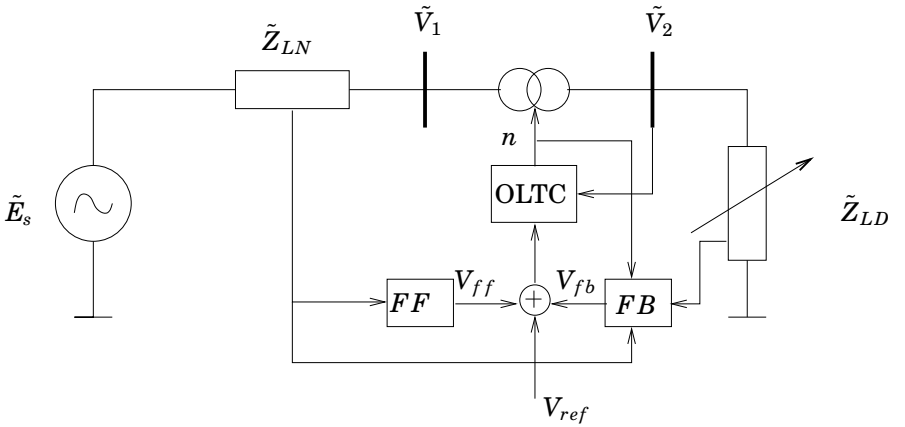

Figure 5.18 Two-node system with generator, transmission line, transformer and load. Compensation of the reference voltage is introduced through the blocks FF and FB.

modifying the friction curve in the same way as the line impedance Z_{LN} changes the active power characteristics.

In addition, the line impedance can be considered measurable. It is natural then to use a feed-forward compensation from the line impedance to diminish the influence of line faults. If the transformer ratio n would be directly accessible for control purposes, the transient influence of line fault could be (at least theoretically) completely removed. Although only V_{ref} is accessible, it is still possible to considerably improve the line-fault behavior of the system.

This compensating subsystem aims to prevent the grid from entering an unstable operating regime. For this it uses information about the line impedance.

A suitable feed-forward compensation is given by the first order filter $H_{ff}(s) = sT_d/(sT + 1)$, where T, T_d are tuning parameters. Then the control signal $V_{ff}(s) = H_{ff}(s)Z_{LN}(s)$.

In case the system enters the unstable region (i.e. $n^2 Y_{LD} Z_{LN} > 1$), another control strategy has to be applied, which is described in the following.

Subsystem 2: Feedback When the system is in the unstable region, it is desirable to drive it back to the stable operation regime. This can be done by reducing the reference voltage as long as the system is in the unstable region. Such a compensation can be achieved by a static nonlinear feedback. In Figure 5.15, as a result of the compensation, the vector

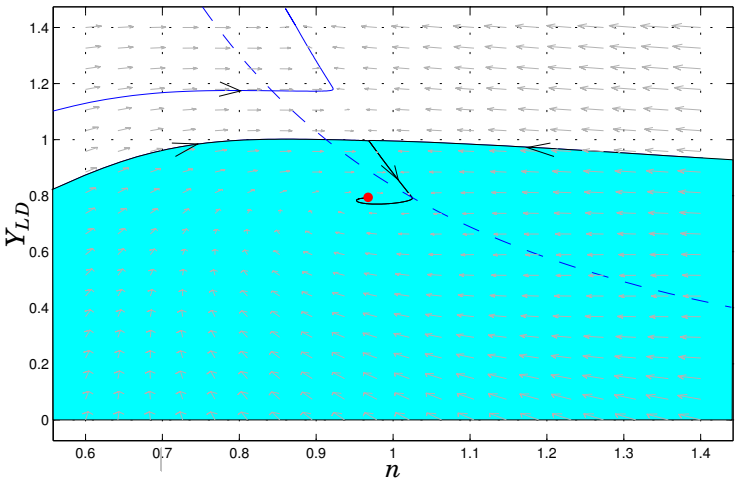

Figure 5.19 Vector field for the design model (5.17) with compensation. The dot marks the stable equilibrium point. The dashed curve is the loci for maximum power transfer, $n^2 Y_{LD} Z_{LN} = 1$. The shaded region represents the region of attraction of the equilibrium point. It has been considerably increased in comparison to the initial system in Figure 5.15.

field above the line $n^2 Y_{LD} Z_{LN} = 1$ will point inwards (see Figure 5.19). It results from the the plots that the region of attraction for the stable equilibrium point has been considerably increased.

It is to be mentioned here that the idea of using the distance from the peak of the function f in voltage stability studies has been recently proposed in [Julian *et al.*, 2000]. However, it has never been used (to the best of the authors knowledge) for dynamic compensation of the voltage reference signal.

Thus the second control subsystem aims to drive the grid from the unstable operation regime to the stable operation regime. For this it uses information about the line impedance, load impedance, and transformer ratio.

A suitable feedback controller is: $V_{fb} = -\max\left(0, \alpha\left(n^2 Y_{LD} - 1/Z_{LN}\right)\right)$, where α is a tuning parameter that is influencing the region of attraction of the equilibrium point. Figure 5.19 shows the phase plot of the system when the reference voltage is augmented by V_{fb}. Notice that the region of attraction (the shaded region) of the compensated system has been significantly increased in comparison to the initial system (see Figure 5.15).

It has been shown in the previous sections that the system does not

necesseraly becomes unstable as the stability limit $n^2 Y_{LD} Z_{LN} = 1$ is passed. However, this stability limit gives a margin up to those values of the load admittance where instabilities appear. This problem has two components:

- from the power control point of view, the critical point is the unstable equilibrium point as shown in Figure 5.14. Since the desired operating point is the stable equilibrium point, the proposed control structure will have no negative effect on the system.
- from the voltage control point of view, the problem is more interesting. Consider the voltage versus load impedance characteristics shown in Figure 5.7. According to equation (5.13), increasing n will have a reversed effect on the load voltage if $Y_{LD} > 1/(Z_{LN} n_1 n_2)$ (where $n_1 < n_2$ are two transformation ratios). Since $1/n_2^2 < 1/(n_1 n_2) < 1/n_1^2$, if the stability margin is surpassed, the inversion effect will appear. Thus a decrease of n is in place if an increase of the load voltage is desired. This is the same type of action that the proposed feedback loop will exhibit.

The two augmenting control signals V_{ff} and V_{fb} can be combined in different ways. The simplest scheme is when they are summed together with the nominal reference value V_{ref}. This way the resulting reference voltage signal that is applied to the OLTC is the sum $V_{ff} + Vfb + V_{ref}$, as shown in Figure 5.18.

Compensation for Static Effects

This control structure should be activated, ideally, only if the maximum loadability of the network is surpassed. However, this depends greatly on the control actions that succeeds the fault. In case of the compensator for dynamic effects proposed above, this would mean that for all possible impedance changes, as long as a stable equilibrium point exists, the controller should stabilize the system. Obviously this means that all these points should be included in the region of attraction of the equilibrium point for the compensated system. Using the above suggested feedback control law, no such guarantees are given, although the region of attraction is enlarged.

As suggested in [Vu and Novosel, 2001], one can use the stability measure $(Z_{LD}/n^2 - Z_{LN})$ as variable to drive this stage of the controller. A simple control law can be an integrator that once a given threshold on the stability margin is exceeded will disconnect a part of the load.

$$\dot{u}_{LS} = \frac{1}{T_{LS}} \mathrm{dzn}(Z_{LD}/n^2 - Z_{LN}) \tag{5.18}$$

The function dzn denotes the dead-zone nonlinearity. In a similar fashion one can use the same idea to connect capacitor banks:

$$\dot{u}_{CB} = \frac{1}{T_{CB}} \mathrm{dzn}(Z_{LD}/n^2 - Z_{LN}) \tag{5.19}$$

In this case, the connected capacitor bank will change the apparent load impedance, increasing this way the power throughput of the system.

Putting it all together

As shown above, there are basically, three available control signals for the system: the transformer ratio n, the capacitor bank, and the load shedding.

An important objective is to keep the amount of disconnected load at minimum. A secondary goal is to keep the number of connected capacitor banks as low as possible. This basically means that there is hierarchy of preferred control:

- The less expensive control input is the *transformation ratio* n. It is desirable to exploit this signal to maximum before any other action is taken. The "Compensator for dynamic effects" introduced in this work uses n as the mean to improve the stability of the power system.
- If the system is not stabilizable by means of altering n, it is desirable to *connect capacitor banks* to the power system, this way increasing that transferable active power.
- When capacitor banks fail to stabilize the system, as a last resort, parts of the load can be disconnected. This is the so called *load shedding*.

Depending on the complexity of the objective function these three stages can be combined in different ways. However, since the study of this mechanism is not the main scope of this work, in the following a simple structure will be used that highlights the usefulness of the proposed compensator for dynamic effects.

The main idea is that if the compensator for dynamic effects fails to stabilize the system, the next stage of control is activated (the considered stage is the load shedding, that is, no capacitor banks are available). The failure to stabilize the system of the first stage is quantized by a threshold on the stability limit. That basically means if $Z_{LD}/n^2 - Z_{LN} < \Delta < 0$, it is assumed that stability can not be regained by dynamic compensation and the load shedding is activated.

5.6 Simulation Results

In order to obtain more realistic simulation results the initial design model has been modified as follows:

- the dynamics have been scaled according to the benchmark model [Larsson, 2003],
- additional dynamics have been introduced for the load argument, Φ,
- load shedding input k has been added,
- saturation and quantization is introduced on the transformer ration n. The latter is intended to simulate the mechanical tap-changer,
- the tap-changer is inherently a discrete system. It changes the transformer ratio n in discrete steps. However, in the time domain, the system can not be viewed as sampled system in the classical sense. The time instances when an actual change of the transformer ratio n occurs, depend on mechanical factors in the tap changer and it can vary from one step to other. Therefore, in the following model the sampling time is denoted h_i and in reality it can vary. In the simulations however h_i is fixed. Moreover, the tap-changer can make only one step at the time.
- to avoid chattering, an OLTC system usually contains a dead-zone on the control error.

This way the simulation model is the following:

$$\begin{cases} \dot{Y}_{LD} = \dfrac{1}{T}\left((1-k)P_{ref} - E^2 \dfrac{Z_{LD}/n^2}{\left|\tilde{Z}_{LN} + \tilde{Z}_{LD}/n^2\right|^2}\cos\Phi\right) \\ \dot{\Phi} = (1-k)Q_{ref} - \dfrac{1}{T}\Phi - E^2 \dfrac{Z_{LD}/n^2}{\left|\tilde{Z}_{LN} + \tilde{Z}_{LD}/n^2\right|^2}\sin\Phi \\ \eta(t+h_i) = \eta(t) + q\ \mathrm{sign}(e(t)) \\ e(t) = \mathrm{dzn}\left(V_{ref} - E\dfrac{Z_{LD}/n}{\left|\tilde{Z}_{LN} + \tilde{Z}_{LD}/n^2\right|}\right) \\ n = \mathrm{sat}(\eta) \end{cases} \tag{5.20}$$

The saturation on n has the limits $n_{min} = 0.75$, $n_{max} = 1.25$ and the dead-zone has the limits ± 0.03. The chosen quantization step q is 0.027. The chosen sampling time is 30 seconds, which approximates the mechanical delay of the tap-changer and the OLTC delay timer.

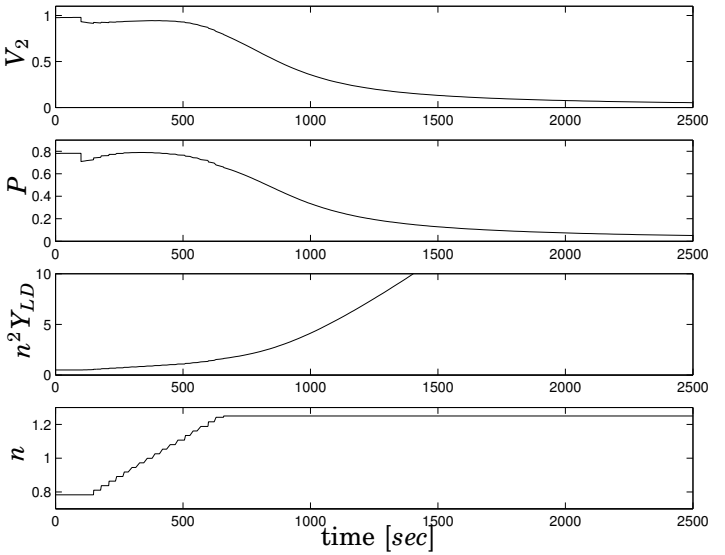

Figure 5.20 At $t = 100$ seconds, a line tripping is simulated by a 20% increase of the line impedance Z_{LN}. The system becomes unstable although a stable equilibrium point exists.

Figure 5.20 shows simulation results fo the before presented model. The model parameters are $V_{ref} = 1$, $P_{ref} = 0.78$, $Q_{ref} = 0.15$, $T = 60$, $E = 1.5$, and $\Theta = 1.47$ radians. Although a stable equilibrium point existe, the system becomes unstable and voltage collapse occurs.

The three-stage control system consists of the following compensator:

- Feed-forward compensation: $H_{ff}(s) = 30s/(20s + 1)$ has a "dirty-derivative" character with the low-pass filter having its time constant comparable with that of the controlled system.
- Feedback compensation: $V_{fb} = -\max\left(0, \alpha\left(n^2 Y_{LD} - 1/Z_{LN}\right)\right)$. The parameter α influences the region of attraction of the equilibrium point. In the simulations $\alpha = 1.1$.
- Load shedding is done according to the following adjustment rule: $\dot{k} = -1/T_{LS}\mathrm{dzn}V_{fb}$. The limits of the dead-zone are design parameter. In the simulation ± 0.2 has been used. This parameter has been tuned by simulations although good physical interpretation exists. The used integrator time constant is $T_{LS} = 10$. The load shedding is based on the VIP.

The first two control signals (V_{ff} and V_{fb}) augment the reference

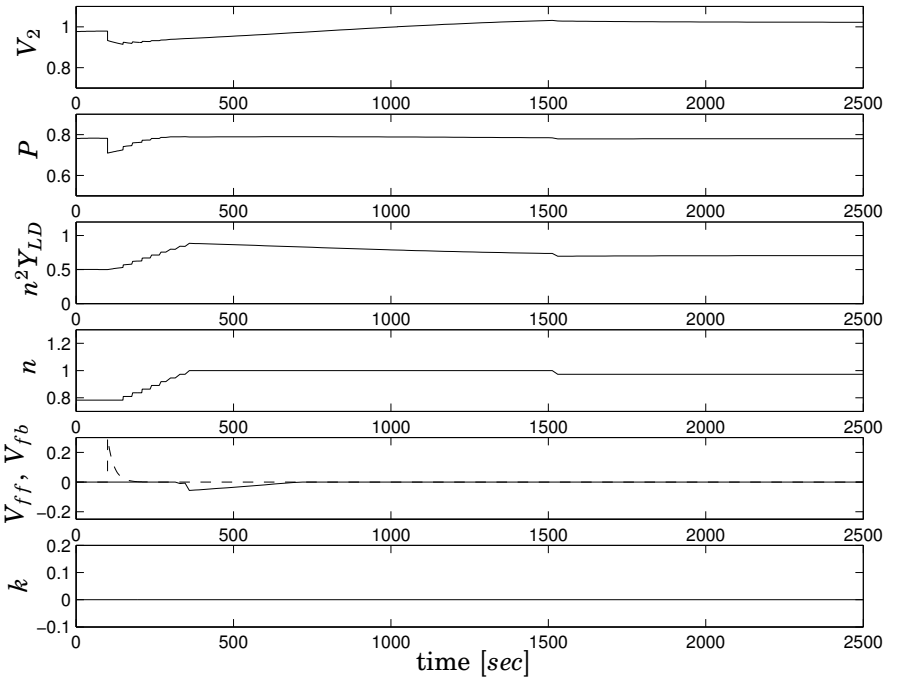

Figure 5.21 At $t = 100$ seconds, a line tripping is simulated by a 20% increase of the line impedance Z_{LN}. By momentary changes of the reference value by augmentation with V_{ff} (dashed line) and V_{fb}, stability is maintained without shedding load. In case the reference voltage had been kept constant, the system would become unstable.

value as follows:

$$e(t) = \mathrm{dzn}\left(V_{ref} + V_{ff} + V_{fb} - E_s \frac{Z_{LD}/n}{\left|\tilde{Z}_{LN} + \tilde{Z}_{LD}/n^2\right|}\right).$$

However, a more complex augmentation is also possible, e.g. V_{ff} is conditioned by V_{fb}.

In the simulations, the following parameters have been used: $V_{ref} = 1$, $P_{ref} = 0.78$, $T = 60$, $E = 1.5$, and $\Theta = 1.47$ radians. In addition, in the simulation from Figure 5.21 the reference reactive power is $Q_{ref} = 0.15$. The scenario consists of a line tripping at $t = 100$ seconds, when the line impedance Z_{LN} is increased from 1 to 1.2. At the moment of the fault, V_{ff} shows a significant increase. However, since the new equilibrium point is not achieved the system ends up in the unstable operating region (at

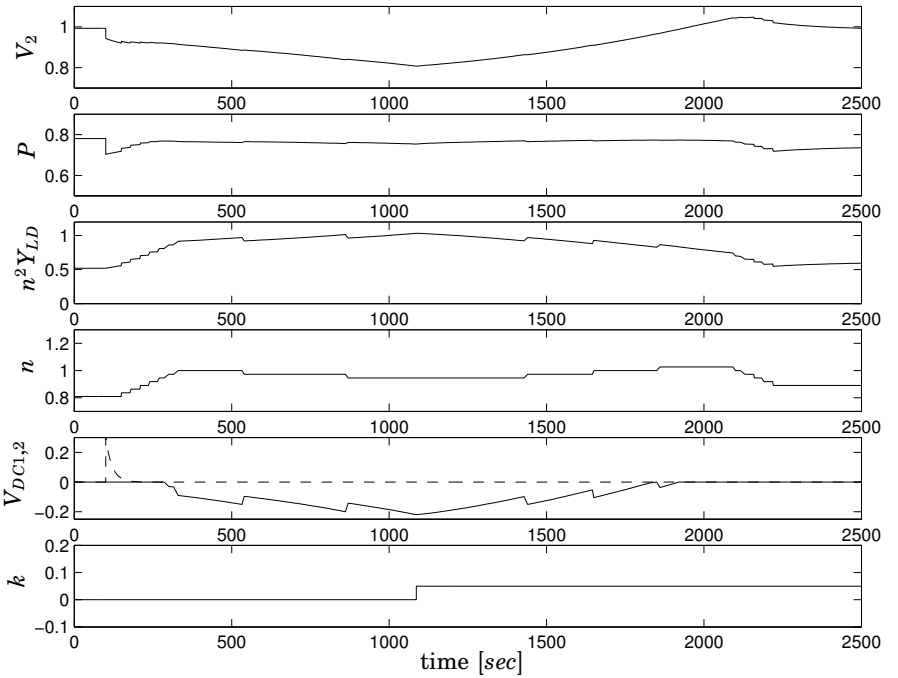

Figure 5.22 At $t = 100$ seconds, a line tripping is simulated by a 20% increase of the line impedance Z_{LN}. The loads power demand can not be met by the network and load shedding is applied at around 1600 seconds.

around 400 seconds). This will trigger the second stage of the controller, decreasing V_{fb}. This will result in a decrease of the overall voltage reference value such that the system is brought back in the stable region. Notice that throughout the entire control sequence, the third control stage (load shedding) is not engaged, i.e. $k = 0$.

It is important to remark that the first step (i.e. V_{ff}) is sensitive to the fault timing due to the low sampling frequency. Similarly if multiple steps (e.g. two) would be possible, the performance would increase significantly. Nevertheless, even in the case of the state-of-the-art OLTCs, where the delay timer is inversely proportional to the control error, considerable improvements can be obtained in compensating for line tripping.

In the next simulation (Figure 5.22), the reference reactive power is increased to $Q_{ref} = 0.2$. This will result in a power demand from the load that can not be satisfied by the network after the line tripping. Consequently load shedding has to be used. This can be seen at approximately

1100 seconds, when one step load shedding is applied. After the load shedding, the secondary control stage is still active, improving the convergence properties of the system.

5.7 A Test-System Illustrating Load-Voltage Dynamics in Power Systems

This test system has been proposed by ABB within the European project CC. It is a benchmark illustrating voltage instability phenomena in a simplified power systems. The load model used is a dynamical model of the form (5.1). Coupled to the network this model give rise to a differential-algebraic form for the studied power system:

$$\begin{cases} \dot{x} = f(x,y,u) \\ 0 = g(x,y,u) \\ f(x,y,u) = \begin{bmatrix} -\frac{x_p}{T_p} + P_0(V_2^{a_s} - V_2^{a_t}) \\ -\frac{x_q}{T_q} + Q_0(V_2^{b_s} - V_2^{b_t}) \end{bmatrix} \\ g(x,y,u) = \begin{bmatrix} \frac{V_2 E}{nZ_{LN}}\sin(\delta) + (1-k)\left(\frac{x_p}{T_p} + P_0 V_2^{a_t}\right) \\ -\frac{V_2 E}{nZ_{LN}}\cos(\delta) + \frac{V_2^2}{n^2 Z_{LN}} - B_0 V_2^2 + (1-k)\left(\frac{x_q}{T_q} + Q_0 V_2^{b_t}\right) \end{bmatrix} \end{cases} \tag{5.21}$$

where $x^T = [x_p,\ x_q]$, $y^T = [V_2,\ \delta]$, $u = [n,\ k]$.

Similarly to model (5.20), the system has two dynamic states x. Additionally, this model has two algebraic states, the voltage on the secondary side of the transformer V_2 and the angle between the generator and the load voltages δ.

Furthermore, this system has an auxiliary capacitor B_0, connected at the load side in order to increase the power transfer capacity of the network. This term can be used as a control input if capacitor bank connections are to be simulated. Naturally, this will mean that the reactance introduced by the capacitor has to be taken into account in the control law. The feedback control law becomes:

$$V_{fb} = -\max\left(0, \alpha\left(n^2(Y_{LD} + B_0) - 1/Z_{LN}\right)\right)$$

That is the equivalent admittance of the load incorporates the capacitor.

The OLTC dynamics is basically governed by an integrator. For sake of simplicity, consider first a continuous dynamics. The integrator time constant T_i is set equal to the some of the mechanical delay T_m and a control delay T_d in the OLTC. The control delay time is a tuning parameter in the OLTC. It is used as a timer until the first control action is taken

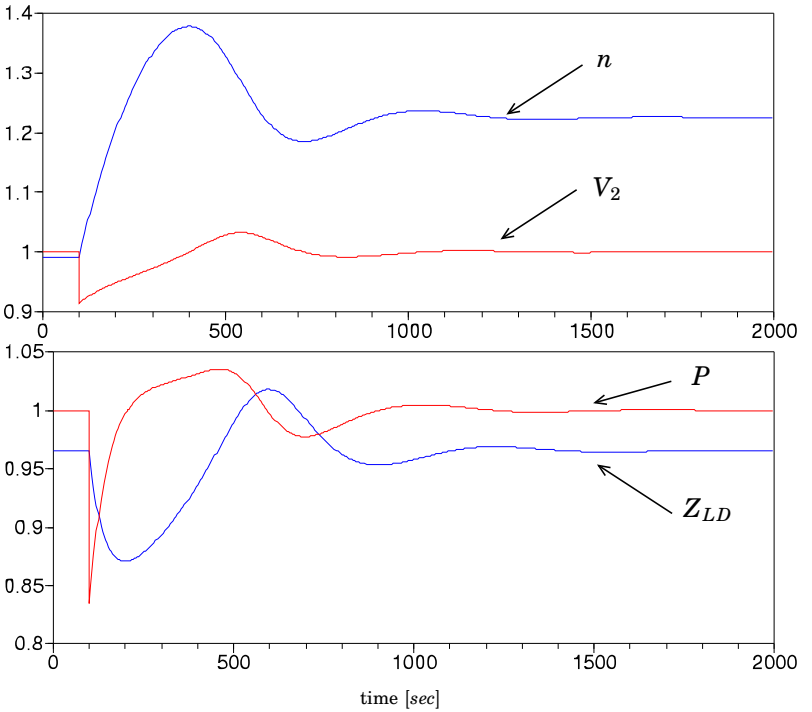

Figure 5.23 At $t = 100$ seconds, a line tripping is simulated by an increase of the line impedance from 0.25 to 0.5. After some transients the system converges to a stable equilibrium point.

after a deviation in the load voltage. Typical values are $T_m = 1 - 5$ sec, $T_d = 30 - 120$ sec.

Similarly to (5.20), after a fault in the line, the system becomes unstable or reattains stability depending on the operating point. Figure 5.23 shows a scenario where after a line fault the system converges to a stable equilibrium point. The parameters used in the simulation are: $P_0 = 1$, $Q_0 = 0.27$, $B_0 = 0.2$, $E = 1.05$, $T_p = T_q = 60$, $T_i = 31$, $a_s = b_s = 0$, and $a_t = b_t = 2$. At $t = 100$ seconds, a line tripping is simulated by an increase of the line impedance from 0.25 to 0.5. After some transients the system converges to a stable equilibrium point.

The same simulation scenario is repeated in case the desired reactive power is set to $Q_0 = 0.28$. In this case the system becomes unstable after the line fault, despite a stable equilibrium point at $(\delta,\ n) = (-0.634,\ 1.25)$.

If the dynamic compensation in the reference voltage is used the sta-

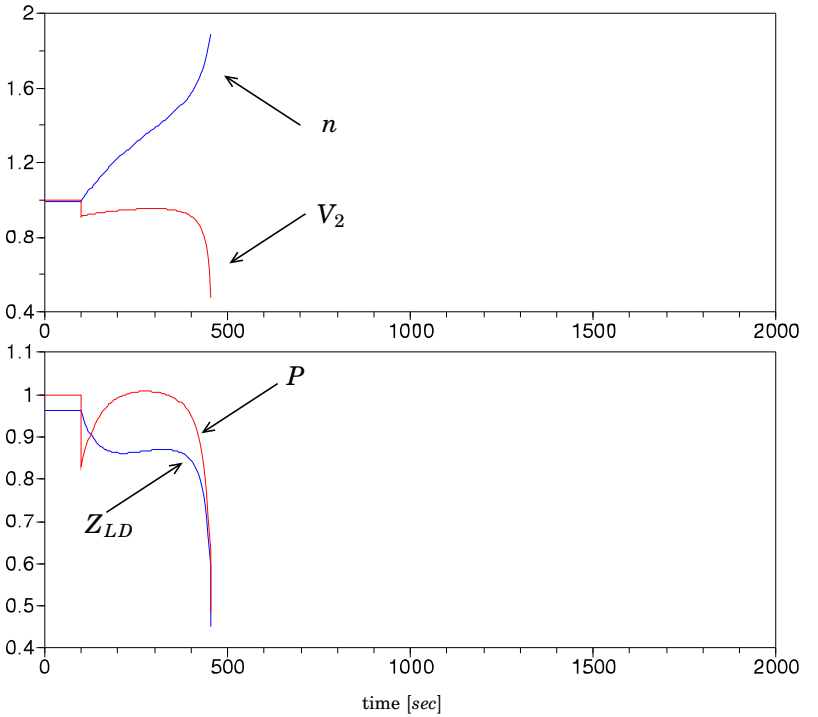

Figure 5.24 At $t = 100$ seconds, a line tripping is simulated by an increase of the line impedance from 0.25 to 0.5. After an initial recovery the voltage will collapse, and the system becomes unstable.

bility can be re-attained. Figure 5.25 shows simulation results in case the reference signal is dynamically adjusted. At the time instant the fault is detected, the feed-forward term will increase the reference signal. This compensation turns out to be sufficient to attain a stable equilibrium point. In this scenario the stable equilibrium point is achieved although the loci $n^2(Y_{LD} + B_0)Z_{LN} = 1$ is surpassed. If the reference is decreased once this barrier is passed, the control action will contribute for a better performance (see Figure 5.26). Notice the typical behavior of the compensated reference signal. When the fault appears, the voltage reference signal is abruptly increased, followed by a mild decrease. If the loci $n^2(Y_{LD}+B_0)Z_{LN} = 1$ is surpassed and the system arrives in the unstable region, the reference signal is again modified, however, in this case it is decreased. After the system arrives to its equilibrium point the reference signal is left unchanged, at its nominal value.

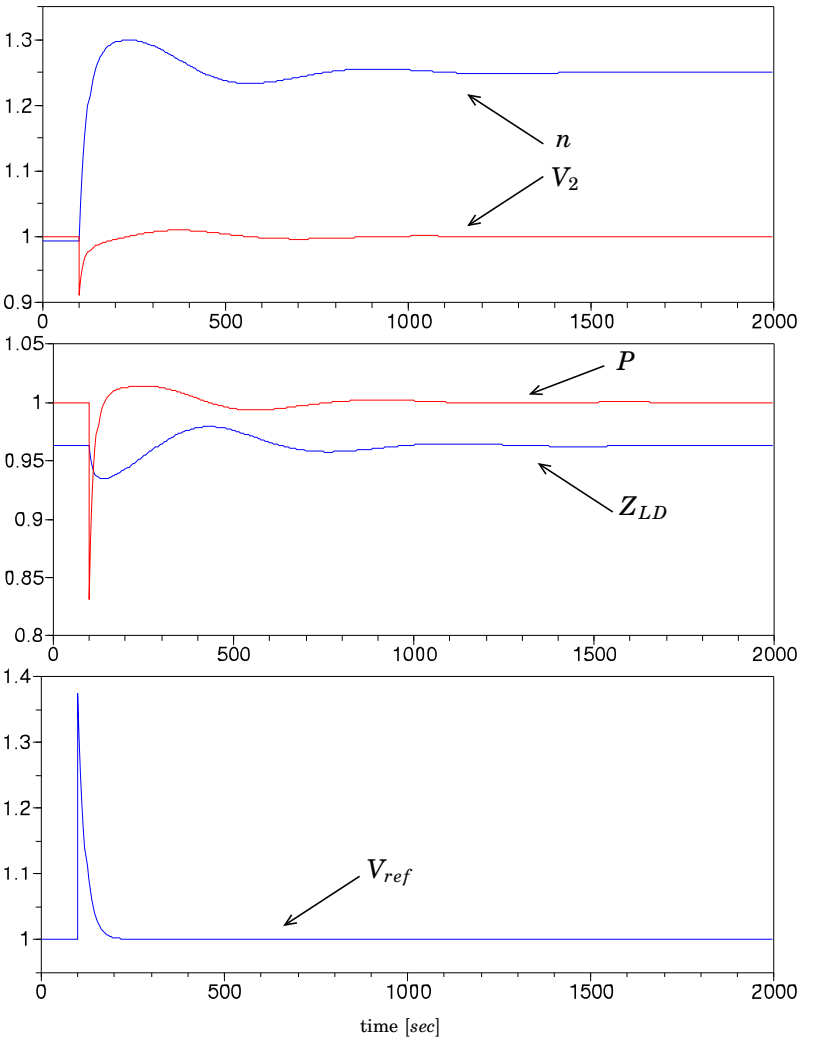

Figure 5.25 At $t = 100$ seconds, a line tripping is simulated by an increase of the line impedance from 0.25 to 0.5. The reference voltage is dynamically changed such that stability is re-attained.

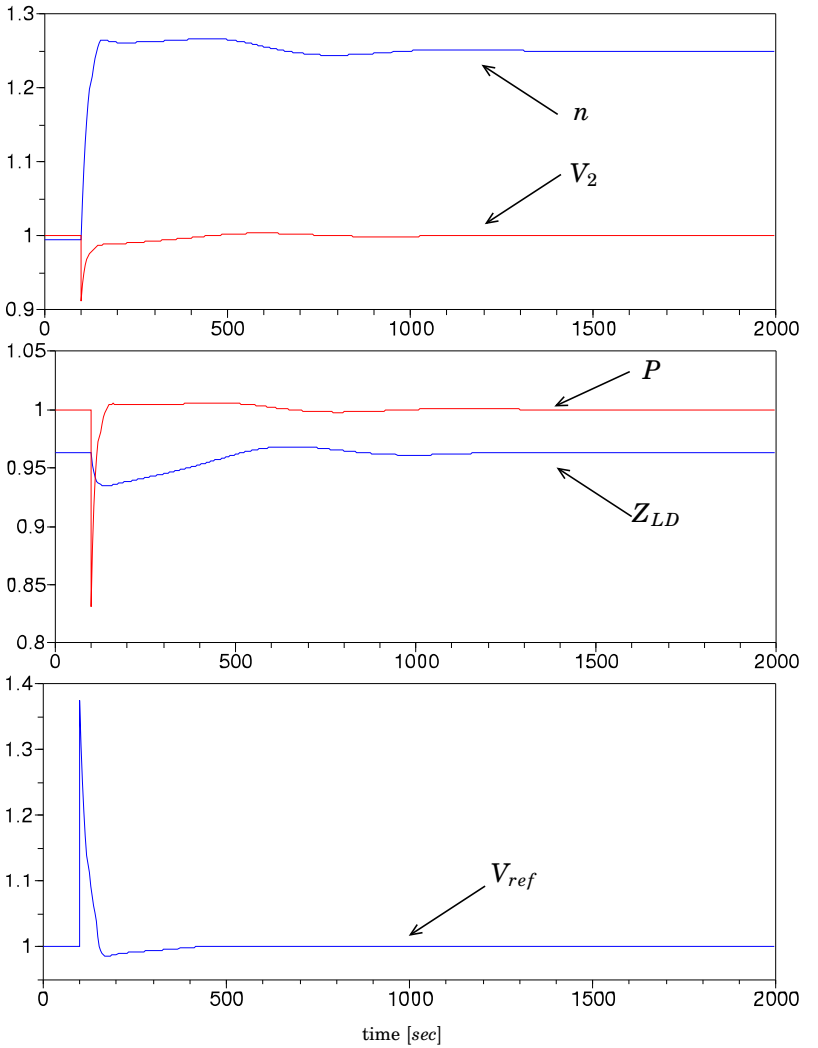

Figure 5.26 At $t = 100$ seconds, a line tripping is simulated by an increase of the line impedance from 0.25 to 0.5. The reference voltage is initially increased and once $n^2 Y_{LD} Z_{LN} > 1$ the reference voltage is decreased. The stable equilibrium point is achieved.

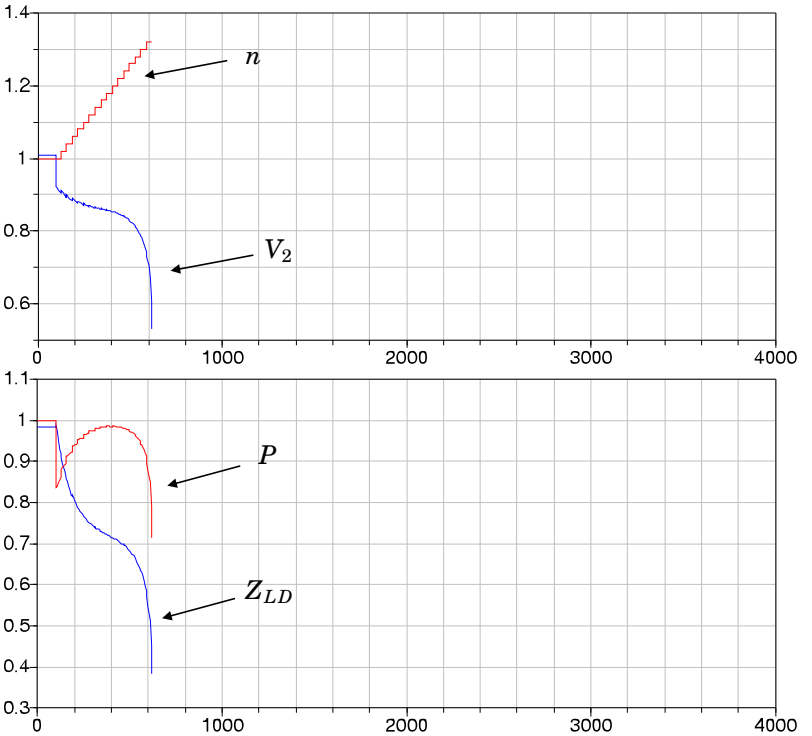

Figure 5.27 At $t = 100$ seconds, a line tripping is simulated by an increase of the line impedance from 0.25 to 0.5. The reference voltage is initially increased and once $n^2(Y_{LD} + B_0)Z_{LN} > 1$ the reference voltage is decreased. Due to the high sampling time and the quantization step of the control signal the system becomes unstable.

A more realistic model for an OLTC is:

$$n(k+h) = \begin{cases} n(k) + 1, \text{ if } V_2 - V_{ref} < DB/2 \text{ and } n(k) < n_{max} \\ \quad n(k), \text{ if } DB/2 < V_2 < DB/2 \\ n(k) - 1, \text{ if } (V_2 - V_{ref}) > DB/2 \text{ and } n(k) > n_{min} \end{cases}$$

This model only gives a good approximation for constant delay time, and the sample time of the discrete-time system should then be chosen as $h = T_d + T_m$. DB denotes a dead-band on the control error which prevents the chattering that can appear due to the quantized control output n. The default values used in simulation are: $h = 30 + 1 = 31$ sec. , $DB = 0.03$. The step size of the OLTC is 0.02.

Figure 5.27 shows the case with $Q_0 = 0.27$ with a discrete OLTC model. Although this case was easy to stabilize in the continuous case, the influence of the high sampling time together with the quantized control output will result in an unstable system.

Not even the tested compensator is able to stabilize the system. However, by reducing the control delay T_d the compensated system will achieve a stable operating point. Figure 5.28 shows a simulation when the control delay is reduced from 30 to 18 seconds.

Similarly, if the step size of the control output n is increased, stability can be achieved. Figure 5.29 shows a simulation result when the step size of the tap changer is increased from 0.02 to 0.04.

Both changes in the OLTC dynamics aims to a quicker response. Nevertheless, it is to point out that without the compensation of the reference voltage the system would still become unstable.

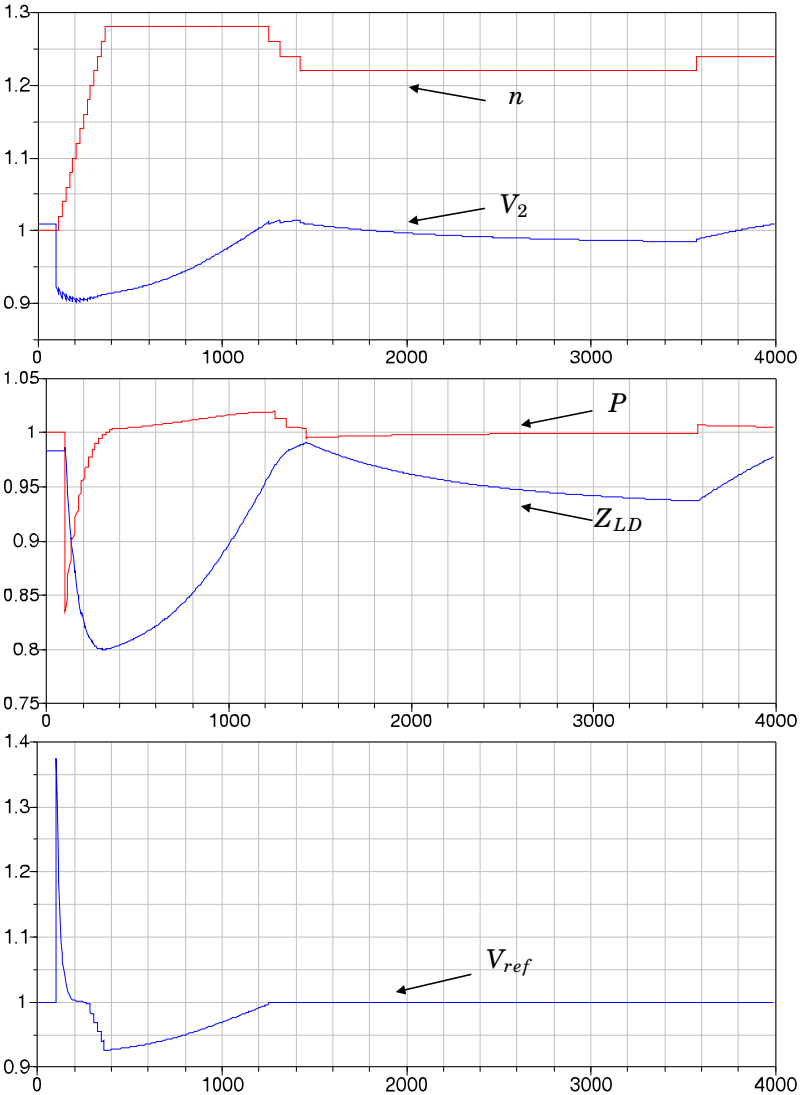

Figure 5.28 At $t = 100$ seconds, a line tripping is simulated by an increase of the line impedance from 0.25 to 0.5. The reference voltage is initially increased and once $n^2(Y_{LD} + B_0)Z_{LN} > 1$ the reference voltage is decreased. The control time delay is reduced from 30 sec. to 18 sec. The system is stabilized.

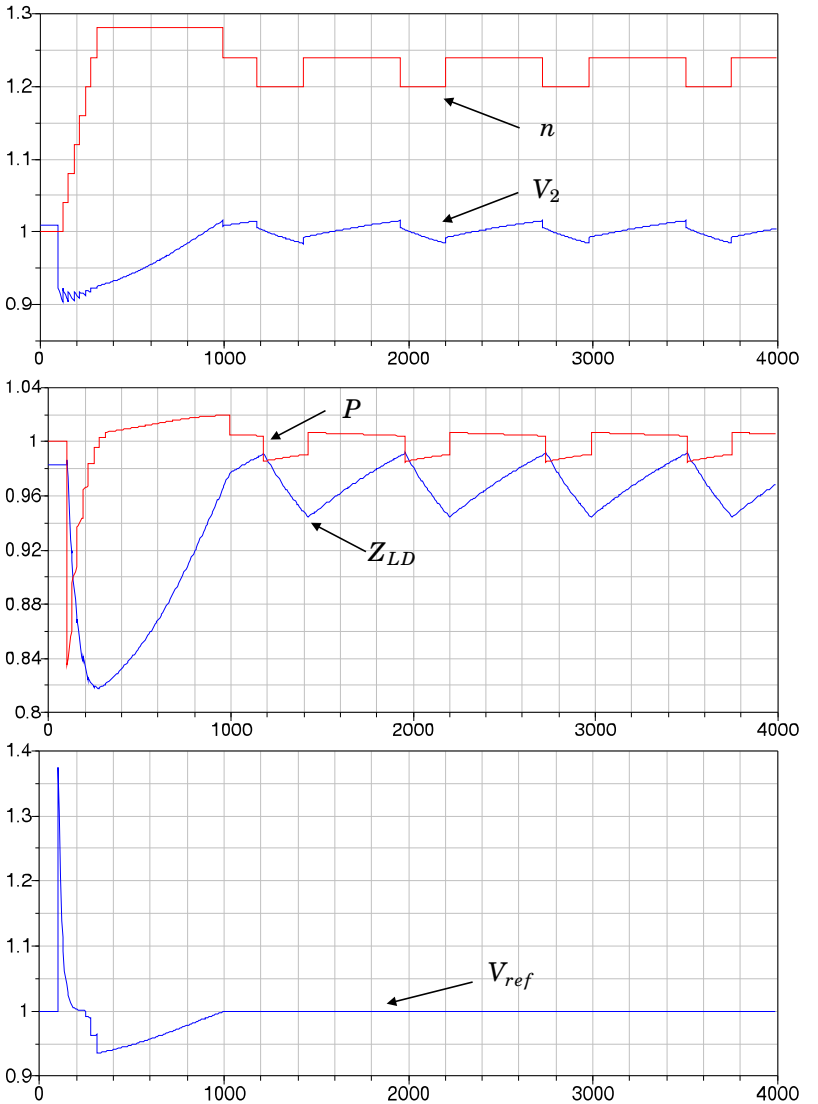

Figure 5.29 At $t = 100$ seconds, a line tripping is simulated by an increase of the line impedance from 0.25 to 0.5. The reference voltage is initially increased and once $n^2(Y_{LD} + B_0)Z_{LN} > 1$ the reference voltage is decreased. The step size of the tap changer is increased from 0.02 to 0.04 . The system is stabilized.

5.8 Conclusion

This work proposes a method for improving the stability properties of power networks. The main concern is the situation when instabilities occurs due to dynamic effects.

The proposed method consists of momentary change of the transformer ratio n so as to avoid the critical operating region. Since in practice the reference voltage V_{ref} is the available signal for compensation the method changes n by means of V_{ref}.

In case the network capacity is exceeded, the method can be easily combined with coupling of capacitor banks and load shedding. This way a complete emergency control scheme is obtained.

Simulation results with different models show the utility of the introduced control structure. The method stabilizes the system returning the voltage to its nominal value while minimizing the amount of disconnected load.

References

Begovic, M. and D. Novosel (2002): "A novel method for voltage instability protection." In *Proceedings of the 35th Hawaii International Conference on System Sciences*.

Begovic, M., D. Novosel, and M. Milisavljevic (2001): "Trends in power system protection and control." In *Decision Support Systems 30*, pp. 269–278.

Guo, Y., D. Hill, and Y. Wang (2000): "Nonlinear decentralized control of large-scale power systems." *Automatica*, **36**, pp. 1275–1289.

Hill, D. (1993): "Nonlinear dynamic load models with recovery for voltage stability studies." *IEEE Transactions on Power Systems*, **8**, pp. 166–176.

IEEE (1990): "Voltage Stability of Power Systems: Concepts, Analytical Tools, and Industry Experience." *IEEE Publication, 90TH-0358-2-PWR*.

Julian, D., R. Schulz, K. Vu, W. Quaintance, N. Bhatt, and D. Novosel (2000): "Quantifying proximity to voltage collapse using the Voltage Instability Predictor (VIP)." In *Power Engineering Society Summer Meeting, IEEE*.

Karlsson, D. and D. Hill (1994): "Modelling and identification of nonlinear dynamic loads in power systems." *IEEE Transactions on Power Systems*, **9:1**, pp. 157–166.

Kundur, P. (1993): *Power System Stability and Control*. McGraw-Hill, Inc.

Larsson, M. (2000): *Coordinated voltage control in electric power systems*. PhD thesis, Lund Institute of Technology, Department of Industrial Electrical Engineering and Automation.

Larsson, M. (2003): "A simple test system illustrating load-voltage dynamics in power sytems." http://www.dii.unisi.it/hybrid/cc/.

Machowski, J., J. W. Bialek, and J. R. Bumby (1997): *Power System Dynamics and Stability*. John Wiley & Sons.

Morison, G., B. Gao, and P. Kundur (1993): "Voltage stability analysis using static and dynamic approaches." *IEEE Transactions on Power Systems*, **8:3**, pp. 1159–1171.

Ohtsuki, H., A. Yokoyama, and Y. Sekine (1991): "Reverse action of on-load tap changer in association with voltage collapse." *IEEE Transaction on Power Systems*, **6:1**, pp. 300–306.

Rosehart, W. D. and C. A. Cañizares (1999): "Bifurcation analysis of various power system models." *International Journal of Electrical Power & Energy Systems*, **21:3**, pp. 171–182.

Schlueter, R., I. Hu, M. Chang, J. C. Lo, and A. Costi (1990): "Methods for determining proximity to voltage collapse." In *IEEE PES Winter Meeting*.

Shahrestani, S. and D. Hill (2000): "Global control with application to bifurcating power systems." *Systems & Control Letters*, **41**, pp. 145–155.

Vu, K. T. and C.-C. Liu (1992): "Shrinking stability regions and voltage collapse in power systems." *IEEE Transactions on Circuits and Systems*, pp. 271–289.

Vu, K. T. and D. Novosel (2001): "Voltage Instability Predictor (VIP) - method and system for performing adaptive control to improve voltage stability in power systems." In *United States Patent Nr. US 6,219,591 B1*.

Zaborszky, J. and Z. Baohua (1989): "Exploration of the conceptual structure of voltage stability." In *Proceedings of the 28th Conference on Decision and Control*.